DEPARTMENT OF THE INTERIOR

U.S. GEOLOGICAL SURVEY

Terrestrial-cosmological correlations in evolutionary processes[a]

by

Herbert R. Shaw[1]

Open-file Report 88-43

This report is preliminary and has not been reviewed for conformity with U.S. Geological Survey editorial standards and stratigraphic nomenclature.

a. This report contains material compiled prior to 4 October, 1984.

[1] U.S. Geological Survey, Menlo Park, CA 94025

UNITED STATES DEPARTMENT OF THE INTERIOR
DONALD PAUL HODEL, SECRETARY
GEOLOGICAL SURVEY
Dallas L. Peck, Director

For additional information write to:

U.S. Geological Survey
MS 910
345 Middlefield Road
Menlo Park, CA 94025

Copies of this report can be purchased from:
Books and Open-file Reports Section
U.S. Geological Survey
Box 25425, Federal Center
Denver, CO 80225
Call (303) 236-7476

TABLE OF CONTENTS

LIST OF TABLES

LIST OF FIGURES

Summary

Time-series records of the following geological-cosmological data are examined for systematic relationships: (1) 74-Myr record of Hawaiian-Emperor (H-E) volcanism, (2) H-E geomagnetic record and reported global geomagnetic periodicities, (3) Phanerozoic record of impact-cratering events on Earth and reported periodicities, (4) Phanerozoic record of strontium isotope variation in the oceans, (5) cosmological model for the history of the Sun's motion in the Milky Way galaxy during the latest 2 Byr, (6) Phanerozoic record of major faunal extinctions and originations, (7) 250-Myr record of faunal extinctions and reported 26-Myr periodicitiy, (8) 70-Myr record of ocean ostracode extinctions and originations, and (9) 140-Myr record of Avian adaptive radiation. Records were examined from the point-of-view of periodic behavior and resemblances between quasiperiodic and episodic behaviors.

Moving window averages, cycle-plots, and power spectra using Fourier transform analysis of H-E volcanism suggest maxima in rate phenomena with periods of about 2, 3, 6, 12 and 15 Myr; evidence of longer periods exists but is unresolved by the 74-Myr record. The 3-Myr volcanic period resembles a 3-Myr average event interval in ocean ostracode data. Histograms of event intervals for the composite of all records show many peaks with a highest peak near a period of 6 Myr. The average of international biostratigraphic stage intervals in studies of faunal extinctions is about 6.2 Myr during the latest 250 Myr. The 12-Myr period resembles an average 12-Myr cycle in geomagnetic polarity durations for the H-E data, and the 15-Myr period resembles a 15-Myr period in the global frequency of geomagnetic reversals. Periodicity arrays are typical of natural records examined, including impact cratering on Earth.

Observed event intervals are tabulated for all systems studied, and histograms of the data are compared with artificial histograms derived from mixed geometric series of the following three types:

$$(2^n)(3^m) \; ; \; (2^n)(3^m)(5^p) \; ; \; (2^n)(3^m)(5^p)(7^q),$$

where exponents are integers. The two-term serial combination approximates the observed distribution, and the four-term series fits all major peaks; the former is considered to represent the most parsimonious periodicity spectrum because no simple sets of harmonic series nor any of the above geometric series taken alone resemble the periodic signatures of the individual or composite records. In both the observed and artificial histograms there is a gap at 28 to 29 Myr; if a 28.4 Myr period exists in the record of impact cratering (Alvarez and Muller, 1984), it is not conspicuous in other terrestrial phenomena (it may be simpler to suppose that this period is an artifact of mixed periods). A maximum exists at about 26 Myr (extinction period of Raup and Sepkoski, 1984), but it is weaker than maxima near 32, 18, and 15 Myr. The 6-Myr maximum dominates all histograms, possibly because multiples of 2-Myr and 3-Myr are common in the volcanic and biologic records. The 32-Myr maximum (subharmonic of 2^n for n=5) is a close second in the simplest artificial histogram, but it is the third highest peak in the histogram of observed values (15$\pm$1 Myr is the second highest peak).

Patterned periodic arrays are characteristic of attractors. These are spatially and(or) temporally recurring periodic patterns produced by iterations of nonlinear dynamical equations (attractor theory is a rapidly growing field of nonlinear dynamics). Numerical data from computer experiments and from fluid dynamic experiments illustrate the properties of attractors. Examples of both types of experimental data come from previous work by the author as well as from the literature of nonlinear dynamics. These experiments, as documented by plots of attractor states and their time-series, illustrate the bifurcational origins of geometric series of

subharmonic and mixed periodicity arrays as well as phenomena such as quasiperiodicity, intermittency, noisy (broadband) periodicity, and mixtures of all these types of periodic behaviors (the latter is sometimes called the regime of chaotic dynamics or deterministic chaos).

Patterns of cosmological evolution implied by the distribution of the planets in the solar system and of the solar system in the Milky Way galaxy are shown to be consistent with the theory of attractors (the nested character of these patterns exemplifies the behavior of strange attractors, a term often used in the literature of chaotic dynamics). By implication, periodic, episodic, and chaotic signatures of derivative phenomena such as cometary and asteroidal distributions and orbital periodicities are aspects of a common frequency spectrum of universal character, giving rise to rhythmic patterns of orchestral proportions. Other phenomena entrained by or resonating with the same cosmological rhythms have similar periodicity suites. An orchestral viewpoint is supported by periodicities found in the record of impact cratering on Earth and in galactic models. Both suites are consistent with geological periodicity arrays. Periodicities of galactic orbital motions range from about 30 Myr for the shortest plane-crossing interval to about 233 Myr for the galactic year (periodic phenomena of shorter durations exist; nearby star formation occurs at episodic intervals of 2 to 3 Myr).

These conclusions imply physical correlations among terrestrial and extraterrestrial phenomena (e.g., bifurcational patterns of biologic rhythms are influenced by mass impact frequencies, volcanic frequencies, glaciation frequencies, and frequencies of other global processes). The evolution of biologic diversity is therefore examined from the viewpoints of attractor theory and universality of periodic processes. When biologic diversity is expressed in terms of rates of change in numbers of taxa, the results are consistent with bifurcation patterns of attractor dynamics. Avian adaptive radiation is used to illustrate a specific bifurcational history in terms of attractor theory. Such systems are tuned by net rate parameters that reflect feedback processes affecting growth (birth, species originations, etc.) and decay (death, species extinctions, etc.). The bifurcation patterns of Avian radiation at the levels of orders and families are described by tuning functions that vary with time in ways that appear to correlate with impact cratering frequencies. Peaks in a plot of bifurcation rates during late Cretaceous and early Tertiary times (marking approaches to plateaus of steady-state diversity in different lineages) correlate with peaks in the record of cratering frequencies. However, the dynamical basis for these correlations is ambiguous. Attractor theory predicts that major changes in simple bifurcation sequences can result from small changes in competing forcing functions. Therefore, diversity can change gradually or explosively at any taxonomic level as a consequence of either small or large changes in environmental forcing (speciation and extinction may be either gradual or punctuated by sudden change, the latter ranging from untimely deaths of individuals to catastrophic extinctions at high taxonomic ranks). From the analysis of Avian radiation it is not possible to specify the relative contributions of cratering energies to processes of extinction and origination, though high cratering frequencies seem to correlate with high rates of evolution. Cause-effect correlations between extinctions and impact events found in other studies are not seen in the Avian record, possibly because they are masked by inclusive effects of the relatively coarse classification scheme.

Correlation of Avian radiation with impact cratering events suggests that biologic evolution over time is controlled by the net effect of environmental (ultimately trophic) energy pulses. A categorical term 'impulse energy' is

used to refer to terrestrial energy cascades related to chains of events connected with cosmic energy sources. This is the dynamical source function for tuning of biologic processes as epitomized by Avian radiation (this does not say that biologic evolution can't also be described by local environmental and biological rate parameters). The net effect of this source (which is both intermittent and episodically continuous) on evolutionary rates can be positive or negative as measured in units of biologic diversity.

Scale effects in nested systems (resonances, self-similarities, universality parameters, etc.) imply that extraterrestrial phenomena such as mass impacts and electromagnetic fluxes are coupled with geological processes such as volcanism, atmosphere and ocean circulations, and transfers of angular momentum between atmosphere, ocean, and mantle (influences on the length-of-day). Concepts of volcanological and geomagnetic coupling suggest that such energy cascades may even perturb the geodynamo. The frequency spectra of 'impulse energy' include galactic pulsations (particle and plasma waves) as well as pulsations in frequencies of impact events influenced by disturbances of reservoirs of cometary and asteroidal objects in the solar system. The present time appears to be one of high impulse energy, but it is not a time of high probabilities for catastrophic encounters with large asteroids or comets according to published data on cratering frequencies. Reexamination of the cratering record suggests that the frequencies of small Earth-crossing objects (meteoroids less than 1 km in diameter and craters less than 10 km in diameter) may have increased relative to large objects (meteoroids larger than 1 km in diameter and craters from 10 to more than 100 km in diameter) during the latest 40 Myr. Pulses of multiple impacts that have fluctuated with time in their populations of object sizes, as well as in their total masses of all impacting objects, may have been characteristic of the cratering record during the Phanerozoic. A companion star hypothesis and(or) other galactic orbital models are consistent with these effects. However, the ages of star-forming events in the Sun's vicinity of the Milky Way galaxy resemble the shorter periodicities of volcanic and biologic processes. Therefore, evidence is reviewed suggesting that an additional effect of astronomical processes on geological periodicities may be provided by the mechanisms and frequencies of star formation in the galaxy.

Introduction

During the early 1970's, E. D. Jackson, K. E. Bargar and I compiled a record of events chronicling the evolution of the Hawaiian-Emperor chain of volcanoes across more than 6000 kilometers of the mid-Pacific. We were excited by evidence of complex cyclic phenomena within which there were also strong elements of order. A synopsis covering the Hawaiian portion was published by Jackson et al. (1975). However, it was not until 1980 that data for the entire chain were published in a volume posthumously honoring Dale Jackson (see Shaw et al., 1980).

Since that study, issues of cyclicity in earth processes have received increasing attention. A recent analysis by Mazaud et al. (1983) identified a 15-Myr periodicity in the frequency of global geomagnetic field reversals during the past 100 Myr. Continental igneous episodes of about twice that period had been proposed by Kistler et al. (1971) and Shaw et al. (1971). I had suspected, without proof, that an approximate 15-Myr period was present in the Hawaiian-Emperor data. Analogous observations concerning the geomagnetic history of the Hawaiian-Emperor chain were made by Moberly and Campbell (1984).

With these and other reported periodicities in mind I have been exploring rheological processes that might reconcile synchronicity among different kinds of geodynamic effects. This involves relationships among plate-tectonic motions, convection in the mantle, melting phenomena related to mantle structure and chemistry, fluid dynamics affecting the geodynamo, other phenomena affecting the geomagnetic field (solar wind, magnetosphere, etc.), and planetary dynamics in general (rotational and orbital effects). These are only a few of the issues raised by correlations of geomagnetic and igneous chronologies. Correlations between igneous events in the evolution of the Earth-Moon system and tidal phenomena during the orbital and rotational evolution of the Earth and Moon were proposed by Shaw (1970), Shaw et al. (1971), Gruntfest and Shaw (1974), Wones and Shaw (1975), and Shaw (1983a). It was demonstrated in these studies that, in principle, major igneous and geodynamic events and their periodicities could be explained by processes of thermomechanical feedback involving interchanges of energy among Earth's internal processes and orbital-rotational processes of the Earth-Moon system (and solar system). It seemed likely that these concepts should also be related to geomagnetic episodes recorded by sea-floor spreading (e.g., Shaw et al., 1971, Figure 5).

These ideas have been converging with periodicity studies by an increasing number of researchers. Where there had been little encouragement a decade ago for correlations of dynamic relationships in Earth's evolution there is now an intense debate concerning geochemical marker-horizons in the biostratigraphic record, frequencies of meteoroid impacts, and periodicities of major biologic extinction events. Speculations concerning global mechanisms of environmental change have acquired great momentum since 1980. Hypotheses of catastrophic asteroid and/or cometary impact have evolved from the status of innovative ideas, in terms of peer acceptance, to a status where major figures in paleontology, geology, geophysics, and astrophysics speak of them with almost factual conviction (e.g., Raup and Sepkoski, 1984; Gould, 1984; Bohor et al., 1984; Rampino and Stothers, 1984; Alvarez and Muller, 1984; Schwartz and James, 1984; Clube and Napier, 1982).

In addition to demonstrations of correspondences between iridium anomalies and the 'K-T boundary claystone' (Alvarez et al., 1980), a remarkable chronostratigraphic event by any criteria (see Bohor et al., 1984), these researches were given great impetus by evidence of correspondences between

periodicities of extinctions and of meteoroid impacts during the past 250 Myr (Raup and Sepkoski, 1984; Alvarez and Muller, 1984). This periodicity varies by a few million years depending on data-set and statistical method, but there is widespread agreement that it is in the neighborhood of 30 Myr (results by various workers range form 26 to 34 Myr).

In retrospect, these developments are not surprising, because many geologists have long been convinced of recurrences in natural processes (this idea is central to concepts of nonlinear dynamics and attractors developed later in this paper). More surprising is the fact that traditions of skepticism among many geologists and paleontologists concerning periodic phenomena in the geologic record, and some of those cited above were in that camp, have swung abruptly or even 'catastrophically' (to some traditionalists) from nonperiodic views of Uniformarianism to periodic views of Catastrophism. But, as pointed out by Gould and Eldredge (1977) and by ancient Chinese sayings, styles of cultural expression (science is assumed to qualify) reflect the dominant themes of their times. For decades the world has been confronted with threats of actual and imminent nuclear explosions and other nuclear disasters. Small wonder that theories about the status of Earth in the Cosmos have become preoccupied with phenomena of cataclysmic nature.

It seems necessary to conclude that we are faced with a revolution in concepts of natural history. This revolution is more profound than is suggested by correlations of volcanic events with paleomagnetic timescales, or correlations of biologic extinction events with meteoroid impact events. It implies a fusion of interdisciplinary researches of the sorts mentioned above. But the most mind-bending implication is the possibility that synchronicity may extend between phenomena as widely separated in space and time as biochemical genetics and intergalactic dynamics. Every type and scale of scientific discipline has been thrown together in ways that violate (or enlighten) long-established traditions of autonomy.

Some aspects of these researches are compared in this paper to concepts of periodic volcanism exemplified by the Hawaiian-Emperor system as described in Shaw et al. (1980) and Moberly and Campbell (1984). In addition to the Hawaiian-Emperor volcanic and geomagnetic record, I include data concerning Mesozoic plutonic periodicities as originally outlined by Evernden and Kistler (1970), Kistler, et al. (1971), and Shaw, et al. (1971). I also reexamine periodicities in the record of Phanerozoic impact-cratering events based on data compiled by Grieve (1982). With reference to the paleontological record, new perspectives are offered by data on originations and extinctions of ostracodes in the world ocean during the latest 70 Myr (Benson, 1975; Benson et al., 1984) and by the record of adaptive radiations among Avian Orders and Families since their expansion beginning in the late Mesozoic (a record of about 140 Myr duration based on the compilation of Fisher, 1967). Geochemical cycles in the world ocean are included in terms of the Phanerozoic record of strontium isotope variations based on data of Burke et al (1982); data on sea level variations during geologic time are being included in work in progress.

Examination of the rates of adaptive radiation in the Avian lineages has revealed two sets of sharply defined events, one in the lower Cretaceous, the other near the K-T boundary. Most of the rate maxima occur near this boundary, but well-defined events occur well before and well after. The range of rate maxima spans about thirty million years; this is generally true for timing of extinction-origination rhythms during the Phanerozoic (Newell, 1982). The two sharpest rate maxima for Avian lineages that span the K/T boundary are represented by the Gruiformes (cranes, rails, etc.) and Charadriiformes (plovers, sandpipers, gulls, and other birds common to the shoreline). Individual rate spikes straddle the K-T boundary and may

represent as little as a few Myr, pending results of taxonomic revisions. (Note: Avian taxonomy is currently under revision using DNA hybridization techniques developed by Sibley and Ahlquist, 1983. This will modify some of the rate curves given in this paper, but it is not likely to change the overall structure of diversity from that compiled by Fisher, 1967).

A focus of attention on ostracodes and birds reflects the availability of data on evolutionary rates. But by coincidence these are biological lineages that should have been sensitive to events in the world oceans and atmosphere. In the case of birds, interaction with major changes in the evolution of global floras and faunas would be expected. Physical connections are also expected with changing ocean dynamics and(or) chemistry, episodic volcanism, mass impact events, electromagnetic effects (e.g., bird migration-navigation phenomena), and so on. It may be significant that the sharpest rate spikes documented here involve Avian lineages that today are characteristic of ocean-margin habitats (i.e., it is likely that physical catastrophes, in contrast with catastrophes caused by biologic epidemics, will have more immediate global effects on such ecological settings than on inland continental and open ocean settings).

Bifurcation patterns of adaptive radiation in Avian lineages has a remarkable resemblance to bifurcational hierarchies in attractor theory (AT), and in nonlinear dynamics in general. Work by Anne Gartner and myself on applications of AT to concepts of evolution of stream drainage networks (Shaw and Gartner, 1983; unpub. data, 1983) is applied to ideas of adaptive radiation, standardization (e.g., Gould, 1983) and canalization (e.g., Niklas, 1982) of biologic diversity patterns. Results show that coupled physical and biological instabilities can arise from either accelerative or decelerative rate phenomena (originations and extinctions both interact with environmental factors that affect the energy sources and tuning of biologic change). The propensity for patterns of evolution to be balanced at the watershed between order and chaos is predicted by computer experiments in AT. These are numerical experiments characterized by cyclic iterations of feedback loops (called recursion cycles, or regenerative feedback cycles).

A central conclusion of this paper is that periodicities of episodic terrestrial processes are consistent with catastrophic extraterrestrial phenomena if they are interpreted as consequences of dynamic feedback among internal terrestrial processes influenced by periodic extraterrestrial processes. That is, principles of nonlinear dynamics predict that internal processes alone would generate complex periodicty patterns, but in order to account for known coupling between Earth and external sources the internal processes must operate in conjunction with the periodic signatures of extraterrestrial processes. This conclusion applies whether or not catastrophism has dominated the rate processes of terrestrial evolution. Synchronizations, approximate or exact, suggest that cyclic phenomena involve coupling of internal physical processes with solar-galactic periodicities as well as with tidal and other periodicities of dissipative and nondissipative orbital mechanics. These correlations constitute forms of long-term harmonic entrainment (resonances). In this rhythm the distribution of impact-cratering events in the geologic record could be viewed as a cosmological 'escapement mechanism' in the workings of a terrestrial clock that is highly nonlinear. The imprint of cosmological rhythms on this nonlinear clock, however, is clear whether or not major impact events have been a significant influence on geologic history.

The ways in which cosmological rhythms can influence terrestrial processes are numerous. Fundamentally, there have been cascades of gravitational and kinetic energy fluctuations throughout geologic history related to the

distributions of mass and electromagnetic radiation in the solar system, interstellar space, and intragalactic space. Spectra of cosmological energy pulsations, including cometary phenomena, star formation, and molecular clouds in the galaxy operate according to the same principles of nonlinear dynamics that determine the timing mechanisms of the terrestrial clock. Some of these processes are reviewed. Cosmological correlations, in terms of similar periodicity arrays, are found for many Earth processes at all time scales examined in this paper.

The Record of Hawaiian-Emperor Volcanism

The chronologic sequence of Hawaiian-Emperor volcanoes (henceforth abbreviated H-E) in Figure 1 is based on data in Shaw et al. (1980); individual volcanoes are identified by numbers in their Table 1. The

Figure 1 near here

chronology is based on a foreshortened length scale that was shown by Jackson et al. (1975) to linearize the time-distance relationship for all segments of the many volcanic loci in the chain. The physical basis for this scale was provided by Jackson and Shaw (1975). Time series plots for relationships among time, distance, and edifice volumes along the composite H-E chain are summarized in Figure 2. This timescale is a conceptually biased one in a

Figure 2 near here

manner analogous to the geomagnetic time scale in that it was devised partly on the basis of physical arguments.

Physically, Figures 1 and 2 invoke the idea that the rates of magma production and directions of propagation of the H-E melting anomaly in the Pacific plate, by whatever mechanism of origination (see Shaw, 1973; Shaw and Jackson, 1973), are recorded by the volcanic alignments and distributions of edifices, and that these properties of the H-E system map the stresses that were active over the indicated time scales in the lithosphere and subjacent mantle. Therefore, volcanic loci record the orientations of effective stress trajectories (Shaw, 1980) on the ocean floor that were dominant during the times of growth of the volcanic chain. Curvatures of loci, represented by tangent azimuths, provide a continuous system of chronological markers in a manner analogous to geomagnetic striping generated by the process of sea-floor spreading. Reconstruction of points of equal curvature were used to generate the distance scale for the migration of the foci of mantle melting relative to the front of propagation, taken at the position of Kilauea. This geochronological construction permitted an evaluation of transient changes in position, size, and shape of the melting anomaly at different stages of evolution and also identified the periodic signatures of the various processes shown in Figure 2 (i.e., we refined the simplistic idea of the Pacific plate moving over a fixed point source, or 'hot spot', of constant eruption rates and propagation speeds).

The correlations in Figures 1 and 2 provide information for four types of kinematic, and implicitly dynamic, parameters of the H-E system: (1) age, (2) propagation direction, (3) propagation length measured from Kilauea, and (4) magma volume. These parameters can be expressed in several ways. Volumes can be subdivided into categories such as edifice volumes, volumes per individual locus of related volcanoes, time-averaged volumes, volumes expressed per unit length of an individual locus or per length of groups of loci, or as cumulative volumes. Each of these can be normalized chronologically to give time-series records of their respective rate changes. In the present discussion we illustrate only the composite relationships for the behavior of the H-E chain as a whole, as condensed in Figure 2 (i.e., we do not consider individual loci or special subgroups of volcanoes). Plots of moving window averages for the variables of Figure 2 are shown in Figures 3 through 5. Cumulative volumes *vs.* time are shown in Figure 6, and magma supply rates

based on slopes of the cumulative record in Figure 6 are shown in Figure 7.

Figures 3, 4, 5, 6, & 7 near here

The data are smoothed in these ways to identify the main periodic signatures of the H-E chain.

Thus, in Figures 3 through 5 and Figure 7 we consider time-series signatures of the following parameters of mid-Pacific volcanism during the latest 74 Myr: (a) average instantaneous azimuths of volcanic loci, (b) total magma volumes, (c) average volumes per unit length of chain, (d) average instantaneous volume rates of edifice growth, (d) average instantaneous propagation rates, and (e) average instantaneous volume rates based on cumulative volumes vs age (these averages were determined by summing all volumes rather than by averaging instantaneous rates as in d). Reference curves are shown in these graphs for other phenomena currently discussed in the literature: the impact cratering record during the latest 100 Myr from Alvarez and Muller (1984); event ages of the three latest biologic extinction peaks from the study by Raup and Sepkoski (1984); curves of geomagnetic reversal data from Moberly and Campbell (1984) and from Mazaud et al. (1983).

A composite of the above time series signatures is given in Figure 8.

Figure 8 near here

Curves have been added in Figure 8 showing the form of the Raup-Sepkoski extinction record and the pattern of ostracode extinctions and originations during the latest 70 Myr (Benson et al., 1984); tick-marks show the Raup-Sepkoski statistical periodicity of 26 Myr compared with the 28.4 Myr statistical periodicity (vertical dashed lines) derived by Alvarez and Muller (1984) from the impact cratering record (curves for their raw and smoothed cratering data are also shown). Curves of geomagnetic reversal frequencies and of the H-E azimuth episodes are placed both above and below other H-E time-series to facilitate comparisons with other signatures. Major global ocean events during this time, from Benson et al. (1984), are shown by arrows with vertical light lines at the bottom of Figure 8.

Correlations Among Phanerozoic Time Series

Phanerozoic patterns of episodic terrestrial processes are summarized in Figure 9. The data include the partial record of extinctions of Raup and

Figure 9 near here

Sepkoski (1984), and the partial record of impact-cratering events of Alvarez and Muller (1984) using data compiled by Grieve (1982). Major intrusive pulses in the Mesozoic record of Sierran plutonic events of Kistler et al. (1971) are combined with the 74-Myr record of H-E volcanism to indicate the form of major magmatic fluctuations during the latest 250 Myr. Additional curves are the long term records of oceanic $^{87}Sr/^{86}Sr$ from Burke et al. (1982), major events of biologic extinctions and originations from Newell (1982), baseline variations in geomagnetic polarity proportions during the Phanerozoic from Tarling (1983), and variations in the galactic density path of the Sun's motion from Innanen et al. (1978).

The periodicity signatures in Figure 9 illustrate a wide range of variations in terrestrial and extraterrestrial processes. The longest oscillations are of the order of the duration of the Phanerozoic. Shorter periods are estimated graphically by plotting the respective peak ages against an apparent cycle number, as shown in Figure 10. Alvarez and Muller (1984) used this kind of plot to discuss the internal consistency of periodicities

Figure 10 near here

determined by statistical methods. The shortest average periods are illustrated by the 70-Myr ostracode record in Figure 10B, which was included to show that some records of seemingly irregular oscillations (see Figure 8) may be reasonably coherent on average.

The 3-Myr slope for the ostracode record in Figure 10B apparently reflects the fact, as pointed out by Benson et al. (1984), that ostracodes are sensitive indicators of systematic environmental changes in the world ocean. That is, it is reasonable to expect that extinction-origination patterns respond to events at many different time scales (see bottom of Figure 8). Slopes representing the extinction data of Raup and Sepkoski (1984), the cratering data of Alvarez and Muller (1984), and the magmatic data of Kistler et al. (1971) and this paper are tightly grouped in the range between 26 and 29 Myr. The oceanic strontium data define a curve with roughly a 42 to 45-Myr slope (perhaps alternating episodes with about 30 and 60 Myr slopes), and the major Phanerozoic extinction-origination events of Newell (1982) vary episodically about a mean slope of about 60 Myr.

There is a suggestion of periodicities roughly in multiples of 3 Myr in Figure 10, as was noted in data for the H-E chain by Jackson et al. (1975) and Shaw et al. (1980). The curvature in the trends of the points in Figure 10 for the H-E events is inferred to represent the effect of mixed periods of from about 3 to 15 Myr, with a greater proportion of higher-frequency pulses in the Emperor portion of the record. However, Figure 7A indicates longer oscillatory variations in the H-E magmatic and geomagnetic signatures, the longest with a cycle-time possibly exceeding 74 Myr.

The grouping of the three data-sets in Figure 10B representing magmatic events (open circles), extinction events (solid dots), and cratering events (crosses) is conspicuous, especially the seeming phase coherence of the first

two sets. However, the five Mesozoic points of the igneous record are a selected set of plutonic events (Kistler et al., 1971), and the three Cenozoic points represent dominant peaks of the H-E volcanic volume record. Thus, the average slope is biased by this mixing, and the older igneous intervals are closer to a 30-Myr slope.

Mixed-frequency effects are expected in complex oscillatory processes. Therefore, they probably exist in other data sets besides the magmatic record. The variety of short-term data in the H-E record makes frequency mixing more conspicuous than in the longer-term records (however, note the episodic variations of slopes in the ocean strontium record from Burke et al., 1982, and in the fossil data from Newell, 1982). The periodicities of galactic plane crossings from Innanen et al. (1978) vary from about 30 to 36 Myr. This is an artifact of the numerical calculations, but the galactic orbital parameters testify to the nonlinear nature of the time series and to effects of more that one frequency.

One of the striking qualitative features of Figure 9 is the mimicry shown by the curve-form of the galactic density sampled by the Sun's intragalactic path and Newell's (1982) evaluation of the major Phanerozoic extinction and origination events. Even the irregularities of amplitude and phase shifts have a resemblance (if the galactic density curve were shifted forward by an amount proportional to the spacings between the extinction-origination peaks, the two curves would roughly coincide). This coincidence is also shown by colinearity of long-term cycle plots in Figure 10B (major biological flourishes of early and late Paleozoic and early and late Mesozoic, and major peaks of galactic density), with slopes ranging from about 130 to 140 Myr (about five times the range 26 to 28 Myr). The variety of periodicity mixing in all records is discussed later (see Table 1 and histograms in Figure 25).

Episodic irregularities in different time series raise important issues of statistical correlation. There is confusion in the literature concerning correlations of periodicities versus correlations of curve-forms (i.e., including information related to amplitude and phase, and effects of frequency mixing). Periodicity correlation can exist in the absence of a correlation of curve-form, and two curve-forms can look similar even if they are constructed from different sets of periodicities. The fact that a curve form can be fitted by summations of sine functions does not mean that these functions represent characteristic physical processes. In some systems of complex but mutually entrained feedback processes, however, statistically significant periodicity mixtures and similarities of asymmetric curve-forms may be preserved to different degrees in different records. This is referred to here as an orchestral signature in which there is a coordinated periodic theme but where different processes (instruments) and groups of processes (instrument sections) display simple to complex subsets of the overall periodicity spectrum of the orchestra.

An orchestral signature is suggested by the general characterisitics of geological time series such as those of Figures 9 and 10. These include the following observations: (1) A dominant periodicity may exist in more than one data set without similarities of overall curve forms (e.g., the igneous, extinction, and cratering signatures of Figure 9). (2) Similar curve forms exist in different records without evidence of identical periodicities (e.g., the Phanerozoic extinction-origination record and the galactic density record in Figure 9). (3) Processes may exist in some records where there are both periodic and nonperiodic components originating from nonlinear resonance phenomena (e.g., the galactic plane-crossing rhythm of Figure 10B discussed later; see Figures 20 and 25, and Table 1). (4) Nonlinear coupling may exist

among many physical processes, and this results in complex frequency mixing in which there may be no exact identities of curve forms or dominant frequencies in different records (e.g., the composite sets of Figures 8 through 10).

Impact Cratering On Earth: Review of Data and Comments on Geologic Effects

Statistics of the Cratering Record.

The curve-forms of data in Figures 2 through 9 include known and unknown physical effects as well as uncertainties in the physical measurements on which they are based. Noise induced by uncertain or erroneous data is conceptually different from noise induced by physical effects of unknown origins. This interpretive factor leads some people to believe only on evidence of statistical correlations, while others distrust statistical conclusions because they can be made without knowledge of coupled and/or interactive physical processes (physical coupling can be either one-way or two-way).

Examples of this dichotomy, and problems of statistical correlation in general, are epitomized by the record of impact cratering. A person who is process-oriented might conclude that the absence of an actual peak in the periodicity analysis of Alvarez and Muller (1984) at about 65 Myr would negate the idea of a correlation of a characteristic impact with the K-T boundary. Another person convinced that there was a major impact at that time and also that the statistical period is real might rationalize the lack of correlation as the effect of a phase shift or minor 'jitter' near that time. Although Alvarez and Muller (1984) do not show a peak at 65 Myr in either the raw data or in their statistical periodicity (the nearest periodicity peak is at about 70 Myr, and the nearest peak in the raw data is between 75 and 80 Myr), there are two factors that mitigate the lack of an exact correlation at the K-T boundary. Alvarez and Muller (1984) included only those craters larger than 10 km from the tabulation of Grieve (1982), and among them they included only the craters for which age uncertainties were known. By comparison, the following review of Grieve's tabulation includes all craters that have been assigned approximate ages. The smoothed time series based on raw data (Figure 11 below) agrees with that of Alvarez and Muller (1984, Figure 1) in most other respects but also has a peak near 65 Myr.

The presence or absence of an event maximum for one or more large craters near the K-T boundary neither corroborates nor denies either the periodic concept of cratering frequencies or the existence of a physical correlation with extinctions and other stratigraphic phenomena at that boundary. Besides the possibility of a minor aberration in a statistical period ('jitter'), there is the possibility of mixed periodicities of the sorts discussed in this paper and the possibility that a 'major impact' could represent a peak event of the extraterrestrial mass flux even though a single large object did not hit the Earth at that time. In view of evidence for nonlinear effects in galactic dynamics (see later discussion of Figure 20), these are likely scenarios whether or not the documented impact record is deficient in coverage and(or) in the accuracy of age determinations.

A difficulty encountered in a hybrid interpretation is that any special periodic mode may be affected differently at different times (there are complex amplitude and phase shifts that represent transient temporal and/or spatial resonances that capture part of the energy into different dynamical modes). For instance, a peculiar forcing effect acting on a special orbit of a reservoir of objects (asteroids or comets) would to some extent influence the system as a whole, particularly the nearby trajectories. This might represent a form of local resonance relative to another system of forcing, but the result would appear to be dissonant relative to a special coherent frequency (both effects would be common to a complex frequency spectrum). This is a different picture than one that treats the record as a pure

frequency with statistical flaws. In the latter case the periodicity can't be counted on (neither extrapolation nor interpolation is valid beyond those peaks actually documented). On the other hand, if the record is the result of nonlinear resonance effects there may be sytematic reasons for the pattern of irregularities even if the pattern is complex and as yet undeciphered. Intervals that do not match a single frequency are not necessarily statistical deviations but might relate to deterministic forcing functions with nonlinear characteristics. With these possibilities in mind, the cratering record is reexamined and expressed as an episodic time series of cratering frequencies (i.e., it is treated as a complex record analogous to the H-E volcanic time series). Possibilities of varying size distributions with time are also examined.

Moving-window averages of all approximately dated impact events of all sizes in Table 2 of Grieve (1982) are portrayed as time series in Figure 11 based on a time scale that varies logarithmically with age. Vertical bars in Figure 11A show the timings of events larger than 10 km in diameter; numbers

---

Figure 11 near here

---

in parentheses show peak values in the smoothed curve of raw data in Alvarez and Muller (1984). The correspondences are close except that amplitudes differ; this produces a peak at 63 Myr where none exists in the Alvarez-Muller time series. The question of large events occurring near the K-T boundary is also discussed by Grieve (1982).

The logarithmic timescale in Figure 11A allows for increasing uncertainty with increasing age, but the effect is exaggerated (resolution is too fine at the youngest age and too coarse at the oldest age). The logarithmic plot also highlights secular variations in the numbers of sampled events with age. If the cratering rate had been constant, and the size distribution invariant, the numbers of events per logarithmic time increment in Figure 11A would increase exponentially with increasing age because of the logarithmic expansion of the age intervals. Although this effect is present, it is small compared to an extrapolation based on the youngest cratering rates. For instance, if the present-day rate for craters equal to or greater than 10 km were one per million years (see discussion below) there would have been about 300 large craters formed during the Paleozoic instead of the 15 shown in Figure 11A; the number would have been several times larger if present-day cratering rates in continental areas estimated by Shoemaker (1983) had existed throughout the Phanerozoic.

Such cumulative differences are large even allowing for areal exposure. At the above rate there could have been many thousands of 10-km or larger craters in late Precambrian rocks, whereas only 4 craters in Grieve's (1982) list have ages greater than 600 Myr and less than 2000 Myr. Shoemaker (1983, p. 485) argued that cratering rates have been roughly steady at the present-day rate during the Phanerozoic (averaged over times of the order 10^8 years), but he noted that the lunar cratering rate over the latest half-billion years was about double the average rate during the last 3.3 Gyr. Evidence reviewed here suggests that there have been fluctuations of both shorter and longer durations for frequencies of Earth-crossing objects (i.e., the signature of impact cratering, like other terrestrial phenomena, probably has several different periodicities). Figure 11B magnifies the logarithmic exaggeration in Figure 11A by using coarser parameters in the moving window averages.

The time-dependence of cratering rates based on the Grieve (1982) sample

taken at face value is illustrated in Figure 12. The average apparent rate

Figure 12 near here

is plotted against the logarithm of age in Figure 12A. Rate values were calculated at intervals of 0.2 log units. Each data point represents the average rate reckoned from the present time back to the age in question (this is given by the total count back to a given age divided by that age). The plot shows a monotonically increasing apparent rate with decreasing age, but there are breaks in slope that may be significant (see Figure 12B). If Figure 12A were linear rather than semilog, the hyperbolic curve would be nearly L-shaped with an apparent instantaneous increase beginning between about 10 and 30 Myr.

The curve in Figure 12A is replotted on doubly logarithmic coordinates in Figure 12B. The mean trend of apparent rates (dashed line) is nearly linear and is fitted by the approximation:

$$\log_{10}K \approx -0.5 \log_{10}A + 0.6 \qquad (1)$$

where K is measured in events per Myr, and A is age in Myr. The apparent rate (i.e., without taking account of size distributions, outcrop area with time, and other physical factors) decreases on average as the square root of increasing age during the latest billion years of Earth's history. The suggestion of episodes in Figure 12A is seen as slope regimes of various age durations (solid lines) in Figure 12B. These are identified as follows: (a) Between about 1 and 4 Myr the apparent rate increase with decreasing age was lower than average; (b) between 4 and about 65 Myr this rate increase was higher than average; (c) between about 65 and 100 Myr the rate was roughly constant; and (d) between about 100 and 600 Myr the rate of increase with decreasing age was close to the average. Within the long interval (d), however, there were probably subintervals analogous to (a) through (c), and within the shorter intervals there were probably yet shorter intervals, and so on (i.e., the fluctuations varied in time in a somewhat self-similar manner).

If the average trend in Figure 12B reflects the changing areas of exposure of rocks of different ages at a constant cratering rate, then exposure area *vs.* age varies according to Eq. (1). The proportions seem qualitatively reasonable, but outcrop area *vs.* age is not documented here. If this pattern were a function only of changing areas of exposure, then the above rate regimes would reflect geological periodicities instead of periodicities in the influx of meteoroids through time. According to Shoemaker (1983, p. 468), however, there is evidence of an increase in lunar cratering rates, hence in the numbers of Earth-crossing objects, during the Phanerozoic relative to the average rate between about 3300 and 600 Myr. Therefore, it is more reasonable to suppose that the apparent rate regimes of Figure 12B reflect a combination of episodic fluctuations in both geological rates and cratering rates.

Equation (1) predicts a sample rate of about 4 events per Myr at an age of 1 Myr (see Figure 12 caption for rates at < 1 Myr). This projected rate is not dominated by any particular age group; it is about the same for all ages, except for the constant interval between about 65 and 100 Myr (it is noted in the next section that there was a lull or pause in rates of Avian radiation during this time interval; see Figures 15 and 16 below). An important question arises, however, concerning the size distribution of craters for any particular total rate as a function of age. Several possibilities exist, such as the following: (1) The size distribution is stationary in time, meaning

that the probability for an event of any given size remains constant with age (compare estimates for objects of different sizes given by Shoemaker, 1983); (2) the size spectrum changes with time, monotonically or periodically; or (3) there is no relation between rate and size, and the mass-energy effects of impacts (including their relationships to biological extinction events) were independent of total event rates; that is, the available reservoirs of Earth-crossing objects were sampled indiscriminately in size even if they were sampled systematically in time (a periodic hit may have been a small object or a big object).

Shoemaker (1983) reviewed the astronomical and geological evidence concerning impact events of different sizes that have been and should have been recorded somewhere in the geologic column. Influenced partly by lunar data for cratering frequencies at ages less than about 3.3 Gyr and partly by astronomical evidence for present-day frequencies of Earth-crossing objects, he estimated that the cratering rate for craters of about 10 km diameter has remained about the same since the Precambrian. This rate is estimated by him to be between 2 and 8 Myr^{-1} impacting the continental areas of the globe. This agrees with an extrapolation of the dashed curve in Figure 12B to the present time, suggesting that whatever causes the apparent dependence of cratering rates of all sizes on age in that plot, the projected rate is consistent with the data of Shoemaker (1983) based on actual counts of Earth-crossing objects (i.e., Grieve's list faithfully records the time-dependence of all processes affecting the geologic record of mass impacts on Earth).

The size distribution in the tabulation of impact craters by Grieve (1982) is examined in Figure 13. A buckshot-like pattern of sizes versus age is shown in Figure 13A, and an inset shows the histogram of total counts per equal logarithmic increments of crater diameters. Figure 13B shows the logarithm of the number of craters in each size increment versus the logarithm of diameter. The sharp maximum at a diameter of about 10 km suggests two alternatives: (1) crater counts at smaller sizes are progressively underestimated, as would be expected for objects too small to survive passage through the atmosphere, as well as on general grounds (this is the case in the statistics of fault-length distributions studied by Shaw et al., 1981, where the fall-off is a function of map scale), or (2) 10-km craters represent a frequency maximum in the size spectrum of impacting objects relative to different power-law distributions of rates vs sizes on either side of this maximum. The first interpretation probably dominates, but the falloff may be more systematic than would be accounted for by these factors alone. Shoemaker (1983) discusses criteria of crater recognition and points out that many craters not yet documented probably exist in recognizeable states if searched for in the appropriate stratigraphic settings (e.g., the midcontinent of North America where there are large areas of relatively undisturbed strata of different ages).

If it were assumed that the right-hand (large-diameter) limb of the distribution in Figure 13B is representative, the relation of the number of craters, N, to diameter, D (km), would be expressed as follows:

$$\log_{10} N = -1.1 \log_{10} D + 2.5 \qquad (2)$$

where the large number of craters of small sizes that would be predicted by an extrapolation below D = 10 km do not exist because: (a) they have been obliterated by erosion and other geological processes, (b) they exist but are difficult to recognize, (c) they never formed because small meteoroid objects do not reach the Earth's surface, or (d) they never formed because the

cumulative numbers of small objects are less than would be predicted by the size vs. frequency relationship for objects larger than 10 km in diameter. If (d) were true, it would be accentuated by factors (a) through (c) because recognition of the larger craters is increasingly favored with increasing age. These effects make it difficult to evaluate the rates for small objects even during the last few million years. An evaluation by Shoemaker (1983, p. 478) suggests that (c) applies to many objects less than about 0.1 km in diameter unless they are dense and coherent (e.g., craters related to iron meteorites), so craters of order 1 km in diameter and less occur with low frequencies compared to the frequencies with which possible crater-forming objects enter the Earth's atmosphere. Thus, Figure 13B reflects a combination of factors, but their proportionate influences remain to be evaluated for crater diameters between about 1 and 10 km.

The truncation of the larger diameters in Figure 13A at ages less than 40 Myr suggests a systematic increase of maximum crater diameters with increasing age up to a limiting size of the order of 100 km in diameter at ages greater than 40 Myr (this relation is enhanced by the fact that these data points are among the values with smallest age uncertainties). Below the size limit given by log D ≈ 2, the regime of apparently increasing size vs age is described by the approximation:

$$\log_{10} D_{max} \approx 0.6 \log_{10} A + 1 \qquad (3)$$

for D in km and age in Myr.

Combining Eqs. (1) and (3) gives an expression for an apparent cratering rate vs. maximum diameter, as follows:

$$\log_{10} K_{max} \approx - 0.83 \log_{10} D_{max} + 1.45 \qquad (4)$$

where K_{max} is the number of events per Myr for craters that are limited by the apparent relationship between maximum diameter, D_{max}, and age, A. For $D_{max} \approx 10$ km, $K_{max} \approx 4$ Myr^{-1}, in agreement with Shoemaker's (1983) estimate of the secular average for 10-km events. Substituting this diameter into Eq. (3) indicates that this rate is satisfied at an age of about 1 Myr. It says nothing about rates at this diameter prior to 1 Myr, but it implies a lower than average rate since that time (i.e., taking Figure 13A and Eq. 3 at face value, there are no 10-km craters in the latest 1 Myr where there should have been about 4). This 'fictive' relation predicts about 30 events per Myr representing 1-km craters and 200 events per Myr representing 100-m craters; the respective ages of apparent falloff in rates for these respective sizes would be near 20,000 yrs and 400 yrs.

The above reasoning suggests the possibility that the cratering rates of the larger objects have been decreasing in the latest 40 Myr relative to cratering rates produced by smaller objects. Shoemaker (1983, p. 482) estimates that about 50 1-km craters have formed on the continents during the last 1 Myr and that about 1000 0.1-km craters have formed during the last 20,000 years (50,000 Myr^{-1}!) based on the statistics of the iron and stony-iron meteorites (these objects represent about 5 percent of present-day Earth-crossing objects). The apparent rate maxima for 1-km and 0.1-km craters calculated from Eq. (4) are much lower than his estimates. By the same apparent relation, however, the 100-km maximum crater would have had an instantaneous rate of about one per 2 Myr at an age of about 40 Myr; this is about ten times the average rate estimated by Shoemaker (1983, p. 486) for craters equal to or larger than 100 km during the Phanerozoic. By either reckoning there should have been more than 2 craters equal to or exceeding 100

km during the latest 40 Myr, whereas Figure 13B shows none.

The fact that Eq. (4) implies a progressive decrease in cratering rates of the larger relative to the smaller objects during the latest 40 Myr, combined with the fact that it predicts lower rates than those determined by Shoemaker (1983) for craters smaller than 10 km in diameter while it predicts higher rates than his for craters of larger diameters, suggests a shift in the size population of craters toward smaller diameters during the last 40 Myr. The overall frequency maximum near 10 km in Figure 13B reflects a compromise between truncation effects at both large and small diameters. Truncation at large diameters reflects the limitations on maximum object sizes vs. age, and truncation at small diameters reflects the increasing importance with age of all factors that mediate against the formation and survival of small craters. It seems likely that the balances of both these factors have fluctuated over time scales of the orders of 1 Myr to 1000 Myr (see Figure 12B) as results of combined geologic and cosmological influences on cratering frequencies but that the present time favors a shift in the population of Earth-crossing objects toward the smaller diameters.

Such peculiarities of the cratering data pose interesting unanswered questions concerning size-frequencies versus time for both terrestrial and extraterrestrial processes. If the distributions discussed above occurred intermittently rather than continuously over time, then there could have been very high pulse-rates for cratering events of all sizes during smaller time intervals. In the limit of high pulse-rates the mass influx of all material entering the atmosphere and ionosphere could have been much greater than the mass represented by large objects. At the small end of the size spectrum something like the blazing sky paradox of cosmology is encountered, because at some level of resolution a nearly continuous layer of meteor-derived material should have become involved with normal weathering and sedimentation cycles. That is, residence times of most chemical elements in the oceans and atmosphere are short compared to the timescales discussed above, so there should be very sharp and characteristic chemical horizons wherever peak flux rates were recorded stratigraphically. Iridium anomalies may qualify as such continuous meteor-derived chemical horizons, so by the above arguments they might represent the result of geologic processes acting on the small particle flux over some characteristic chemical residence time rather than representing instantaneous deposition of material derived from individual impacts of the largest objects.

In view of such composite factors, a complex but systematic frequency signature is likely for extraterrestrial phenomena that have been recorded via the agencies of geologic processes. Extraterrestrial factors include: (a) the size spectra vs. age of the reservoirs of asteroid and cometary objects (i.e., factors genetically related to the evolution of the solar system), and (b) the galactic mass distributions vs. time that affected the evolution of the solar system hence the dynamics of those reservoirs. The galactic role is at least two-fold: it controls the long-term structures of the distributions of objects, and it controls those instantaneous factors that gravitationally perturb the orbital parameters of those objects (see Hills, 1981). The graph of galactic density sketched in Figure 9 shows an episodic pattern in which the densities have been generally increasing during the past 500 Myr, with a maximum during the latest 40 Myr.

Geologic Processes and the Extraterrestrial Mass Flux.

At least two types of physical effects are of interest to correlations between global volcanism and global effects of extraterrestrial processes: (1) factors that might influence volcanic propagation directions and rates,

and (2) factors that might influence rates of magma generation and transport. In a general model of magmatic evolution these volcanic phenomena are part of a global system of regenerative feedback lacking any specific cause (Shaw et al., 1971). It might seem that periodic signatures would not be expected in such feedback systems. On the contrary, however, there are dynamical reasons to predict that such systems are capable of producing episodicities and(or) specific mixtures of simple periodicities of many kinds. Therefore, volcanic phenomena (including their paleomagnetic signatures) are relevant to composite geologic periodicities mentioned above as well as to relationships between geological and cosmological phenomena where physical effects are known to exist (tidal phenomena originating in various forms of gravitational and electromagnetic coupling).

Several episodic phenomena were summarized over the latest 70 Myr or so in Figure 8. Excluding biologic processes, they represented phenomena of five types: (a) the geomagnetic record, (b) rates of volcanic propagation across the Pacific Plate, (c) intraplate magma production rates, (d) changing azimuths of plate stresses and(or) plate rotations, and (e) impact cratering. Arrows along the bottom of Figure 8 identify significant physical events in the geologic record of oceanic phenomena from Benson (1975) and Benson et al. (1984), as follows: (1) the Pliocene event at ~ 3 Myr, (2) the terminal Miocene event at ~ 6 Myr, (3) the mid-Miocene event at ~ 15 Myr, (4) the terminal Oligocene event at ~ 25 Myr, (5) the "40-Myr" event, (6) the "52-Myr" event, and (7) the K-T event at ~ 65 Myr. The timing of these events is approximate (see age-ranges described by Benson et al., 1984), but their precision is good relative to uncertainties in the cratering record. Relative to that record, events (3), (4), (5) and (7) match peaks of crater counts in Figure 11A; event (1) occurs at the slope change in Figure 12B. The oceanic events also generally occur at times near significant maxima, minima or reversals in the magmatic-geomagnetic phenomena of Figure 8. Some qualitative mechanism by which these four types of phenomena (magma dynamics, magnetodynamics, ocean dynamics, impact dynamics) might be coupled are sketched below.

Azimuths of tangents to H-E volcanic loci map the trace of the maximum principal stress in the Pacific plate. Jackson and Shaw (1975) and Jackson et al. (1975) argued that swings in tangent azimuths are correlated with boundary tractions on lithospheric plates but that no great force imbalance is required to change stress orientations. The effect is like the jiggling motion of a piston sliding along roughened cylinder walls. Slight hangups at plate margins cause transient hesitations and oscillations of stresses within the moving plate as a whole. The net direction and general speed of motion (kinematic rotations), however, may or may not be affected. Thus, volcanic loci record subtle imbalances in the dynamics of the Pacific plate that must also correlate with changing global conditions of many kinds, including vertical tectonic motions and ocean circulations. The global jostling of plates in turn correlates with forcing functions of global convective motions in the deeper mantle. They are also coupled in some way with interactions between the ocean and atmosphere recorded by short-term transfers of momentum from the atmosphere to the mantle (e.g., Carter et al., 1984).

In short, the forcing function for plate motions is periodic over many different timescales. It is influenced by the net balances of differential rotations of a mosaically faulted and stratified Earth. Any extraterrestrial process that contributes to one or more effects can modify the net balance. Such a process contributes directly to the episodicity of volcanic azimuth variations. Tidal and orbital-rotational forcing effects are important, and other effects come from electromagnetic coupling between Earth and the

interplanetary plasma flux via the ionosphere and from the direct inputs of kinetic energy of mass impacts. Large-scale cratering events also trigger a variety of atmospheric, oceanographic, and tectonic mechanisms that could shift the global balances near conditions of unstable equilibrium (i.e., where the vector sum of two opposing large forces can be changed in direction or sign by the action of a much smaller force).

The record of volcanic volumes along the Hawaiian-Emperor chain reflect the power of magma production in the mantle and the duration of eruption at a given locality. Such effects are sensitive to nonlinear instabilities associated with mechanisms of shear melting (Shaw, 1970; Shaw, 1973; Gruntfest and Shaw, 1974; Shaw et al., 1971; Shaw et al., 1980). The timing of such instabilities is marked by nonlinear episodes (which may be intermittent or periodic) of variables such as volcanic volume rates and propagation rates. These rate episodes are directly coupled with transient surging effects of plate and mantle motions which, however, may not be conspicuous in kinematic records of average plate motions. In special circumstances these 'thermal runaways' (Anderson and Perkins, 1975) can occur in the absence of transient plate motions and are analogous to local eddies in the steady-state regime of a glacier (i.e., between accelerative episodes, or 'surges'). Some of these kinematic effects are described by Shaw and Jackson (1973).

Generally speaking, the patterns and synchronizations of magmatic volume and propagation rates are coordinated with the mass balances of sea-floor spreading. Episodicities in the latter are automatically imprinted in the timing of the patterns of magnetic striping, hence in the geomagnetic time scale and in the correlations between oscillations of volcanic rate parameters and geomagnetic reversal frequencies. If there are periodicities in the global magmatic record they must also be contained in the geomagnetic record. This inference is supported by correlations in Figures 3, 7, and 8 and by the cycle plots in Figure 10A.

The involvement of impact-cratering events in the interactions of magmatic and geomagnetic rate phenomena may be direct in some instances, but in others it may be manifested by circumstantial chains of events starting, for example, with the triggering of a continental magmatic event. That is, the global magmatic engine, in conjunction with tectonic processes, represents a net balance of all magmatic events, hence any rate transient is compensated by changes throughout the system. If such events occurred throughout Earth's history, periodicities in magmatic-geomagnetic episodes would have become entrained (resonated with) the periodicities of cratering events. The 'pacemaker' effects of cratering events (more accurately all inputs from extraterrestrial sources) on global magmatic processes are therefore dependent on the secular variations of the impact record. This does not exclude direct cause-effect connections with individual geological events. The general result includes local cause-effect signatures combined with global resonances over long times. If oscillations of the impact record are irregular or contain multiple periodicities, as is argued in the present paper, then this synchronization will be manifested by a frequency spectrum in which the frequencies of the cratering record represent a subset of a richer frequency spectrum of magmatic processes.

The coordinated effects of extraterrestrial, magmatic, and geomagnetic events are reinforced by coupling with other geological processes. The class of processes that includes sea-level variations, glaciations, ocean temperature fluctuations, and ocean-atmosphere circulations represents a key intermediary between geological processes in general and the rhythm of biological evolution on Earth. Therefore, it is anticipated that there has been an analogous long-term periodicity entrainment of biological processes

with the periodicities of geologic and impact-related processes in addition to the instantaneous effects of catastrophic impact events. It is easy to see in the biological case that the instantaneous effects feed back into the long-term effects, hence the periodicities of the secular biological record represent the folding together of the several types of phenomena. The principle is the same as the relationship between individual impact-triggered magmatic events and the global signature of impact-related magmatic phenomena over geologic time.

Besides these general classes of coupled phenomena there are biologically important subclasses. For instance, weather cycles and atmospheric circulation are involved directly in the patterns of evolution of nonmarine flora and fauna. Also, fluctuations in the Earth's magnetic field related to extraterrestrial phenomena as well as to coupled magmatic-geomagnetic effects and the core dynamo must have contributed to the complex mutual relationships involved in patterns of flower-insect-bird evolution via influences on navigational mechanisms, migratory patterns, and so on. The timing of episodic variations in rates of Avian evolution is examined in the next section.

The above varieties of coupled processes also imply involvement of periodic oscillations in the operation of the core dynamo. Therefore, long-term variations of Earth's rotational modes are coupled with the circumstantial chains of events documented by Plate Tectonics, geomagnetic time scales, and magmatic cycles. The coupling of core motions with the geomagnetic field is modified by other geodynamic processes, and perhaps the question is moot whether core motions drive other geomagnetic effects or are considered to be driven by other geomagnetic processes via secular mechanisms (e.g., the long-term relationship between tidal phenomena and magnetospheric phenomena that may influence the length-of-day; cf., Carter et al., 1984). In this sense, it is reasonable to expect entrainment of the timing of core motions and impact cratering frequencies via relationships with global magma-tectonic phenomena. At this level of comparison such resonances are orchestrated by cosmological rhythms that influence the nonlinear dynamic periodicities of galactic processes. These processes are reviewed following a discussion of dynamical factors that may influence rates of biological change.

Rate-Controlled Bifurcations in Biologic Radiation

Avian Adaptive Radiation and the K-T Transformation.

The term transformation is meant to refer to a paradigmatic shift in the patterns and rates of evolution. It does not necessarily imply physical events of catastrophic nature, but some form of dynamic impetus is implied that changes the patterns of global biologic diversity. The rates of adaptive radiation of Avian lineages at the levels of orders and families as documented by Fisher (1967) are used to illustrate such a transformation. Genetic tuning that is influenced by environmental changes, which are in turn governed by terrestrial and(or) extraterrestrial rate processes, varies episodically with time according to the degree of synchronization with other geological periodicities. Cyclic synchronicity and resonances are meant to imply the same sorts of entrainment and orchestral effects in biologic evolution that are found in correlations of terrestrial and extraterrestrial physical phenomena discussed in the previous section.

Figure 14 reproduces Fisher's (1967) portrayal of adaptive radiation in the evolution of Avian lineages. Birds represent particularly interesting

---

Figure 14 near here

---

biologic forms because they demonstrate both local and global dynamic effects. It has been pointed out that the statistics are biased in favor of waterbirds because they are the most likely to be preserved in the fossil record. On the other hand, this fact automatically selects those lineages which are most likely to reflect important changes in the global environment. Lineages such as the Pelecaniformes (pelicans, cormorants and frigate birds) are highly pelagic, whereas some lineages of Passeriformes are geographically restricted ("perching birds," dwellers of diverse ecological settings involving woodlands, marshes, watercourses in semiarid climates, and so on; they include songbirds, thrushes, wrens, starlings, swallows, crows, etc.). Thus, environmental effects involving air-water, air-land, and land-water interactions are all involved in the rates of Avian evolution.

Figure 15 shows the logarithm of the number of taxa counted within familial sets of generally related lineages versus age, using the time scale of Fisher (1967) for internal consistency (comparison with the revised time scale of Harland et al., 1982, is shown in Figure 16 below). The 'explosive'

Figure 15 near here

---

nature of the overall rates of radiation is evident. Such an acceleration of evolution is cited by numerous authors as evidence of the filling of a genetic vacuum left by a major extinction. It is argued, however, that such patterns are characteristic of changes in biologic diversity and that an internally consistent bifurcation process operated before, during, and after times when major impact events were most likely (e.g., the 40-Myr and 65-Myr oceanic events of Figure 9, and the 40-Myr, 65-Myr, 100-Myr, 130-Myr, and 160-Myr cratering episodes of Figure 11A)). It is also evident that the same form of acceleration applies at every taxonomic level from that of Avian radiation in general down to the patterns of each familial set (and implicitly at the levels of genera and species). The timing of accelerations in individual sets spans ages from about 140 Myr to 40 Myr (about 150 to 40 Myr on the revised timescale). If the general pattern represents a response to catastrophic

extinction events of impact origin or otherwise, multiple events were involved. There are strong suggestions in the patterns of acceleration that the energy (tuning) of changes in Avian diversity was renewed several times during the time interval 150 to 40 Myr.

The rate curves of Figure 15 resemble rocket trajectories. Avian adaptive radiation in general (all orders) experienced an initial episode of acceleration about 140 (150) Myr ago and a second episode 'fired' in multiple bursts between about 80 and 60 Myr ago. Overall the assemblage of orders was established in a stable configuration by about 40 (38) Myr ago where it has remained until the present time (with suggestions of negative accelerations among some lineages). This satellite-like scenario is emphasized by near coincidences of the above stages with peaks in the impact-cratering record of Figure 11A (cf., Figure 16).

The subsidiary accelerations within familial sets that span ages from about 80 (83) Myr to 60 (55) Myr ago represent a time interval when there was a distributed pattern of cratering events (Figure 11A). The lifestyles of the Pelecaniformes is mimicked by a drifting trajectory of radiation beginning about the same time as the dominant expansion but accelerating somewhat at about 120 (128) Myr ago. This acceleration event peaked at about 60 (55) Myr, and subsequently degenerated to its present diversity at about 10 (5) Myr ago.

Reversals of diversity trends suggested by the Pelecaniformes and the ostrich-like forms are also seen over different time intervals in other lineages. Perhaps Avian evolution, as recorded by fossil groups, is on the decline at the level of families unless another impetus comes along to renew the trajectories of acceleration, as happened during the late Cretaceous. Alternatively, the pattern may continue in the direction of decreasing diversity and extinction. That is, the patterns of diversity of the fossil forms suggests that some degree of renewed impetus is required even to maintain the status quo. However, such an event might have occurred during the last few million years, in that the fossil record does not adequately represent the diversiy patterns of modern forms. Figure 11A and the previous discussion of cratering frequencies suggest that the last 3 Myr may be an important interval of time to search for effects of rejuvenation in more detailed records of diversity at the levels of genera and species (if it happened, it involved 'showers' of small events rather than single large impact events).

These observations raise questions concerning why the cratering events of the Cenozoic after about 60 Myr, and especially near ages of 40 myr and 15 Myr, didn't cause major renewals in Avian radiation; after all, the largest Phanerozoic crater in Grieve's (1982) list has an age of about 40 Myr (Popigai, Siberia; diameter 100 km, age 39$\pm$ 9 Myr). Evidently a pulse of adaptive response requires a critical impetus relative to existing rates of evolution. By analogy with rocket trajectories, the response depends on the net energy, 'burn rate', etc., required to change a preexisting trajectory to a new one. Except for the 40-Myr event, this interpretation is consistent with the idea of decreasing maximum events with increasing frequencies of occurrence in the cratering record over the latest 40 Myr (Figure 13A).

The 100-km cratering event at 39 $\pm$ 9 Myr appears to contradict the impulse model. However, Figure 15 does show changes near 40 Myr in lineages such as the Procellariiformes (albatrosses, storm petrels, etc.), Coraciiformes (kingfishers, etc.), Piciformes (woodpeckers, etc.) and Passeriformes (songbirds, etc.). At about this time reversals(negative responses) occurred in the Falconiformes (birds-of-prey), Pelecaniformes (pelicans, etc.) and Gruiformes (cranes, etc.).

Another way to characterize accelerative pulses is to plot the slopes of curves in Figure 15, as shown in Figure 16. The ordinate is the change in

Figure 16 near here

log(# of taxa) with change in age, thus having the dimensions of a temporal frequency (expressed in Myr^{-1}). Tick marks are shown for the peaks of impact cratering in Figure 11A. Because the impulse-energy events may have either positive or negative effects (e.g., the 40-Myr events just described in Figure 15) one might look for correlations of cratering events with either maxima (transitions from accelerative to decelerative episodes) or minima (transitions from decelerative to accelerative episodes). In detail, episodic cratering rates should be compared with the second derivative, or rates of change in rates, but the records are not adequate for that purpose. The correspondences between the beginnings and endings of the composite record of acceleration-deceleration trends in Figure 16 (dashed curve at top) with impact events are reasonably close.

It is conceivable that an impulse-energy scale could be established for rates of evolution. This would involve magnitudes of both positive and negative responses in that a given type of event, whether related to impacts or to major terrestrial influences such as volcanism, can theoretically contribute either to rates of originations or extinctions. Different lineages and ranks within lineages would require different scaling coefficients as to both magnitude and sign. But such a scheme, calibrated by detailed patterns of diversity in the fossil record, might provide a refined chronology of events for comparison with time series data of geological-extraterrestrial processes. Sensitive lineages (e.g., deep ocean ostracodes, higher mammals) might be used to calibrate the energy scaling during the latest 15 Myr. This would be of particular interest in view of the 15-Myr correlations among impact-cratering, geomagnetic, and magmatic episodes. If such an approach proved valid, the scaling law would be a composite one that accounts for cascade-like compounding of extraterrestrial-terrestrial event sequences.

In a similar vein, it would be valuable to examine relative changes in contemporaneous faunal lineages (for instance, lineages that may have been more sensitive to energetic events than the relatively stabilized Avian lineages during the latest 40 Myr). Such a study probably would have to be done at the levels of genera and species. Of particular interest would be comparative rates of evolution in Avian, Cetacean, and Primate lineages (particularly with regard to rates of change in cranial capacity in the latter two groups, and perhaps a comparison of navigational capabilities between cetaceans and birds). As a conjecture, rate episodes in Cetacean evolution might correlate with the 52-Myr, 40-Myr, terminal Oligocene (~ 25-Myr) and mid-Miocene (15-Myr) events (Figure 8), and rate episodes of Primate evolution might correlate with events at and post-dating the 15-Myr event, particularly events near 3 Myr and less (cf., Figures 10 and 11A, and Table 1).

Numerical Dynamics of Rate-Controlled Bifurcations.

The graphical behavior of an algorithm designed to illustrate numerical dynamics of birth-death feedback cycles is illustrated in Figure 17 (this is a system with one type of genetic quantity and one governing rate parameter; the latter is called the tuning parameter). The genetic quantity represents a

Figure 17 near here

population that varies in numbers depending on a time-dependent net rate function made up of factors affecting reproduction and death rates. The population may be individuals or taxa for which birthrates (origination events) and deathrates (extinction events) define rates of speciation and bifurcations within genera, families, etc. The population of taxa that is analogous to numbers of individuals in such instances is the diversity.

Application of the same type of equation to taxonomic populations is justified as a conceptual guide on the grounds that it models the types of patterns that may be associated with increased vs. decreased diversity. It is also justified on the grounds that at all taxonomic levels we are dealing with fundamental feedback processes of types analogous to those that describe the nonlinear dynamics of physical systems. These are the relationships among diverse genetic entities (cells, bacteria, viruses, genes, DNA-RNA cycles, etc.). Exploration of hierarchical self-similarity in such feedback systems is a primary reason for experiments in numerical dynamics.

This approach to evolutionary models resembles the ideas of the previous section concerning impulse energy events. The positive-negative balances of such events represent the competitive birth-death rates symbolized by the tuning parameters of Figure 17. Changes in such rate balances arise because in some domains consecutive iterations of birth-steps and death-steps carry the genetic quantity progressively farther away from a given stability condition toward one or more new ones or toward conditions of irregularly oscillating states. In the former case this may involve oscillations among several stable sets of populations that take the place of the previous stable population, and in the latter case it may involve chaotic oscillations or unstable genetic trends. Such trajectories of convergent (attracting) and divergent (repelling) behavior, relative to a given genetic locus, give rise to the name "attractors" for the stable bifurcation structures. In this respect the behavior also resembles limit-cycles of nonlinear oscillations in mechanically, thermally, or thermomechanically forced systems. Hence, it applies conceptually to any system of nonlinearly interacting effects, including the long-term behavior of astrophysical systems (e.g., Helleman, 1983; Shaw, 1983a,b). These include processes of star formation and destruction, and galactic density structures. Such conceptual parallels are the basis for what I have called entrainment and orchestral effects in the correlations of terrestrial and extraterrestrial processes. I return to this idea later in an analysis of mixed periodicities.

Figures 17A and 17B differ only in the fact that Figure 17A is scaled in proportion to the genetic quantity, X, and rate parameter, λ, while Figure 17B is scaled to the logarithms of these quantities and is restricted to the period-doubling regime. Self-similarity shown by Figure 17B occurs because the tuning parameter is plotted as the difference between the critical value λ_c (transition to chaos) and smaller values of λ. The difference function - log (λ_c - λ) expands indefinitely in almost invariant and period-doubling sets of logarithmically proportionate intervals of X (log ΔX). Thus, the numbers of X-values increase theoretically without limit according to the progression 2^n, and each of the bundles that splits off approximately duplicates the bifurcation history of the previous bundle. In this respect there is a parallel with the taxonomic bifurcation style of Figure 14. If the lower main stem represented a class of organisms, then one of the bundles is analogous to an order and its bifurcations symbolize families and lower taxa. Although the analogy is suggestive it is incomplete (i.e., Figure 17 would represent a very simple genetic lineage that responded to only one kind of genetic tuning).

Scale-invariances among attractor bifurcation sets is called universality,

a property common to many attractor structures (see Feigenbaum, 1980; Helleman, 1983). In Figure 17 the entire pattern is characterized by only three numbers: a critical tuning parameter, a logarithmic proportionality constant that determines the bifurcation numbers relative to a change in tuning parameter, and a packing coefficient that describes the relative spacing of X-values in each bundle. Although it is beyond the scope of this discussion, the same universal structures apply to subsets of stable bifurcations within certain windows of parameter values in the chaotic regime (see Ott, 1981; Shaw, 1981; Sparrow, 1982; Helleman, 1983). This property of attractor dynamics has a metaphorical resemblance to the nature of the balances between order and chaos in evolutionary structures. It is in this vein that a comparison is made between biologic and attractor bifurcation sets (i.e., in every case we are dealing with relatively simplified subsets or windows of order in a more general pattern that is analogous to the chaotic regime of attractor dynamics).

The resemblance between Figure 17B and the patterns of Avian radiation in Figure 14 is explored farther in Figure 18 relative to the time-dependence of

---

Figure 18 near here

---

the rate parameter, λ. If λ increases linearly with time, then the sets of bifurcating structures grow exponentially over narrower and narrower time intervals. Equal durations for consecutive bifurcational episodes therefore imply that the rate parameter increases with time at a decreasing rate, corresponding to the logarithmic function of Figure 17B. Accordingly, any energy function that drives or triggers such a time-dependent increase in the rate parameter, λ, must be proportioned to the function $-\log(\Delta\lambda)$.

In order to drive an evolving system to ever higher and higher levels of diversity, other things being equal, large increases in energy input rates might be expected. An example might be logarithmically increasing impact energies of extraterrestrial objects if they represented the total energy potential for biologic change of the type shown by the Avian record. However, other terrestrial processes such as magma-tectonic, oceanic, and atmospheric cycles modify the energy scaling by interaction with processes that are the aftermaths of impacts. The energies of such processes also vary over orders of magnitude (e.g., volume rates of H-E volcanism span at least three decades in power over short geologic timespans). Therefore it is likely that dynamical tuning as reflected in biologic diversity represents some sort of difference function among all of these processes. That is, the critical point of the period-doubling regime in Figures 17 and 18 would correspond to a critical balance of physical to biogenic energy-consuming processes. If too much energy is fed into the biosphere it reacts with chaotic patterns of diversity, implying a potential for selective and/or wholesale extinctions. Therefore, an important aspect of the response of the biosphere to external inputs such as mass impacts is how the Earth responds in terms of energy partitioning among all available physical processes as well as biologic processes.

The cumulative energy of prior evolutionary processes, physical and biological, sets the stage for a given episode of adaptive radiations. This background provides the framework within which a given state of complexity must be viewed. In one sense, each such state (e.g., at a given time in Figure 18) represents a bifurcational window within a matrix of both relatively stable structures and chaotic structures. Such a viewpoint is necessary to reconcile the relative scales of order and disorder in any given

biologic structure at all levels of genetic development from the individual organism to the evolution of higher taxa through geologic time (the same reasoning applies to concepts that have been offered by various researchers concerning possibilities of extraterrestrial biogenic processes).

Coupled effects in the control of rate parameters give rise to more degrees of freedom than are considered in Figures 17 and 18. The numerical properties of bifurcational instabilities are conceptually similar, but the varieties of time-dependent paths and structural domains are enriched. The additional degrees of freedom give rise to oscillations in time and space which describe structural domains of complex periodicities with regard to both phase and amplitude. Such patterns may appear to be stochastic and(or) intermittently periodic even when they are generated by the same deterministic set of equations.

Structures of this type are sometimes called 'strange attractors' because they combine elements that are periodic with other elements that are nonperiodic to produce complex patterns that are geometrically self-similar and reproducible (instead of a closed geometric curve with a distinct period, trajectories in phase portraits of state parameters are fuzzy sets that retain structural similarity under magnification). The mixed periodic-chaotic orbital history of the solar system in the galaxy, as shown in Figure 20 below, is probably a strange attractor (a phase portrait would be constructed by plotting together the rotation angle relative to the galactic center and the z-motion normal to the galactic plane as a description of the trajectory of motion of the Sun in the Milky Way galaxy; such a plot would look something like an endless basket weave rather than a system of closed orbits).

A bifurcation diagram generated by two rate parameters, but portrayed in the same manner as the one-dimensional system of Figure 17, is shown in Figure 19. In this case values of the net rate parameter are represented by a

---

Figure 19 near here

---

hypersurface. This algorithm was designed to explore structures produced by superpositions of rate relations resembling those in Figures 17 and 18.

Figure 19 illustrates the fact that bifurcational diversity can be reduced as well as increased by a monotonic increase in the net tuning parameter. Simplicity and complexity in patterns of lineage diversity do not necessarily go, respectively, with low and high dynamic rates, although this can be true for any lineage described by a one-dimensional model such as Figure 18. This is not meant to imply that a given set of genetic strains is reversibly contracted and expanded in diversity relative to a convergent bifurcational interval such as that in Figure 19. In those regions the degrees of freedom are reduced because the trajectories of potential diversity are fed into (slaved to) a smaller set of stable structures. The resulting diversity pattern is standardized relative to what it might have been. However, the genetic content of the contracting lineages on the left is different from, though related to, the content of the expanding lineages on the right.

In the algorithm of Figure 19 a sufficiently high summation of rate parameters leads to wholesale extinction of the genetic class in the sense that numerical trajectories totally escape from the defined hyperspace to undefined trajectories outside the parameter space of the attractor (such trajectories are sometimes called repellors). Such events, labeled ESCAPE in Figure 19 symbolize a transformation or shift in paradigm in which new genetic entities, of whatever form, are not directly traceable to these prior structural states. That is, there is a discontinuity or jump from one type of

attractor structure to a new one, analogous to a major mutational event in genetics. Time-dependent oscillations in the various classes of behavior are shown in Figure 19B.

Numerical dynamics predicts that correlations between terrestrial and extraterrestrial processes that result in what is called here an event of impulse energy, whether dominated by one or the other source, may be associated with either an increase or decrease in biologic diversity. Therefore, events in the paleontologic record have to be tested for correspondences between both positive and negative magnitudes and rates of change in the combined system of biological-geological states.

Whether extinctions occur as a result of excessively low or excessively high driving rates of genetic evolution, an energy threshold is implied. Low-power extinctions are probably more localized and subtle than high-power extinctions, although removal of the energy supply from a high trophic state can result in a dramatic crash. But such distinctions can only be made in a broad multilineage context relative to the total trophic energy supply rate. On the other hand, transformational extinctions of the sort symbolized by the righthand limit of Figure 19 might occur as cascades of increasing impulse energy. However, their effectiveness also depends on the context of differing scales and histories of genetic structures. In either case documentation is needed at every taxonomic level from the species to the phyllum, and at every biochemical level from the virus to the most complex multicellular organism.

In the absence of such comprehensive programs of correlation among energy input rates and lineage diversities, ambiguities will persist between two sorts of biologic effects: (1) Rapid cascades of high energy inputs can lead to almost instantaneous disappearance of previously standardized lineages that consumed large fractions of the trophic energy supply relative to other lineages. (2) Population crashes can also be caused by energy loss from the system as a whole, but they imply time-dependent changes in other trophic balances and might not be as devastating to an individual lineage.

In the case of high energy input rates, diversification can't keep up with the approach to the ESCAPE condition of Figure 19. Physically, this is analogous to the loss of integrity of a major river system because of rapid tectonic uplift or tilting. At the same time, however, lineages (or rivers) that consumed little energy and are of low and nonstandardized diversity may experience an acceleration of diversity (e.g., near the beginnings of the Avian radiation events documented by Figure 14). Differences in the time-dependent variations of the ratios of impulse energy to diversity may themselves be functions of energy level. For instance, genera and species of simple organisms interacting directly with a globally coordinated environment (e.g., the ocean) probably respond more immediately to small changes than do the taxonomic levels of families, orders, and classes of organisms interacting with a variety of heterogeneous and interdependent environments (e.g., the ostracode record in Figure 8 vis a vis the total faunal record in Figure 9). This does not mean, however, as is exemplified by river piracy, that a major taxonomic feature is not sometimes subject to wholesale extinction caused by a relatively small environmental change.

Galactic Evolution as a Strange Attractor: The Path of the Solar System

Figure 20 shows a synopsis of the history of the solar system relative to its encounters with galactic density distributions and galactic plane crossings as described by Innanen et al. (1978) on the basis of galactic density models computed by Clutton-Brock et al. (1977). The density record

---

Figure 20 near here

---

during the latest 600 Myr of Figure 20A is compared with the paleontologic record in Figure 9.

Besides the periodic character of the galactic plane-crossing paths emphasized by others in their interpretations of impact cratering events, Figure 20 has implications concerning other events of episodic character in the history of the solar system. There are several periodic features in both graphs of Figure 20 that resemble effects found in the behavior of strange attractors (Figure 19B). There is a beat-like repetition of about 930 Myr; its harmonic of 465 Myr is the time taken for the Solar System to overtake and pass all the spiral density arms of the Milky Way galaxy which revolve at about half the velocity of star systems outside the galactic nucleus (the nucleus extends out to about 3 kpc and the Sun is at about 10 kpc from the center; a parsec, pc, is 3.26 light years). Another harmonic of about 233 Myr is the galactic year, which is the time taken by the Sun, other stars, and molecular cloud complexes to circumnavigate the galaxy relative to an externally fixed coordinate system. These are not exact figures. For example, Rubin (1983) reports the galactic year as 225 Myr.

It takes about two galactic years for the solar system to experience the variety of density environments in the galaxy relative to the spiral arms. Because this duration is nearly as long as the Phanerozoic, the solar system has experienced an ever new and unique galactic environment during the time that biologic diversity has flowered to its present-day complexity. As described below, the route and the time of passage through the galactic environment are not passive phenomena. The temporal and spatial scales of star birth and death events make it likely that the solar system has been influenced by many major disturbances of the galactic mass distribution (cf., Seiden and Gerola, 1982). Figure 20A represents spatial-temporal averaging based on a knowledge of present galactic structure, hence it does not reveal the details of more localized and transient effects. There are numerous features of almost but not quite periodic character, and other features of irregular and unpredictable chaotic character.

Such dynamical trajectories of motion are typical of strange attractors in numerical dynamics. A laboratory analog is shown below (Figure 24) where the parameters of state are clearly defined and adjustable yet the patterns of motion in time and space have strong resemblances to galactic structure. On the galactic scale, forcing functions are relative to even more comprehensive processes that are not fully known and ultimately may be undefinable except in terms of a framework that encompasses the largest known system.

As pointed out by Bok (1984) the diversity of relative motions within the galaxy mean that it is perpetually changing in its configurations. During the transits of the galactic spiral arms the solar system experiences the changes associated with star formation and also more specific effects related to disturbances of the Oort cloud and the inner reservoir of cometary objects (Roberts, 1975; Hills, 1981). Although it is beyond the scope of this paper to attempt specific correlations at the galactic scale, it is evident that the

dynamical history of the solar system is coordinated with galactic dynamics on many scales of interaction in time and space.

The generalized relations of mass and luminosity for stars of different types is shown in Figure 21A after Rubin (1984); approximate ages are those of Main Sequence stars. Figure 21B shows localized star-birth events in the Orion sub-arm of the Milky Way galaxy (Orion is where the solar system is located at the present time (Spitzer, 1982). Star formation is episodic with

---

Figure 21 near here

---

events occurring at intervals of 2 to 4 Myr over the latest 12 Myr. These loci of star formation are about 1500 light years (0.5 kpc) from the Sun, a distance too great to imply cause-effect correlations. However, the process is intermittently continuous (Seiden and Gerola, 1982), so these events record a perpetual system of disturbances (like waves and white caps in the open ocean) at the temporal and spatial scales of star-forming density structures. Pulsations of such episodicity have been occurring since the origin of the solar system, and their intensity is presumably greatest when the solar system is in the vicinity of a spiral arm and associated molecular cloud complexes.

The spiral density arms are about 1 kpc in width. This gives a residence time of a star within the arm of the order of 10 Myr at a relative velocity (about half the orbital velocity) of the order of 10^2 km sec^{-1} (a parsec is roughly 3 x 10^{13} km). This assumes that the path is approximately normal to the arm; oblique paths at the position of the Sun take longer, so the residence time is 10 to 20 Myr, allowing for variations in width. Molecular cloud complexes also revolve in the galaxy at speeds similar to those of the stars and the Sun (the Sun's present orbital velocity in the galaxy is about 220 km sec^{-1}), so the net gravitational effects during such a traverse relate to several kinds of interactions with the spiral arms (see Blitz, 1982; Hodge, 1984). The shock-like phenomena thought to be responsible for the spiral structure itself also relate to episodes of star formation associated with transits of the arms by the older stars (e.g., the Sun) and the cloud complexes (Spitzer, 1982).

Some time estimates indicate the possible varieties of periodic effects (compare with Figures 8 through 10). For a two-arm galaxy (four intervals per 360 degrees of arc) the total time spent between arms is about 460 Myr (2 x 230 Myr) minus 4 x (10 to 20) Myr, or 380 to 420 Myr. The average transit time between two half-arms is about a fourth of this total, or about 95 to 105 Myr. However there are at present two sub-arms, one of which is the Orion arm where the solar system and star-forming events of Figure 21 are located. So there are other subintervals of the order of 40 to 50 Myr between peak intervals for star formation. If cascades of star formation occur during each passage, there have been episodes of the order of 10 Myr of maximum likelihoods separated by 40 to 50 Myr of minimum liklihoods, or about 55 ± 10 Myr maximum to maximum. This period resembles intervals between extinction events and origination events during the Phanerozoic (e.g., Figure 9).

Moving backwards from the present location of the solar system, the above timing would suggest that ages of zero to 5 or 10 Myr represented a likely peak interval for star formation (cf., events in Figure 8). From 5 or 10 to between 45 and 60 Myr the likelihood of local star formation is lower, and it is again high at ages somewhere between 45 and 70 Myr, depending on any changes of arm width. In the meantime, galactic plane crossings have occurred at the more regular intervals of about 30 to 36 Myr as shown in Figure 20. The Sun is presently close to the galactic plane as well as just passing

through a period of nearby star formation. The next previous crossing was about 31 Myr ago.

The variety of episodic phenomena can be refined by appeal to specific orbital calculations. Models by Harrison (1977), Whitmire and Jackson (1984), and Davis et al. (1984) postulate an as yet undiscovered solar companion star to explain differences in the timing of galactic plane crossings, impact cratering maxima, and the extinction maxima of Raup and Sepkoski (1984).

Of more importance than the existence of special periodicities is the overall signature involving mixed periodicities of the galactic strange attractor. During times of proximity to regions containing molecular cloud complexes the various episodic phenomena mentioned above are supplemented by shorter-term density fluctuations. Whether or not a solar companion star is verified, the variety of galactic disturbances that have interacted with the solar system via cometary, electromagnetic (plasma winds, etc.) and other unknown effects may range from periods less than 2 Myr to periods exceeding the Phanerozoic record. This periodicity range is consistent with the dominant cycles seen in the records summarized in Figure 10.

The notion of a solar companion star would appear to be reasonable based on the statistics of binary star systems in the universe. Binary star formation is a common process (see Huang, 1975; Sexl and Sexl, 1979). The concept of binary star formation also has contributed to an understanding of the evolution of planetary nebulae and possible stages in the evolution of the solar system. Figure 22 shows a relation illustrated by Huang (1975) between rotational velocities of stars and their spectral type shown in Figure 21.

Figure 22 near here

At a certain age along the Main Sequence stars may experience an abrupt decrease in rotational velocity associated with the creation of planetary systems. It is possible that a binary star model could explain certain features of the planetary mass distributions in the solar system. For instance, the distribution of orbital kinetic energies of the planets is shown in Figure 23. This signature, like the galactic structure, has elements of

---

Figure 23 near here

---

chaotic behavior in addition to the classical regularities described by Kepler's laws and the Titius-Bode relation. The latter empirical relation, which has never been explained, may be related to an attractor-like evolution of planetary distributions (Shaw, 1983b).

Regression lines for the orbital kinetic energies versus planetary masses have different trends for the inner terrestrial planets and the major outer planets of the solar system. It is speculated that the intersection of the trend for the terrestrial planets with that of the outer planets may point toward a mass state that represents a missing object at about 0.1 the Sun's mass. This mass is consistent with the theoretical mass of a companion star. Such an interpretation would identify the terrestrial planets as possible relicts of events during which the solar companion star passed through a critical distance from the Sun and receded to its (hypothetical) present loosely bound orbit (see Davis et al., 1984; Whitmire and Jackson, 1984). However, it is possible that the formation of the planets is the only record of a more violent event during which the companion star was lost from the solar system (orbital fissioning was so energetic that there was ejection of

the smaller object and the present distribution of masses and kinetic energies in Figure 23 represent the only remaining record of the event, in a manner analogous to the ESCAPE trajectory in the attractor evolution of Figure 19).

If the latter interpretation is favored it implies that the companion star model would not explain present-day gravitational disturbances of the cometary reservoirs. However, such a direct cause-effect model is not needed if the solar system and attendant cometary reservoirs constitute a substructure of the galactic strange attractor. Such an interpretation is consistent with the complex structures seen in Figure 23 despite the precise regularities of the planetary orbits. The latter would be analogous to stable periodic windows in the chaotic regimes of Figures 17 and 19. The periodicity of cometary showers represents the long-term oscillatory structures of the strange attractor.

Episodic and Periodic Signatures in the Geologic Record Interpreted According to Numerical Structures Found in Attractor Dynamics

Clues From Experimental and Numerical Attractor Behaviors.

The mixed character of Hawaiian-Emperor volcanic episodes and of biologic episodes has been illustrated in several ways. The history of the Sun's path in the Milky Way galaxy also has periodicities of mixed character. In both cases there are strong hints of coherence as well as strong evidence of irregular or chaotic behavior. Such simultaneous indications of order and disorder are characteristic of attractor structures in general and strange attractors (also called chaotic attractors) in particular. An experimental strange attractor is shown in Figure 24. In this instance, the behavior is

---

Figure 24 near here

---

not explained by such things as statistical uncertainties in the sampling of ages, nor is it an artifact of theory or computer modeling. The forcing frequency is specifically defined, and sources of secondary forcing frequencies are also known (in this experiment there were small diurnal fluctuations in room temperature and electrical power). If the pattern was expanded self-similarly to the galactic scale, it would resemble the record of the Sun's episodic path through the galaxy (compare Figures 20, 23, and 24).

Such resemblances between different types of systems reflect the variety of periodic and aperiodic modes imbedded in the structures of strange attractors. The potential diversity of patterns is unlimited, but there is a universal system of structural repetitions that always look somewhat alike (structural similarity is described by universality parameters). Such patterns are not random, but neither are they restricted to fixed sets such as the planetary orbital periods or the rotational period of the laboratory rheometer. Attractor structures have elements of scale-invariance (self-similarity) and universality (characteristic dynamical coefficients independent of material system or scale). This means that attractor signatures have similar properties that are independent of the material type of system and of the scales of time and size used to describe the system. Perhaps a simpler way of putting it is to say that the potential types and complexities of patterns we can recognize in nature are not scale dependent and are the same everywhere. This is, of course, conjectural at the limits of cosmic distances and(or) subatomic particles (i.e., there is no theoretical limit, but there are cutoffs in the criteria for measurements of time and size).

Kinematic comparison of Figures 20 and 24 illustrates similarities that result from nonlinear dynamics. The scale ratio of time is of the order 10^{11} (10^9 years to 100 hours) and the length ratio is of the order 10^{22} (100 kpc to 30 cm; 1 pc $\approx 3 \times 10^{13}$ km). Thus, the frequencies vary roughly as the inverse square root of the length scales. In detail this results from dynamical relationships that are not examined quantitatively here. Qualitatively, the experimental fluid is highly viscous (10^3 poise), and the torque input produces sharp thermomechanical instabilities (nonlinear oscillations of shear stresses, shear rates, temperatures, viscosities, and particle velocities). These pulsations are kinematically analogous to star formation in the galaxy and are responsible for the chaotic structure (and its regularities) in the experimental system.

The analogous episodes of star formation are explained kinematically as resulting from density instabilities characteristic of gas dynamics (e.g.,

Seiden and Gerola, 1982). There are certain optimal but unpredictable conditions for the occurrences of instabilities which are, on average, repetitive in the cases of both viscous fluids and compressible gases. The timing of these instabilities is sensitive to slight departures from the mean thermodynamic states in either case (sensitive dependence on initial conditions and to changes in ambient boundary conditions). Therefore, the time-records of behavior in viscous liquids and compressible gases have common elements of periodic regularity and irregularity reflecting a 'mixture' of order and disorder (this is the regime labeled chaos in attractor studies such as Figures 17 and 19).

In the traditional fluid dynamic view, the experimental conditions of Figure 24 resemble laminar boundary layer flow with local episodes of quickly damped turbulence (i.e., the motion of a marker particle for the most part follows simple stream lines that look like trajectories of laminar flow). From a numerical dynamic viewpoint, however, the behavior is statistically mixing, or turbulent, although it is far from a state of statistically homogeneous turbulence. This is seen in the fact that though the marker trajectories are stream-like, they are not invertible owing to the elements of mixing and intermittency. Essentially the same statement can be made about a marker trajectory such as the path of a star in the galaxy. This exemplifies the universality of dynamical structures even for two systems that are not geometrically similar and differ greatly in size and periodicities.

An important point discovered in numerical studies of attractor structures is the great diversity of periodic and chaotic modes encountered. It was shown by May (1976), and in many other studies including ours, that there are systematic bifurcation sequences within chaotic regimes such as those of Figures 17 and 19. In the chaotic regime mixed odd- and even-period windows are found (Figure 17A). In systems with one degree of freedom the most conspicuous and persistent window is a period-doubling sequence of period 3 (repeats of 3, 6, 12, 24, etc., in a branching structure), but all integer periods appear to be possible with sufficiently detailed resolution. In systems of two or more degrees of freedom (multiple rate parameters), sequences based on 3, 5, and 7 are conspicuous. In general (but not always), the larger the prime number base the narrower and harder to find are the corresponding periodic windows.

Attractor-Like Periods in Natural Records.

These observations suggest an approach to the search for mixed periodicities in natural systems of attractors. The approach is analogous to 'maximum parsimony' invoked in models of genetic branching. Applied to time series data of a physical process, however, there may be relationships between period and amplitude. In a case where the total energy of a process increases with its longevity, most of the energy will be represented by long-period fluctuations. Therefore, in a power spectrum the highest power is at the lowest frequencies. This effect is evident in the episodic signatures examined in this paper, and an eventual goal of this analysis is to develop a scheme that will elucidate such energy-magnitude scaling. For the time being, however, energy ratios are ignored and we focus on numerical properties of the time distributions.

Table 1 lists numerical series representing period-doubling and mixed regimes; May (1976) enumerates the theoretical distribution of periods for

---

Table 1 near here

---

the one-dimensional case. At short periods nearly all integer values between about 1 and 12 are represented by the simple combinations $(2^n)(3^m)$; see column with this heading in Table 1. As the possible variety of periods gets larger, however, the likelihood of periods not represented by maximum parsimony among sequences requiring more than one base increases unless there is a tendency for convergences toward simple attractor sets. The product $(2^n)(3^m)$ defines the most parsimonious mixed set because sequences of a single base are excluded (i.e., we are referring to the greatest simplicity among mixed sets). Over the numerical range 0 to 48 in Table 1, there is about a 4:1 chance that a random period will fall at values between those given by $(2^n)(3^m)$ periods; the chance is 6:1 for a range from 0 to 64, and is again about 4:1 over a range from 0 to 108.

The numerical structure of such series is interesting from the standpoint of randomness expressed by departures of the observed intervals of periodic phenomena from simple geometric series. If terms involving the series to the prime bases 5, 7, 11, 13, 17, etc. were allowed, of course, all integer periods eventually would be represented. In place of such unlimited series of integers, it is possible that sets based on irrational numbers would be more parsimonious. In the present instance, however, comparisons beyond those of Table 1 are not warranted. Inclusion of 5 and 7 improves the fit to periodicities at ~ 135 (± 4), 60, 42, 45, 30, and 15 in Figure 10. If there is a 26-Myr period, the prime number 13 also has to be included as one of the bases. Tests have not been attempted as yet for noninteger periods.

Table 1 lists all of the peak-to-peak intervals found in the time series examined in this paper. That is, mixtures of repeat intervals are examined without regard to phase differences between records. Establishment of specific phase differences between periods would require high chronological precision or long records of rather simple periodicities. The viewpoint advocated here is that the search for a single unique period, or even a simple set of periods, is unrealistic in the face of overwhelming evidence for chaotic dynamics with consequent hierarchies of complex bifurcating phenomena whether the viewpoint is terrestrial or extraterrestrial.

Histograms of peak-to-peak intervals listed in Table 1 for periods from 0 to 100 Myr are compared in Figure 25A with histograms compiled from nearest-neighbor geometric series. Each age value was counted as a 2-Myr

---

Figure 25 near here

---

sample (integer value of time interval ± 1 Myr), so a unit count is represented by a square of area 2 in Figure 25A. Overlapping counts were summed within 1 Myr intervals, accounting for the existence of half-counts between adjacent values of integer time intervals.

Artificial histograms in Figure 25A correspond to those portions of the data accounted for by each of the series $(2^n)(3^m)$, $(2^n)(3^m)(5^p)$, and $(2^n)(3^m)(5^p)(7^q)$. This was accomplished by taking those numerical values in each series that were nearest to an observed age interval and summing them as was done for the raw data. Where the difference was equally divided on either side of the observed value the entire age span between the two numerical values was included in the count, so the counts were proportioned according to fractions of the (1 x 2 Myr) area (i.e., normalized by the inclusive range), giving fractional counts of 1/4, 1/3, etc., units. The sharpness of the maxima indicates that such ambiguities were infrequent.

The resemblances of the artificial and observed histogram shapes is evident. The simplest series $(2^n)(3^m)$ mimics the overall distribution

fairly well (this is the most parsimonious artificial set by the convention defined above). Disagreements mean that age intervals involving multiples of 5, 7, or higher primes are needed to account for the observed distribution. For instance, gaps in the series $(2^n)(3^m)$ are found near ~ 15, ~ 20, ~ 30, and ~ 40 Myr, and peaks at 32, 36, 48, 54, 64, 72, and 96 Myr are too large. Inclusion of a series to base 5 improves the resemblance, and inclusion of a series to base 7 nearly duplicates the histogram of the raw data.

The comparisons in Figure 25A and Table 1 indicate that the natural record is indistinguishable from ordered periodic progressions, even though this order is numerically complex. Regardless of the lengths and types of records included, an assumption of periods in the most parsimonious series gives a reasonable fit of the data, and periods in the series $(2^n)(3^m)(5^p)(7^q)$ fit nearly all the data. The maximum deviation is about 3 Myr, and the correspondences are usually ± 1 Myr. A theoretical reason why the sequence $(2^n)(3^m)$ may be the most parsimonious is because it reflects the dominant numerical periods of chaotic attractor regimes (see chaotic bifurcations in Figures 17A and 19A). The period-doubling regime (2^n) is simpler, but patterns limited to this stable sequence are as unrealistic as simple harmonic series based on a single fundamental frequency.

The simplest physical interpretation consistent with these comparisons is that every period in the series $(2^n)(3^m)$ was generated by terrestrial and(or) cosmological processes for time scales between 2 Myr and 500 Myr. Processes that generated selected periods in the series (5^p) and (7^q) existed but were not as conspicuous in this sample of records, nor would they be if the processes were simulated by one-dimensional numerical attractor models.

The extent to which all numerical series are represented in the geologic data is suggested by comparing counts of different periods in the different columns of Table 1. For instance, there are 30 different periods in the set $(2^n)(3^m)$ between the values 1 and 325 Myr, and there are about three times as many (85) different periods in the set $(2^n)(3^m)(5^p)(7^q)$ over the same range. The column labeled "Obs." summarizes all of the observed geologic time intervals of this data set. Without taking account of age uncertainties it has 66 different 'periods' (the galactic year is counted only once). If it is assumed that ages differing by 1 Myr are indistinguishable, then there are 43 different 'periods'. This number can always be reduced by increasing the age uncertainty, but these counts generally concur with the above conclusion that bases in addition to 2 and 3 are required to fit the data. That is, there are more different periods than are present in the most parsimonious set (43 *vs*. 30 in the set 2,3) and fewer than in the most inclusive set (66 *vs*. 85 in the set 2,3,5,7).

These differences in part reflect the limited number of records available for analysis. As additional and more precise records are included (e.g., sea level data, oxygen isotope data, other paleontologic data), the comparison with the (2,3,5,7) set should improve, and more inclusive numerical sets (e.g., 2,3,5,7,11,13) may be required to fit all the data. This would be expected if the numerical progressions occur in self-similar arrays, because more and more of the possible subsets will be represented as the sample becomes more and more complete. Given a large enough data base it would be possible to compare populations of periods in the geologic data with populations of periods in numerical attractor models with varying degrees of freedom (e.g., populations of periodicities in the chaotic regime of Figure 17 *vis a vis* those in models such as Figure 19). The latter has not been done quantitatively, but qualitatively the proportions are different than those

given by May (1976) because there are more ways to generate complexity.

The relationship between the present method and specific statistical analyses such as those of Raup and Sepkoski (1984) and Alvarez and Muller (1984), representing periods of 26 and 28.4 Myr, respectively, are not evaluated here. Special periods could result from biased mixtures of the periodic sets of Figure 25 or possibly from the existence of bases with higher prime numbers (e.g., period 13; 28.4 is probably not distinguishable from 2^2x7^1). In the former case, weighting could result from physical effects that dominate different types of data sets, or it could reflect differing types of uncertainties in the periodic subsets of different processes.

Figure 25B shows the shorter-term periodicities not resolved in Figure 25A. It is dominated by three sets of data: (a) the ostracode data of Benson et al. (1984), (b) the Hawaiian-Emperor data, and (c) the data of this paper on Avian adaptive radiation. It suggests that periodicities considered at the shorter intervals of time have distributions resembling the overall data set. For example, if the periodic interval between about 30 and 44 Myr in Figure 25B were expanded by a factor of two it would roughly resemble the interval between 0 and 28 Myr. If the same interval were expanded by a factor of five or six, it would resemble the overall pattern in Figure 25A. Similar comparisons might be found with finer and finer sampling of time intervals, limited only by the shortest time record that has approximately the same number of cycles. In Figure 10B such self-similarity would be represented by steeper and steeper curves. If the shortest period were normalized to fundamentals less than 1 Myr, then the clustering of periodicities would become dense and nearly vertical at the lefthand ordinate axis.

Self-similarity is a property of numerical sets based on geometric progressions. The data of Table 1 and histograms of Figure 25 suggest that natural processes mimic such numerical self-similarity. However, to make this demonstration complete, it will be necessary to expand the analysis to other types of natural time series and to processes that have been documented with precisions better than 1 Myr. It may then be possible to classify the numbers of periods within different bandwidths of self-similarity and to express this property in terms of characteristic dimensional indices. Self-similarity can sometimes be described by noninteger fractions called fractal dimensions (see Mandelbrot, 1982), suggesting that the periodicity arrays of Table 1 and Figure 25 may be fractals or variable spectra of multifractal dimensions.

Figure 25C shows a histogram constructed as in Figure 25A (observed) but representing intervals measured between minima in the episodic record rather than maxima. If it is assumed that all episodic intervals are significant in terms of the orchestral signature, then the same periodicity spectra should describe the timings of minima as well as maxima. Because extinction events were included in the set of maxima, origination events are included with the minima. However, according to earlier discussions there is ambiguity as to how energy maxima of physical processes correlate with records of extinctions and originations. Therefore, physical correlations are not implied by this arbitrary distinction (Figures 25A and 25C are two sets of numbers that represent the same episodic phenomena).

The histogram in Figure 25C has roughly the same pattern as the histogram of observed intervals in Figure 25A and the artificial histogram based on the series $(2^n)(3^m)(5^p)(7^q)$. The main difference is that contributions from the series $(3^m)(5^p)(7^q)$ are more conspicuous in Figure 25C, reflected by peaks near 35 Myr, 45 Myr, 56 Myr and 90 Myr. However, minima in the time series are not as sharply defined as maxima for some geologic processes, and uncertainties are larger in Figure 25C than in Figure 25A.

The Uniqueness of Evolution: A Conjectural Reconstruction

The solar system was born as a closely coupled binary star system more than 10 Gyr ago; it evolved to the present G(1) state of the Sun during about half that lifetime (see Figures 21 and 22). About 5 Gyr ago the paired orbital motions around the center of mass encountered dissipative instabilities that also involved satellitic masses formed during the earlier condensation. The binary orbit as well as the orbital distributions of satellite bodies (proto-planets) were severely disrupted at that time. The rotational kinetic energies of the larger stellar mass about the center of the system and about its own spin axis were drastically reduced by the disruptive processes while the proto-planets were dissipatively rearranged ('mixed up') to give the present orbital distribution of masses and velocities around the Sun. The companion star (which has been named Nemesis but might be renamed Genesis according to the scenario of this paper; Gould, 1984, suggested Siva) was about one-tenth the Sun's mass. It left evidence of its existence in the orbital kinetic energies and chemistries of the terrestrial planets, while the larger outer planets tracked the loss of kinetic energy of the Sun and binary system as a whole.

This was a process that is not easy to visualize or reconstruct; possibly there were jet-like ejections of mass from inner regions at an earlier nebular stage, as is seen in modern observations of star-forming events. During these processes interaction with other events of star formation in the molecular cloud complexes and with shock waves in the ever changing structure of the Milky Way galaxy established a secular rhythm that influenced the types of coupling that evolved among galactic, solar-system, and planetary dynamics. The system that had begun as a very disordered chaotic attractor was progressively self-tuned by the redistributions of mass and energy. In the process chaotic resonances developed that converged to the system of stabilized planetary orbits that exists today. Fine-tuning of planetary orbits and systems of planetary satellites occurred through the action of local dissipative phenomena (gravitational and electromagnetic dissipation of various types and kinetic dissipation related to mass impacts). The general process of relaxation has been called the principle of "least interaction action" by Ovenden (1975, 1976). It is conceivble that the companion star remains in a loosely bound orbit, as in the models of Davis et al. (1984) and Whitmire and Jackson (1984), as one of the trajectories of motion of the chaotic attractor that is the solar system. This possibility, however, is not essential to the existence of other periodic resonances, including periodicities of meteoroid impacts on Earth.

During the latest 4 Gyr the periodic and quasiperiodic regularities of the chaotic attractor, including such effects as the Earth's rotation and revolution around the Sun, optimized chances for biochemical selection in the primordial oceans (whether directly or aided by 'panspermia'; see Hoyle and Wickramasinghe, 1981). Subsequent events of genetic bifurcations and increased cellular complexity were orchestrated by the solar-galactic rhythm. Evolving episodes of extinction, origination, and adaptive radiation tracked this long-established rhythm with ever more involuted and convoluted tuning. This resulted simultaneously in great complexity and in generally robust and standardized biologic forms that have been rejuvenated from time-to-time. Rejuvenation was associated with major episodes of impulse-energy events that had mixed periodicities related to resonances of cometary showers with geologic processes such as volcanism, ocean circulation, etc. The existence of mixed periodicities was a property of nonlinear dynamics and was expressed by geometric bifurcation structures of types characteristic of attractors

(Figures 17 through 19, 25, and Table 1).

The existence of mixed periodicities made up of geometric series such as $(2^n)(3^m)$, etc., suggests that there were also mixed periodicities (harmonics) that involved rational fractions of these series. Therefore, sub-multiples of 1 Myr are implied by the attractor scenarios as well as the longer periods discussed in this paper. A concept of self-similar attractor periodicities ties together our perceptions of the 'immediate' and of the 'secular'. If this orchestration represents a universal attractor it also ties together concepts of periodicities down to the limits of atomic interactions and quantum uncertainty (e.g., Shaw, 1981).

The present time is not a maximum in the probabilities of large cometary impacts, but it is in phase with the galactic rhythm of density structures and star formation. Therefore it represents a time of high probabilities of shower-like impacts of the smaller Earth-crossing objects of all types. It may not be far-fetched to suggest that events of star formation in our vicinity of the galaxy correlate at some level with events of biologic origination (large-scale galactic pulsations echoed by small-scale pulsations of terrestrial biology). If so, the evolution of biological intelligence in the solar system is the net resultant of the above rhythms. It could be said that the brain is itself a description of bifurcating sets in a local chaotic structure of the solar-galactic attractor (relating the local concept of thought to a universal concept of mind).

The probability of the occurrence of intelligent life elsewhere in this galaxy and other galaxies is not defined solely by the likelihood of comparable thermodynamic environments. By analogy with trajectories of motion of strange attractors, the trajectories of motion that constitute intelligence are potentially represented by diverse types of composite periodic-nonperiodic structures. The possibility that the same rhythms and bifurcation structures that exist on Earth also exist somewhere else in the universe is not subject to prediction (the bifurcation structures of chaotic attractors are in general unpredictable even when they are generated by deterministic functions). But by the same principle, the possibility that analogous complexities exist is high (the existence of complex attractor structures that have common elements of universality is far more probable than the existence of identical attractor structures). Therefore, other patterns of intelligent rhythms and life forms may exist with a probability that approaches one hundred percent. However, the extent to which these forms are mutually recognizable is a property of the evolutionary states of the universal attractor with which research on Earth is currently engaged.

References

Alvarez, L.W., Alvarez, W., Asaro, F. and Michel, H.V., 1980, Extraterrestrial causes for the Cretaceous-Tertiary extinction: Science, v. 208, p. 1095-1108.

Alvarez, Walter and Muller, R. A., 1984, Evidence from crater ages for periodic impacts on Earth: Nature, v. 308, p. 718-720.

Anderson, O. L. and Perkins, P. C., 1975, A plate tectonics model involving nonlaminar asthenospheric flow to account for irregular patterns of magmatism in the southwestern United States: Physics and Chemistry of the Earth, v. 9, p.113-122.

Benson, R. H., 1975, The origin of the psychrosphere as recorded in changes of deep-sea ostracodes: Lethaia, v. 8, p. 69-83.

Benson, R. A., Chapman, R. E. and Deck, L. T., 1984, Paleoceanographic events and deep-sea ostracodes: Science, v. 224, p. 1334-1336.

Blitz, Leo, 1982, Giant molecular-cloud complexes in the galaxy: Scientific American, v. 246, p. 84-94.

Bohor, B. F., Foord,, E. E. Modreski, P. J. and Triplehorn, D. M., 1984, Mineralogic evidence for an impact event at the Cretaceous-Tertiary boundary: Science, v. 224, p. 867-869.

Bok, B. J., 1984, The Milky Way galaxy, in P. W. Hodge, ed. The Universe of Galaxies: N.Y., W. H. Freeman and Co., p. 5-21 (Readings from Scientific American).

Burke, W. H., Denison, R. E., Hetherington, E. A., Koepnick, R. B., Nelson, H. F. and Otto, J. B., 1982, Variaton of seawater $^{87}Sr/^{86}Sr$ throughout Phanerozoic time: Geology, v. 10, p. 516-519.

Carter, W. E., Robertson, D. S., Pettey, J. E., Tapley, B. D., Schutz, B. E., Eanes, R.J., and Lufeng, M., 1984, Variations in the rotation of the earth: Science, v. 224, p. 957-961.

Clube, V. and Napier, B., 1982, The Cosmic Serpent: N.Y. Universe Books, 299 p.

Clutton-Brock, M. K., Innanen, A. and Papp, K. A., 1977, A theory for the gravitational potentials of spheroidal stellar systems and its application to the galaxy: Astrophysics and Space Science, v. 47, p. 299-314.

Davis, Marc, Hut, P. and Muller, R. A., 1984, Extinction of species by periodic cometary showers: Nature, v. 308, p. 715-717.

Evernden, J. F. and Kistler, R. W., 1970, Chronology of emplacement of Mesozoic batholithic complexes in California and western Nevada: U.S. Geological Survey, Professional Paper 623, 42 p.

Feigenbaum, M. J., 1980, Universal behavior in nonlinear systems: Los Alamos Science, Summer/1980, p. 4-27.

Fisher, James, 1967, Fossil birds and their adaptive radiation: in W. B. Harland, C. H. Holland, M. R. House, N. F. Hughes, A. B. Reynolds, M.J.S. Rudwick, G. E. Satherthwaite, L. B. H. Tarlo, and E. C. Willey (eds.) The Fossil Record, London, Geological Society of London, p. 133-154.

Gollub, J. P., Benson, S. V. and Steinman, J., 1980, Subharmonic route to turbulent convection, in, R. H. G. Helleman, ed. Nonlinear Dynamics Annals, N.Y. Academy Science, v. 357, p. 22-27.

Gould, S. J., 1983, Nature's great era of experiments: Natural History, v. 92, p. 12-21.

Gould, S. J., 1984, The cosmic dance of Siva: Natural history, v. 93, p.14-19.

Gould, S. J. and Eldredge, N., 1977, Punctuated equilibria: The tempo and mode of evolution reconsidered: Paleobiology, v. 3, p. 115-151.

Grieve, R. A. F., 1982, The record of impact on Earth: Implications for a major Cretaceous/Tertiary impact event: in L. T. Silver and P. H. Schultz (eds.), Geological Implications of Large Asteroids and Comets on Earth: Geological Society America, Special Paper 190, p. 25-37.

Gruntfest, I. J. and Shaw, H. R., 1974, Scale effects in the study of earth tides: Transactions Society Rheology, v. 18, p. 287-297.

Harland, W. B., Cox, A. V., Llewellyn, P. G., Pickton, C. A. G., Smith, A. G., and Walters, R., 1982, A Geologic Time Scale: Cambridge, University Press, 131 p.

Harrison, E. R., 1977, Has the Sun a companion star?: Nature, v. 270, p.324-326.

Helleman, R. H. G., 1983, One mechanism for the onsets of large-scale chaos in conservative and dissipative systems: in, C. W. Horton Jr., L. E. Reichl and V. G. Szebehely (eds.), Long-Time Prediction in Dynamics, N.Y., Wiley, p. 95-126.

Hills, J. G., 1981, Comet showers and the steady-state infall of comets from the Oort cloud: Astronomy Journal, v. 86, p. 1730-1740.

Hodge, P. W., 1984, The Universe of Galaxies: N. Y., W. H. Freeman and Co. (Readings from Scientific American), 113 p.

Hoyle, Fred and Wickramasinghe, C., 1981, Evolution From Space: N.Y., Simon and Schuster, Inc., 176 p.

Huang, S.-S. , 1975, Life outside the Solar System: in New Frontiers in Astronomy, San Francisco, W. H. Freeman and Co., p. 104-112 (Readings from Scientific American).

Innanen, K. A., Patrick, A. T. and Duley, W. W., 1978, The interaction of the spiral density wave and the Sun's galactic orbit: Astrophysics and Space Science, v. 57, p. 511-515.

International Mathematics and Statistic Library (IMSL), Edition 9 (1982) Houston, Texas, IMSL, Inc., Vol 2, Chapt F, FTFREQ, p 1-3.

Jackson, E. D. and Shaw, H. R., 1975, Stress fields in central portions of the Pacific Plate: Delineated in time by linear volcanic chains: Journal Geophysical Research, v. 80, p. 1861-1874.

Jackson, E. D., Shaw, H. R. and Bargar, K. E., 1975, Calculated chronology and stress field orientations along the Hawaiian chain: Earth Planetary Science Letters, v. 26, p. 145-155.

Kaula, W. M., 1968, An Introduction to Planetary Physics. N.Y., Wiley, 490 p.

Kistler, R. W., Evernden, J. F. and Shaw, H. R., 1971, The Sierra Nevada plutonic cycle: Part I, The origin of composite granitic batholiths: Geological Society America, Bulletin, v. 82, p. 853-868.

Lowrie, W. and Alvarez, W., 1981, One hundred million years of geomagnetic polarity history: Geology, v. 9, p. 392-397.

May, R. M., 1976, Simple mathematical models with very complicated dynamics: Nature, v. 261, p. 459-467.

Mandelbrot, B. B., 1982, The Fractal Geometry of Nature: San Francisco, W.H. Freeman, 460 p.

Mazaud, A., Laj, C., de Seze, L. and Verosub, K. L., 1983, 15-Myr periodicity in the frequency of geomagnetic reversals since 100 Myr: Nature, v. 304, p. 328-330.

Moberly, Ralph and Campbell, J. F., 1984, Hawaiian hotspot volcanism mainly during geomagnetic normal intervals: Geology, v. 12, p. 459-463.

Negi, J. G. and Tiwari, R. K., 1983, Matching long term periodicities of geomagnetic reversals and galactic motions of the Solar System: Geophysical Research Letters, v. 10, p. 713-716.

Newell, N. D., 1982, Mass extinctions - Illusions or realities?, in L. T. Silver and P. H. Schultz (eds.), Geological Implications of Impacts of Large Asteroids and Comets on Earth: Geological Society America, Special Paper 190, p. 257-263.

Niklas, K., 1982, Computer simulations of early land plant morphologies; canalization of patterns during evolution?: Paleobiology, v. 8, p. 196-210.

Ott, Edward, 1981, Strange attractors and chaotic motions of dynamical systems: Reviews of Modern Physics, v. 53, p. 655-671.

Ovenden, M. W., 1975, Bode's Law - truth or consequences: Vistas in Astronomy, v. 18, p. 473-496.

Ovenden, M. W., 1976, The Principle of Least Interaction Action, in V. Szebehely and B. D. Tapley (eds.) Long-Time Predictions in Dynamics: Boston, D. Reidel Publ. Co., p. 295-305.

Rampino, M. R. and Stothers, R. B., 1984, Terrestrial mass extinctions, cometary impacts and the Sun's motion perpendicular to the galactic plane: Nature, v. 308, p. 709-712.

Raup, D. M. and Sepkoski, J. J., Jr., 1984, Periodicity of extinctions in the geologic past: Proceedings National Academy Science, v. 81, p. 801-805.

Roberts, W. W., Jr., 1975, Theoretical aspects of galactic research: Vistas in Astronomy, v. 19, p. 91-109.

Rubin, V. C., 1983, The rotation of spiral galaxies: Science, v 220, p.1339-1344.

Rubin, Vera, 1984, Dark matter in spiral galaxies, in P. W. Hodge, ed. The Universe of Galaxies: N. Y., W. H. Freeman and Co., p. 31-43 (Readings from Scientific American).

Schwartz, R. D. and James, P. B., 1984, Periodic mass extinctions and the Sun's oscillation about the galactic plane: Nature, v. 308, p. 712-713.

Seiden, P.E. and Gerola, H., 1982, Propagating star formation and the structure and evolution of galaxies. Fundmentals Cosmic Physics, v. 7, p.241-311.

Sexl, R. and Sexl, H., 1979, White Dwarfs - Black Holes: An Introduction to Relativistic Astrophysics: N.Y., Academic Press, 203 p.

Shaw, H. R., 1970, Earth tides, global heat flow, and tectonics: Science, v. 168, p. 1084-1087.

Shaw, H. R., 1973, Mantle convection and volcanic periodicity in the Pacific: Evidence from Hawaii: Geological Society of America, Bulletin, v. 84, p. 1505-1526.

Shaw, H. R., 1980, The fracture mechanisms of magma rise from the mantle to the surface: in R.B. Hargraves ed. Phycics of Magmatic Processes, Princeton, NJ, Princeton University Press, p. 201-264.

Shaw, H. R., 1983a, Magmatic processes and orbital evolution. Geological Society of America, Abstracts with Programs, v. 15, p. 684.

Shaw, H. R., 1983b, Mathematical attractor theory and geological patterns: The distribution of the planets as a resonant mapping of chaos: Preprint, 32 pp, 9 figs.

Shaw, H. R. and Jackson, E. D., 1973, Linear island chains in the Pacific: Result of thermal plumes or gravitational anchors? Journal of Geophysical Research, v. 78, p. 8634-8652.

Shaw H. R., and Gartner, A. E., 1983, Mathematical theory of attractors and the evolution of order in branching systems, hydrologic, biologic and tectonic: Geological Society America, Abstracts w. Programs, v. 15, p. 329.

Shaw, H. R., Kistler R. W., and Evernden, J. F., 1971, The Sierra Nevada plutonic cycle: Part 2, Tidal energy and a hypothesis for orogenic-epeirogenic periodicities: Geolological Society America, Bulletin, v. 82, p. 869-896.

Shaw, H. R., Jackson, E. D. and Bargar, K. E., 1980, Volcanic periodicity along the Hawaiian-Emperor chain: American Journal Science, v. 280-A, p. 667-708.

Shaw, H. R., Gartner, A. E., and Lusso, F., 1981, Statistical data for movements on young faults of the conterminous United States; paleoseismic implications and regional earthquake forecasting: U.S. Geological Survey, Open-file Report 81-946, 353 p.

Shaw, Robert, 1981, Strange attractors, chaotic behavior and information flow: Zeitschrift fuer Naturforschung A, v. 36a, p. 80-112.

Shoemaker, E. H., 1983, Asteroid and comet bombardment of the Earth: Annual Review Earth Planetary Science, v. 11, p. 461-494.

Sibley, C.G. and Ahlquist, J.E., 1983, The phylogeny and classification of birds, based on the data of DNA-DNA hybridization: in R.F. Johnston, ed. Current Ornithology, N. Y., Plenum Press, v. 1, p. 245-292.

Sparrow, Colin, 1982, The Loranz Equations: Bifurcations, Choas, and Strange Attractors: N.Y., Springer-Verlag, 269 p.

Spitzer, Lyman, Jr., 1982, Searching Between The Stars: New Haven, Yale University Press, 179 p.

Tarling, D. H., 1983, Paleomagnetism: N.Y., Chapman and Hall, 379 p.

Whitmire, D. P. and Jackson II, A. A., 1984, Are periodic mass extinctions driven by a distant solar companion?: Nature, v. 308, p. 713-715.

Wones, D. R. and Shaw, H. R., 1975, Tidal dissipation: a possible heat source for mare basalt magmas: Lunar Science VI, Lunar Science Institute, p. 878-880.

Table 1. Values of the geometric series 2^n, 3^m, 5^p, and 7^q and their products for integer values of the exponents compared with peak-to-peak age intervals for selected sets of geologic data identified in columns 1 through 12, as follows: (1) record of biologic extinctions in the latest 250 Myr according to Raup and Sepkoski (1984), (2) record of impact cratering during the latest 250 Myr according to Alvarez and Muller (1984), (3) Phanerozoic record of impact cratering as determined in this paper based on analysis of data compiled by Grieve (1982), (4) record of Hawaiian-Emperor volcanism during the latest 73 Myr according to Shaw et al. (1980), and record of Mesozoic plutonism in the Sierra Nevada batholith according to Kistler et al. (1971), (5) record of Phanerozoic variations in strontium isotope ratios in the oceans according to Burke et al. (1982), (6) major biologic extinctions in the Phanerozoic according to Newell (1982), (7) major biologic originations in the Phanerozoic according to Newell (1982), (8) record of ostracode extinctions and originations during the latest 70 Myr according to Benson et al. (1984), (9) record of Avian radiation events (this paper), (10) analysis of galactic plane crossings by the Sun during the Phanerozoic according to Innanen et al. (1978), (11) analysis of galactic density variation along the Sun's path during the Phanerozoic according to Innanen et al. (1978), (12) analysis of geomagnetic reversal frequencies according to Moberly and Campbell (1984), Mazaud et al. (1983), Negi and Tiwari (1983), and Tarling (1983). Also see histograms in Figure 25; data from Moberly and Campbell (1984) are not included in the histograms because they are essentially the same set as those of Hawaiian-Emperor magmatism. The galactic year of 225 Myr in Col. 11 is from Rubin (1983) and 233 Myr is from Innanen et al. (1978).

Table 1.

Periodicities[a]

Shaw 9/15/84

	Numerical								Geological											
Index	2^n	3^m	5^p	7^q	2^n3^m	$2^n3^m5^p$	$2^n3^m5^p7^q$	Obs.	1	2	3	4	5	6	7	8	9	10	11	12
1	1	1	1	1	1	1	1	--	--	--	--	--	--	--	--	--	--	--	--	--
2	2	--	--	--	2	2	2	2	--	--	--	2(3)	--	--	--	2(4)	2(2)	--	--	--
3	--	3	--	--	3	3	3	3	--	--	3	3	--	--	--	3(4)	3(2)	--	--	--
4	4	--	--	--	4	4	4	4	--	--	--	4(4)	--	--	--	4(3)	4	--	--	--
5	--	--	5	--	--	5	5	5	5	--	5	5(4)	--	--	--	--	5	--	--	5(3)
6	--	--	--	--	6	6	6	6	--	--	6	6(7)	--	--	--	6	6	--	--	--
7	--	--	--	7	--	--	7	7	--	--	--	7(5)	--	--	--	--	--	--	--	7(3)
8	8	--	--	--	8	8	8	8	--	--	--	8(6)	--	--	--	8(2)	8	--	--	8
9	--	9	--	--	9	9	9	9	--	--	--	9	--	--	--	9	--	--	--	--
10	--	--	--	--	--	10	10	10	--	--	10	10(2)	--	--	--	--	10	--	--	--
11	--	--	--	--	--	--	--	11	--	--	--	--	--	--	--	--	--	--	--	11
12	--	--	--	--	12	12	12	12	12	--	--	12(3)	--	--	--	--	12	--	--	12(2)
13	--	--	--	--	--	--	--	13	--	--	--	13	--	--	--	--	--	--	--	13(2)
14	--	--	--	--	--	--	14	14	--	--	--	14(3)	--	--	--	--	--	--	--	--
15	--	--	--	--	--	15	15	15	--	--	15	15	--	--	--	--	--	--	--	15(4)
16	16	--	--	--	16	16	16	16	--	--	16	--	--	--	--	--	--	--	--	16
17	--	--	--	--	--	--	--	17	--	--	--	17	--	--	--	--	--	--	--	--
18	--	--	--	--	18	18	18	18	--	--	--	18	--	--	--	--	--	--	--	--
19	--	--	--	--	--	--	--	19	19(3)	--	--	19	--	--	--	--	--	--	--	--
20	--	--	--	--	--	20	20	20	--	--	--	20	--	--	--	--	--	--	--	--
21	--	--	--	--	--	--	21	21	--	--	21	--	--	--	--	--	--	--	--	--
22	--	--	--	--	--	--	--	22	--	22	--	22	--	--	--	--	22	--	--	--
23	--	--	--	--	--	--	--	23	--	23(2)	23	--	--	--	--	--	--	--	--	--
24	--	--	--	--	24	24	24	24	24	--	--	--	--	--	--	--	--	--	--	--
25	--	--	25	--	--	25	25	25	25	--	--	25(2)	--	--	--	--	--	--	--	--
26	--	--	--	--	--	--	--	26	26	--	26	--	--	--	--	--	--	--	--	--
27	--	27	--	--	27	27	27	27	27(2)	27	--	--	--	--	--	--	--	--	--	--
28	--	--	--	--	--	--	28	--	--	--	--	--	--	--	--	--	--	--	--	--
29	--	--	--	--	--	--	--	--	--	--	--	--	--	--	--	--	--	--	--	--
30	--	--	--	--	--	30	30	30	--	30(2)	--	30(2)	--	--	--	--	--	30	--	--
31	--	--	--	--	--	--	--	31	--	--	--	--	--	--	--	--	--	31(3)	--	--
32	32	--	--	--	32	32	32	32	--	--	32	32	32	--	--	--	--	32	--	--
33	--	--	--	--	--	--	--	33	--	--	--	--	33	--	--	--	33	33	--	--
34	--	--	--	--	--	--	--	34	34	--	--	--	34	--	--	--	--	--	--	34
35	--	--	--	--	--	--	35	35	--	--	--	--	--	--	--	--	--	35	--	--
36	--	--	--	--	36	36	36	36	--	--	--	--	--	--	--	--	--	36	--	--
37	--	--	--	--	--	--	--	37	--	--	--	--	--	37(2)	--	--	--	--	--	--
38	--	--	--	--	--	--	--	--	--	--	--	--	--	--	--	--	--	--	--	--
39	--	--	--	--	--	--	--	39	--	--	--	--	--	--	39	--	--	--	--	--
40	--	--	--	--	--	40	40	40	--	40	--	--	--	--	--	--	--	--	--	--
41	--	--	--	--	--	--	--	41	--	--	--	--	41	--	--	--	--	--	--	--
42	--	--	--	--	--	--	42	42	--	--	42	--	42	--	--	--	--	--	--	--
43	--	--	--	--	--	--	--	--	--	--	--	--	--	--	--	--	--	--	--	--
44	--	--	--	--	--	--	--	44	--	--	--	--	--	--	44	--	--	--	--	--
45	--	--	--	--	--	45	45	--	--	--	--	--	--	--	--	--	--	--	--	--
46	--	--	--	--	--	--	--	--	--	--	--	--	--	--	--	--	--	--	--	--
47	--	--	--	--	--	--	--	47	--	--	--	--	--	--	--	--	--	--	--	47
48	--	--	--	--	48	48	48	--	--	--	--	--	--	--	--	--	--	--	--	--
49	--	--	--	49	--	--	49	--	--	--	--	--	--	--	--	--	--	--	--	--
50	--	--	--	--	--	50	50	50	--	--	--	--	50	50	--	--	--	--	--	--

Table 1. Periodicities--Continued

Index	2^n	3^m	5^p	7^q	2^n3^m	$2^n3^m5^p$	$2^n3^m5^p7^q$	Obs.	1	2	3	4	5	6	7	8	9	10	11	12
51	--	--	--	--	--	--	--	51	--	--	51(2)	--	--	--	--	--	--	--	--	--
52	--	--	--	--	--	--	--	--	--	--	--	--	--	--	--	--	--	--	--	--
53	--	--	--	--	--	--	--	--	--	--	--	--	--	--	--	--	--	--	--	--
54	--	--	--	--	54	54	54	--	--	--	--	--	--	--	--	--	--	--	--	--
55	--	--	--	--	--	--	--	55	--	--	--	--	--	55	--	--	--	--	--	--
56	--	--	--	--	--	--	56	--	--	--	--	--	--	--	--	--	--	--	--	--
57	--	--	--	--	--	--	--	57	--	--	--	--	--	--	57	--	--	--	--	--
58	--	--	--	--	--	--	--	--	--	--	--	--	--	--	--	--	--	--	--	--
59	--	--	--	--	--	--	--	59	--	--	--	--	59	--	--	--	--	--	--	--
60	--	--	--	--	--	60	60	--	--	--	--	--	--	--	--	--	--	--	--	--
61	--	--	--	--	--	--	--	61	--	--	--	--	--	--	61	--	--	--	--	--
62	--	--	--	--	--	--	--	--	--	--	--	--	--	--	--	--	--	--	--	--
63	--	--	--	--	--	--	63	63	--	--	--	--	--	63	--	--	--	--	--	--
64	64	--	--	--	64	64	64	64	--	--	--	--	--	--	--	--	--	--	--	64
65	--	--	--	--	--	--	--	--	--	--	--	--	--	--	--	--	--	--	--	--
66	--	--	--	--	--	--	--	--	--	--	--	--	--	--	--	--	--	--	--	--
67	--	--	--	--	--	--	--	--	--	--	--	--	--	--	--	--	--	--	--	--
68	--	--	--	--	--	--	--	68	--	--	--	--	--	--	68	--	--	--	68	--
69	--	--	--	--	--	--	--	--	--	--	--	--	--	--	--	--	--	--	--	--
70	--	--	--	--	--	--	70	--	--	--	--	--	--	--	--	--	--	--	--	--
71	--	--	--	--	--	--	--	--	--	--	--	--	--	--	--	--	--	--	--	--
72	--	--	--	--	72	72	72	--	--	--	--	--	--	--	--	--	--	--	--	--
73	--	--	--	--	--	--	--	73	--	--	--	--	--	--	73	--	--	--	--	--
74	--	--	--	--	--	--	--	--	--	--	--	--	--	--	--	--	--	--	--	--
75	--	--	--	--	--	75	75	--	--	--	--	--	--	--	--	--	--	--	--	--
76	--	--	--	--	--	--	--	76	--	--	--	--	--	76	--	--	--	--	--	--
77	--	--	--	--	--	--	--	--	--	--	--	--	--	--	--	--	--	--	--	--
78	--	--	--	--	--	--	--	--	--	--	--	--	--	--	--	--	--	--	--	--
79	--	--	--	--	--	--	--	--	--	--	--	--	--	--	--	--	--	--	--	--
80	--	--	--	--	--	80	80	80	--	--	--	--	80	--	--	--	--	--	--	--
81	--	81	--	--	81	81	81	81	--	--	81	--	--	--	--	--	--	--	--	--
82	--	--	--	--	--	--	--	--	--	--	--	--	--	--	--	--	--	--	--	--
83	--	--	--	--	--	--	--	--	--	--	--	--	--	--	--	--	--	--	--	--
84	--	--	--	--	--	--	84	--	--	--	--	--	--	--	--	--	--	--	--	--
85	--	--	--	--	--	--	--	--	--	--	--	--	--	--	--	--	--	--	--	--
86	--	--	--	--	--	--	--	--	--	--	--	--	--	--	--	--	--	--	--	--
87	--	--	--	--	--	--	--	--	--	--	--	--	--	--	--	--	--	--	--	--
88	--	--	--	--	--	--	--	--	--	--	--	--	--	--	--	--	--	--	--	--
89	--	--	--	--	--	--	--	--	--	--	--	--	--	--	--	--	--	--	--	--
90	--	--	--	--	--	90	90	--	--	--	--	--	--	--	--	--	--	--	--	--
91	--	--	--	--	--	--	--	--	--	--	--	--	--	--	--	--	--	--	--	--
92	--	--	--	--	--	--	--	92	--	--	--	--	--	--	--	--	--	--	92	--
93	--	--	--	--	--	--	--	--	--	--	--	--	--	--	--	--	--	--	--	--
94	--	--	--	--	--	--	--	94	--	--	--	--	--	--	--	--	--	--	94	--
95	--	--	--	--	--	--	--	--	--	--	--	--	--	--	--	--	--	--	--	--
96	--	--	--	--	96	96	96	96	--	--	96	--	--	--	--	--	--	--	--	--
97	--	--	--	--	--	--	--	--	--	--	--	--	--	--	--	--	--	--	--	--
98	--	--	--	--	--	--	98	--	--	--	--	--	--	--	--	--	--	--	--	--
99	--	--	--	--	--	--	--	--	--	--	--	--	--	--	--	--	--	--	--	--
100	--	--	--	--	--	100	100	--	--	--	--	--	--	--	--	--	--	--	--	--

9 Sh

Index	2^n	3^m	5^p	7^q	2^n3^m	$2^n3^m5^p$	$2^n3^m5^p7^q$	Obs.	1	2	3	4	5	6	7	8	9	10	11	12
101	--	--	--	--	--	--	--	--	--	--	--	--	--	--	--	--	--	--	--	--
102	--	--	--	--	--	--	--	--	--	--	--	--	--	--	--	--	--	--	--	--
103	--	--	--	--	--	--	--	--	--	--	--	--	--	--	--	--	--	--	--	--
104	--	--	--	--	--	--	--	104	--	--	--	--	--	--	104	--	--	--	--	--
105	--	--	--	--	--	--	105	--	--	--	--	--	--	--	--	--	--	--	--	--
106	--	--	--	--	--	--	--	--	--	--	--	--	--	--	--	--	--	--	--	--
107	--	--	--	--	--	--	--	--	--	--	--	--	--	--	--	--	--	--	--	--
108	--	--	--	--	108	108	108	--	--	--	--	--	--	--	--	--	--	--	--	--
109	--	--	--	--	--	--	--	--	--	--	--	--	--	--	--	--	--	--	--	--
110	--	--	--	--	--	--	--	--	--	--	--	--	--	--	--	--	--	--	--	--
111	--	--	--	--	--	--	--	--	--	--	--	--	--	--	--	--	--	--	--	--
112	--	--	--	--	--	--	112	--	--	--	--	--	--	--	--	--	--	--	--	--
113	--	--	--	--	--	--	--	--	--	--	--	--	--	--	--	--	--	--	--	--
114	--	--	--	--	--	--	--	114	--	--	--	--	--	--	--	--	--	--	--	114
115	--	--	--	--	--	--	--	115	--	--	--	--	--	115	--	--	--	--	--	--
116	--	--	--	--	--	--	--	--	--	--	--	--	--	--	--	--	--	--	--	--
117	--	--	--	--	--	--	--	--	--	--	--	--	--	--	--	--	--	--	--	--
118	--	--	--	--	--	--	--	--	--	--	--	--	--	--	--	--	--	--	--	--
119	--	--	--	--	--	--	--	--	--	--	--	--	--	--	--	--	--	--	--	--
120	--	--	--	--	--	120	120	--	--	--	--	--	--	--	--	--	--	--	--	--
121	--	--	--	--	--	--	--	--	--	--	--	--	--	--	--	--	--	--	--	--
122	--	--	--	--	--	--	--	--	--	--	--	--	--	--	--	--	--	--	--	--
123	--	--	--	--	--	--	--	--	--	--	--	--	--	--	--	--	--	--	--	--
124	--	--	--	--	--	--	--	--	--	--	--	--	--	--	--	--	--	--	--	--
125	--	--	125	--	--	125	125	--	--	--	--	--	--	--	--	--	--	--	--	--
126	--	--	--	--	--	--	126	--	--	--	--	--	--	--	--	--	--	--	--	--
127	--	--	--	--	--	--	--	--	--	--	--	--	--	--	--	--	--	--	--	--
128	128	--	--	--	128	128	128	--	--	--	--	--	--	--	--	--	--	--	--	--
129	--	--	--	--	--	--	--	--	--	--	--	--	--	--	--	--	--	--	--	--
130	--	--	--	--	--	--	--	--	--	--	--	--	--	--	--	--	--	--	--	--
131	--	--	--	--	--	--	--	--	--	--	--	--	--	--	--	--	--	--	--	--
132	--	--	--	--	--	--	--	--	--	--	--	--	--	--	--	--	--	--	--	--
133	--	--	--	--	--	--	--	--	--	--	--	--	--	--	--	--	--	--	--	--
134	--	--	--	--	--	--	--	134	--	--	--	--	--	--	--	--	--	--	134	--
135	--	--	--	--	--	135	135	--	--	--	--	--	--	--	--	--	--	--	--	--
136	--	--	--	--	--	--	--	--	--	--	--	--	--	--	--	--	--	--	--	--
137	--	--	--	--	--	--	--	--	--	--	--	--	--	--	--	--	--	--	--	--
138	--	--	--	--	--	--	--	--	--	--	--	--	--	--	--	--	--	--	--	--
139	--	--	--	--	--	--	--	--	--	--	--	--	--	--	--	--	--	--	--	--
140	--	--	--	--	--	--	140	140	--	--	--	--	--	--	--	--	--	--	140	--
141	--	--	--	--	--	--	--	--	--	--	--	--	--	--	--	--	--	--	--	--
142	--	--	--	--	--	--	--	--	--	--	--	--	--	--	--	--	--	--	--	--
143	--	--	--	--	--	--	--	--	--	--	--	--	--	--	--	--	--	--	--	--
144	--	--	--	--	144	144	144	--	--	--	--	--	--	--	--	--	--	--	--	--
145	--	--	--	--	--	--	--	--	--	--	--	--	--	--	--	--	--	--	--	--
146	--	--	--	--	--	--	--	--	--	--	--	--	--	--	--	--	--	--	--	--
147	--	--	--	--	--	--	147	--	--	--	--	--	--	--	--	--	--	--	--	--
148	--	--	--	--	--	--	--	--	--	--	--	--	--	--	--	--	--	--	--	--
149	--	--	--	--	--	--	--	--	--	--	--	--	--	--	--	--	--	--	--	--
150	--	--	--	--	--	150	150	--	--	--	--	--	--	--	--	--	--	--	--	--

Index	2^n	3^m	5^p	7^q	2^n3^m	$2^n3^m5^p$	$2^n3^m5^p7^q$	Obs.	1	2	3	4	5	6	7	8	9	10	11	12
151	--	--	--	--	--	--	--	--	--	--	--	--	--	--	--	--	--	--	--	--
152	--	--	--	--	--	--	--	--	--	--	--	--	--	--	--	--	--	--	--	--
153	--	--	--	--	--	--	--	--	--	--	--	--	--	--	--	--	--	--	--	--
154	--	--	--	--	--	--	--	--	--	--	--	--	--	--	--	--	--	--	--	--
155	--	--	--	--	--	--	--	--	--	--	--	--	--	--	--	--	--	--	--	--
156	--	--	--	--	--	--	--	--	--	--	--	--	--	--	--	--	--	--	--	--
157	--	--	--	--	--	--	--	--	--	--	--	--	--	--	--	--	--	--	--	--
158	--	--	--	--	--	--	--	--	--	--	--	--	--	--	--	--	--	--	--	--
159	--	--	--	--	--	--	--	--	--	--	--	--	--	--	--	--	--	--	--	--
160	--	--	--	--	--	160	160	--	--	--	--	--	--	--	--	--	--	--	--	--
161	--	--	--	--	--	--	--	--	--	--	--	--	--	--	--	--	--	--	--	--
162	--	--	--	--	162	162	162	--	--	--	--	--	--	--	--	--	--	--	--	--
163	--	--	--	--	--	--	--	--	--	--	--	--	--	--	--	--	--	--	--	--
164	--	--	--	--	--	--	--	--	--	--	--	--	--	--	--	--	--	--	--	--
165	--	--	--	--	--	--	--	--	--	--	--	--	--	--	--	--	--	--	--	--
166	--	--	--	--	--	--	--	--	--	--	--	--	--	--	--	--	--	--	--	--
167	--	--	--	--	--	--	--	--	--	--	--	--	--	--	--	--	--	--	--	--
168	--	--	--	--	--	--	168	--	--	--	--	--	--	--	--	--	--	--	--	--
169	--	--	--	--	--	--	--	--	--	--	--	--	--	--	--	--	--	--	--	--
170	--	--	--	--	--	--	--	--	--	--	--	--	--	--	--	--	--	--	--	--
171	--	--	--	--	--	--	--	--	--	--	--	--	--	--	--	--	--	--	--	--
172	--	--	--	--	--	--	--	--	--	--	--	--	--	--	--	--	--	--	--	--
173	--	--	--	--	--	--	--	--	--	--	--	--	--	--	--	--	--	--	--	--
174	--	--	--	--	--	--	--	--	--	--	--	--	--	--	--	--	--	--	--	--
175	--	--	--	--	--	--	175	--	--	--	--	--	--	--	--	--	--	--	--	--
176	--	--	--	--	--	--	--	--	--	--	--	--	--	--	--	--	--	--	--	--
177	--	--	--	--	--	--	--	--	--	--	--	--	--	--	--	--	--	--	--	--
178	--	--	--	--	--	--	--	--	--	--	--	--	--	--	--	--	--	--	--	--
179	--	--	--	--	--	--	--	--	--	--	--	--	--	--	--	--	--	--	--	--
180	--	--	--	--	--	180	180	--	--	--	--	--	--	--	--	--	--	--	--	--
181	--	--	--	--	--	--	--	--	--	--	--	--	--	--	--	--	--	--	--	--
182	--	--	--	--	--	--	--	--	--	--	--	--	--	--	--	--	--	--	--	--
183	--	--	--	--	--	--	--	--	--	--	--	--	--	--	--	--	--	--	--	--
184	--	--	--	--	--	--	--	--	--	--	--	--	--	--	--	--	--	--	--	--
185	--	--	--	--	--	--	--	--	--	--	--	--	--	--	--	--	--	--	--	--
186	--	--	--	--	--	--	--	--	--	--	--	--	--	--	--	--	--	--	--	--
187	--	--	--	--	--	--	--	--	--	--	--	--	--	--	--	--	--	--	--	--
188	--	--	--	--	--	--	--	--	--	--	--	--	--	--	--	--	--	--	--	--
189	--	--	--	--	--	--	189	--	--	--	--	--	--	--	--	--	--	--	--	--
190	--	--	--	--	--	--	--	--	--	--	--	--	--	--	--	--	--	--	--	--
191	--	--	--	--	--	--	--	--	--	--	--	--	--	--	--	--	--	--	--	--
192	--	--	--	--	192	192	192	--	--	--	--	--	--	--	--	--	--	--	--	--
193	--	--	--	--	--	--	--	--	--	--	--	--	--	--	--	--	--	--	--	--
194	--	--	--	--	--	--	--	--	--	--	--	--	--	--	--	--	--	--	--	--
195	--	--	--	--	--	--	--	--	--	--	--	--	--	--	--	--	--	--	--	--
196	--	--	--	--	--	--	196	--	--	--	--	--	--	--	--	--	--	--	--	--
197	--	--	--	--	--	--	--	--	--	--	--	--	--	--	--	--	--	--	--	--
198	--	--	--	--	--	--	--	--	--	--	--	--	--	--	--	--	--	--	--	--
199	--	--	--	--	--	--	--	--	--	--	--	--	--	--	--	--	--	--	--	--
200	--	--	--	--	--	200	200	--	--	--	--	--	--	--	--	--	--	--	--	--

Index	2^n	3^m	5^p	7^q	2^n3^m	$2^n3^m5^p$	$2^n3^m5^p7^q$	Obs.	1	2	3	4	5	6	7	8	9	10	11	12
201	--	--	--	--	--	--	--	--	--	--	--	--	--	--	--	--	--	--	--	--
202	--	--	--	--	--	--	--	--	--	--	--	--	--	--	--	--	--	--	--	--
203	--	--	--	--	--	--	--	--	--	--	--	--	--	--	--	--	--	--	--	--
204	--	--	--	--	--	--	--	--	--	--	--	--	--	--	--	--	--	--	--	--
205	--	--	--	--	--	--	--	--	--	--	--	--	--	--	--	--	--	--	--	--
206	--	--	--	--	--	--	--	--	--	--	--	--	--	--	--	--	--	--	--	--
207	--	--	--	--	--	--	--	--	--	--	--	--	--	--	--	--	--	--	--	--
209	--	--	--	--	--	--	--	--	--	--	--	--	--	--	--	--	--	--	--	--
210	--	--	--	--	--	--	210	--	--	--	--	--	--	--	--	--	--	--	--	--
211	--	--	--	--	--	--	--	--	--	--	--	--	--	--	--	--	--	--	--	--
212	--	--	--	--	--	--	--	--	--	--	--	--	--	--	--	--	--	--	--	--
213	--	--	--	--	--	--	--	--	--	--	--	--	--	--	--	--	--	--	--	--
214	--	--	--	--	--	--	--	--	--	--	--	--	--	--	--	--	--	--	--	--
215	--	--	--	--	--	--	--	--	--	--	--	--	--	--	--	--	--	--	--	--
216	--	--	--	--	216	216	216	--	--	--	--	--	--	--	--	--	--	--	--	--
217	--	--	--	--	--	--	--	--	--	--	--	--	--	--	--	--	--	--	--	--
218	--	--	--	--	--	--	--	--	--	--	--	--	--	--	--	--	--	--	--	--
219	--	--	--	--	--	--	--	--	--	--	--	--	--	--	--	--	--	--	--	--
220	--	--	--	--	--	--	--	--	--	--	--	--	--	--	--	--	--	--	--	--
221	--	--	--	--	--	--	--	--	--	--	--	--	--	--	--	--	--	--	--	--
222	--	--	--	--	--	--	--	--	--	--	--	--	--	--	--	--	--	--	--	--
223	--	--	--	--	--	--	--	--	--	--	--	--	--	--	--	--	--	--	--	--
224	--	--	--	--	--	--	224	--	--	--	--	--	--	--	--	--	--	--	--	--
225	--	--	--	--	--	225	225	225**	--	--	--	--	--	--	--	--	--	--	225**	--
226	--	--	--	--	--	--	--	--	--	--	--	--	--	--	--	--	--	--	--	--
227	--	--	--	--	--	--	--	--	--	--	--	--	--	--	--	--	--	--	--	--
228	--	--	--	--	--	--	--	--	--	--	--	--	--	--	--	--	--	--	--	--
229	--	--	--	--	--	--	--	--	--	--	--	--	--	--	--	--	--	--	--	--
230	--	--	--	--	--	--	--	--	--	--	--	--	--	--	--	--	--	--	--	--
231	--	--	--	--	--	--	--	--	--	--	--	--	--	--	--	--	--	--	--	--
232	--	--	--	--	--	--	--	--	--	--	--	--	--	--	--	--	--	--	--	--
233	--	--	--	--	--	--	--	233*	--	--	--	--	--	--	--	--	--	--	233*	--
234	--	--	--	--	--	--	--	--	--	--	--	--	--	--	--	--	--	--	--	--
235	--	--	--	--	--	--	--	--	--	--	--	--	--	--	--	--	--	--	--	--
236	--	--	--	--	--	--	--	--	--	--	--	--	--	--	--	--	--	--	--	--
237	--	--	--	--	--	--	--	--	--	--	--	--	--	--	--	--	--	--	--	--
238	--	--	--	--	--	--	--	--	--	--	--	--	--	--	--	--	--	--	--	--
239	--	--	--	--	--	--	--	--	--	--	--	--	--	--	--	--	--	--	--	--
240	--	--	--	--	--	240	240	--	--	--	--	--	--	--	--	--	--	--	--	--
241	--	--	--	--	--	--	--	--	--	--	--	--	--	--	--	--	--	--	--	--
242	--	--	--	--	--	--	--	--	--	--	--	--	--	--	--	--	--	--	--	--
243	--	243	--	--	243	243	243	--	--	--	--	--	--	--	--	--	--	--	--	--
244	--	--	--	--	--	--	--	--	--	--	--	--	--	--	--	--	--	--	--	--
245	--	--	--	--	--	--	245	--	--	--	--	--	--	--	--	--	--	--	--	--
246	--	--	--	--	--	--	--	--	--	--	--	--	--	--	--	--	--	--	--	--
247	--	--	--	--	--	--	--	--	--	--	--	--	--	--	--	--	--	--	--	--
248	--	--	--	--	--	--	--	--	--	--	--	--	--	--	--	--	--	--	--	--
249	--	--	--	--	--	--	--	--	--	--	--	--	--	--	--	--	--	--	--	--
250	--	--	--	--	--	250	250	--	--	--	--	--	--	--	--	--	--	--	--	--

Index	2^n	3^m	5^p	7^q	2^n3^m	$2^n3^m5^p$	$2^n3^m5^p7^q$	Obs.	1	2	3	4	5	6	7	8	9	10	11	12
251	--	--	--	--	--	--	--	--	--	--	--	--	--	--	--	--	--	--	--	--
252	--	--	--	--	--	--	252	--	--	--	--	--	--	--	--	--	--	--	--	--
253	--	--	--	--	--	--	--	--	--	--	--	--	--	--	--	--	--	--	--	--
254	--	--	--	--	--	--	--	254	--	--	--	--	--	--	--	--	--	--	--	254
255	--	--	--	--	--	--	--	--	--	--	--	--	--	--	--	--	--	--	--	--
256	256	--	--	--	256	256	256	--	--	--	--	--	--	--	--	--	--	--	--	--
257	--	--	--	--	--	--	--	--	--	--	--	--	--	--	--	--	--	--	--	--
258	--	--	--	--	--	--	--	--	--	--	--	--	--	--	--	--	--	--	--	--
259	--	--	--	--	--	--	--	--	--	--	--	--	--	--	--	--	--	--	--	--
260	--	--	--	--	--	--	--	--	--	--	--	--	--	--	--	--	--	--	--	--
261	--	--	--	--	--	--	--	--	--	--	--	--	--	--	--	--	--	--	--	--
262	--	--	--	--	--	--	--	--	--	--	--	--	--	--	--	--	--	--	--	--
263	--	--	--	--	--	--	--	--	--	--	--	--	--	--	--	--	--	--	--	--
264	--	--	--	--	--	--	--	--	--	--	--	--	--	--	--	--	--	--	--	--
265	--	--	--	--	--	--	--	--	--	--	--	--	--	--	--	--	--	--	--	--
266	--	--	--	--	--	--	--	--	--	--	--	--	--	--	--	--	--	--	--	--
267	--	--	--	--	--	--	--	--	--	--	--	--	--	--	--	--	--	--	--	--
268	--	--	--	--	--	--	--	--	--	--	--	--	--	--	--	--	--	--	--	--
269	--	--	--	--	--	--	--	--	--	--	--	--	--	--	--	--	--	--	--	--
270	--	--	--	--	--	270	270	--	--	--	--	--	--	--	--	--	--	--	--	--
271	--	--	--	--	--	--	--	--	--	--	--	--	--	--	--	--	--	--	--	--
272	--	--	--	--	--	--	--	--	--	--	--	--	--	--	--	--	--	--	--	--
273	--	--	--	--	--	--	--	--	--	--	--	--	--	--	--	--	--	--	--	--
274	--	--	--	--	--	--	--	--	--	--	--	--	--	--	--	--	--	--	--	--
275	--	--	--	--	--	--	--	--	--	--	--	--	--	--	--	--	--	--	--	--
276	--	--	--	--	--	--	--	--	--	--	--	--	--	--	--	--	--	--	--	--
277	--	--	--	--	--	--	--	--	--	--	--	--	--	--	--	--	--	--	--	--
278	--	--	--	--	--	--	--	--	--	--	--	--	--	--	--	--	--	--	--	--
279	--	--	--	--	--	--	--	--	--	--	--	--	--	--	--	--	--	--	--	--
280	--	--	--	--	--	--	280	280	--	--	--	--	--	--	--	--	--	--	--	280
281	--	--	--	--	--	--	--	--	--	--	--	--	--	--	--	--	--	--	--	--
282	--	--	--	--	--	--	--	--	--	--	--	--	--	--	--	--	--	--	--	--
283	--	--	--	--	--	--	--	--	--	--	--	--	--	--	--	--	--	--	--	--
284	--	--	--	--	--	--	--	--	--	--	--	--	--	--	--	--	--	--	--	--
285	--	--	--	--	--	--	--	285	--	--	--	--	--	--	--	--	--	--	--	285
286	--	--	--	--	--	--	--	--	--	--	--	--	--	--	--	--	--	--	--	--
287	--	--	--	--	--	--	--	--	--	--	--	--	--	--	--	--	--	--	--	--
288	--	--	--	--	288	288	288	--	--	--	--	--	--	--	--	--	--	--	--	--
289	--	--	--	--	--	--	--	--	--	--	--	--	--	--	--	--	--	--	--	--
290	--	--	--	--	--	--	--	--	--	--	--	--	--	--	--	--	--	--	--	--
291	--	--	--	--	--	--	--	--	--	--	--	--	--	--	--	--	--	--	--	--
292	--	--	--	--	--	--	--	--	--	--	--	--	--	--	--	--	--	--	--	--
293	--	--	--	--	--	--	--	--	--	--	--	--	--	--	--	--	--	--	--	--
294	--	--	--	--	--	--	294	--	--	--	--	--	--	--	--	--	--	--	--	--
295	--	--	--	--	--	--	--	--	--	--	--	--	--	--	--	--	--	--	--	--
296	--	--	--	--	--	--	--	--	--	--	--	--	--	--	--	--	--	--	--	--
297	--	--	--	--	--	--	--	--	--	--	--	--	--	--	--	--	--	--	--	--
298	--	--	--	--	--	--	--	--	--	--	--	--	--	--	--	--	--	--	--	--
299	--	--	--	--	--	--	--	--	--	--	--	--	--	--	--	--	--	--	--	--
300	--	--	--	--	--	300	300	--	--	--	--	--	--	--	--	--	--	--	--	--

Index	2^n	3^m	5^p	7^q	2^n3^m	$2^n3^m5^p$	$2^n3^m5^p7^q$	Obs.	1	2	3	4	5	6	7	8	9	10	11	12
301	--	--	--	--	--	--	--	--	--	--	--	--	--	--	--	--	--	--	--	--
302	--	--	--	--	--	--	--	--	--	--	--	--	--	--	--	--	--	--	--	--
303	--	--	--	--	--	--	--	--	--	--	--	--	--	--	--	--	--	--	--	--
304	--	--	--	--	--	--	--	--	--	--	--	--	--	--	--	--	--	--	--	--
305	--	--	--	--	--	--	--	--	--	--	--	--	--	--	--	--	--	--	--	--
306	--	--	--	--	--	--	--	--	--	--	--	--	--	--	--	--	--	--	--	--
307	--	--	--	--	--	--	--	--	--	--	--	--	--	--	--	--	--	--	--	--
308	--	--	--	--	--	--	--	--	--	--	--	--	--	--	--	--	--	--	--	--
309	--	--	--	--	--	--	--	--	--	--	--	--	--	--	--	--	--	--	--	--
310	--	--	--	--	--	--	--	--	--	--	--	--	--	--	--	--	--	--	--	--
311	--	--	--	--	--	--	--	--	--	--	--	--	--	--	--	--	--	--	--	--
312	--	--	--	--	--	--	--	--	--	--	--	--	--	--	--	--	--	--	--	--
313	--	--	--	--	--	--	--	--	--	--	--	--	--	--	--	--	--	--	--	--
314	--	--	--	--	--	--	--	--	--	--	--	--	--	--	--	--	--	--	--	--
315	--	--	--	--	--	--	315	--	--	--	--	--	--	--	--	--	--	--	--	--
316	--	--	--	--	--	--	--	--	--	--	--	--	--	--	--	--	--	--	--	--
317	--	--	--	--	--	--	--	--	--	--	--	--	--	--	--	--	--	--	--	--
318	--	--	--	--	--	--	--	--	--	--	--	--	--	--	--	--	--	--	--	--
319	--	--	--	--	--	--	--	--	--	--	--	--	--	--	--	--	--	--	--	--
320	--	--	--	--	--	320	320	--	--	--	--	--	--	--	--	--	--	--	--	--
321	--	--	--	--	--	--	--	--	--	--	--	--	--	--	--	--	--	--	--	--
322	--	--	--	--	--	--	--	--	--	--	--	--	--	--	--	--	--	--	--	--
323	--	--	--	--	--	--	--	--	--	--	--	--	--	--	--	--	--	--	--	--
324	--	--	--	--	324	324	324	--	--	--	--	--	--	--	--	--	--	--	--	--
325	--	--	--	--	--	--	--	--	--	--	--	--	--	--	--	--	--	--	--	--

a. Entries are given for all numerical periods in combinations of the geometric series 2^n, 3^m, 5^p, and 7^q. Numbered columns give time intervals between events for various geologic processes (numbers in parentheses indicate multiple values of the same time interval). The column headed Obs. is a summary of observed time intervals from all data sources:

1. Extinction maxima during latest 250 Myr from Raup and Sepkoski (1984).
2. Maxima of impact cratering during latest 250 Myr (crater diameters exceeding 10 km) from Alvarez and Muller (1984).
3. Maxima of impact cratering during Phanerozoic (all crater diameters) from Figure 11A of this paper.
4. Volume rate maxima of Hawaiian-Emperor magmatism during the latest 73 Myr from Shaw et al. (1980), and Mesozoic Sierra Nevada intrusive events from Kistler et al. (1971).
5. Maxima of $^{87}Sr/^{86}Sr$ variations in the oceans throughout the Phanerozoic from Burke et al. (1982).
6. Phanerozoic extinction maxima from Newell (1982).
7. Phanerozoic origination maxima from Newell (1982).
8. Extinction maxima of ocean ostracodes during the latest 70 Myr from Benson et al. (1984).
9. Peak events of Avian radiation during the latest 130 Myr from Figure 16 of this paper.
10. Galactic plane crossings by the solar system during the latest 260 Myr from Innanen et al. (1978).
11. Maxima of galactic density variations in the Sun's vicinity during the latest 600 Myr from Innanen et al. (1978); the entry 233* is the nominal galactic year according to Innanen et al. (1978), and the entry 225** is the galactic year according to Rubin et al (1983).
12. Maxima of geomagnetic reversal frequencies from Moberly and Campbell (1984), Mazaud et al. (1983), Negi and Tiwari (1983), and Tarling (1983).

Figure 1. Age calibration for Hawaiian-Emperor volcanism as given by Shaw et al. (1980). The upper graph shows observed ages with least squares regression lines; the bottom graph shows the distribution of distances and inferred ages for all volcanic edifices in the chain as recorded in Tables 1 and 2 of the above reference. Note: The right-hand side of Table 2 in Shaw et al. (1980) is misaligned in the upper right quadrant; each row in columns 5 to 9 is off by one row down to Volcano No. 49 (i.e., No. 49 is age 20.9, volume 2.2; No. 1 is age 0, volume 19.4, and so on):.

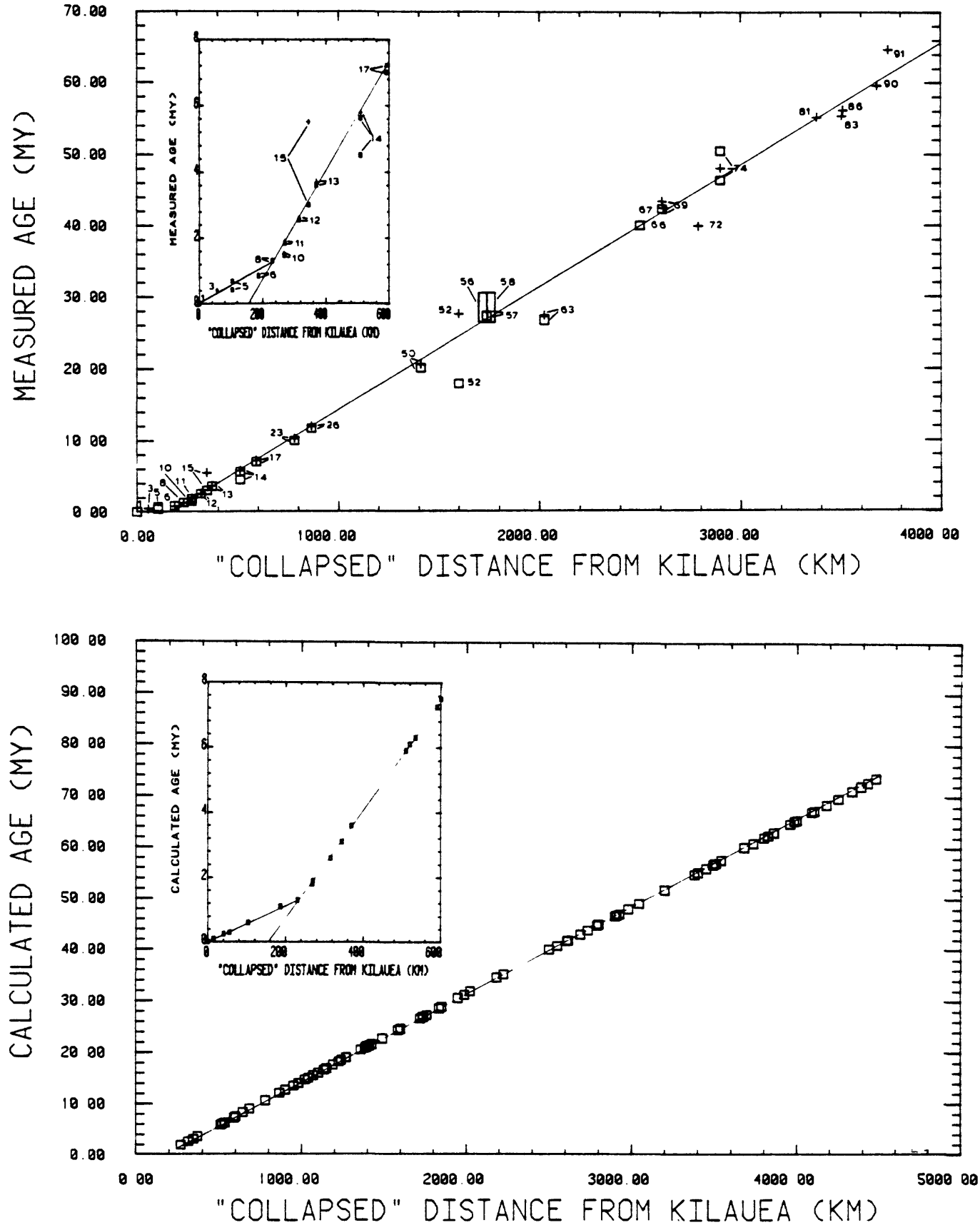
MEASURED AGE (MY)
"COLLAPSED" DISTANCE FROM KILAUEA (KM)
CALCULATED AGE (MY)
"COLLAPSED" DISTANCE FROM KILAUEA (KM)

Fig.1

Figure 2. Compilation showing time variations of unsmoothed H-E data from Shaw et al. (1980). The plot of tangent azimuths indicates the age sequences for numbered volcanoes. The dashed curve for propagation rates represents the ratio of values $(\Delta V/\Delta t)/(\Delta V/\Delta x)$, hence it is a measure of the coherence between the various sets of volume-distance-age data.

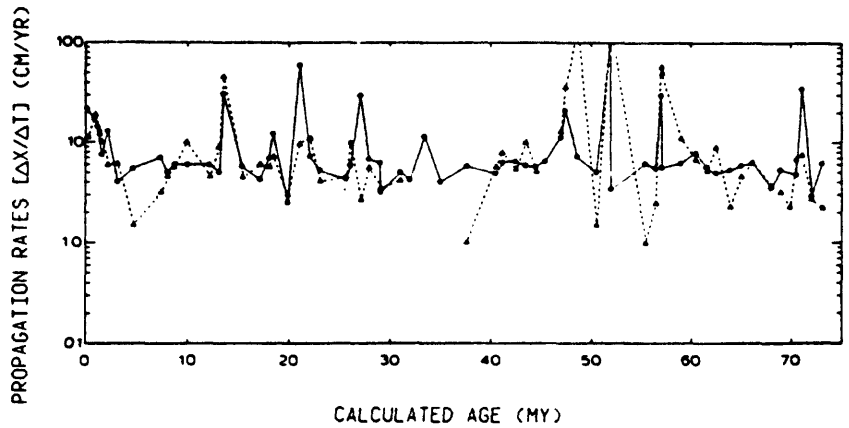
PROPAGATION RATES [ΔX/ΔT] (CM/YR)
100
10
1
0
10
20
30
40
50
60
70
CALCULATED AGE (MY)

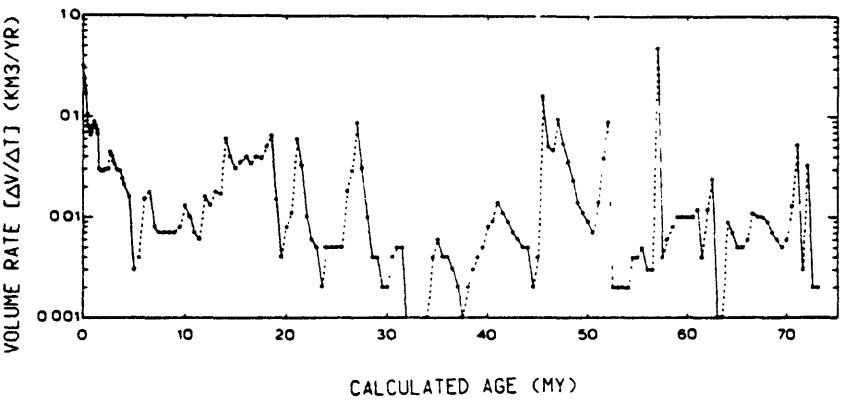
VOLUME RATE [ΔV/ΔT] (KM3/YR)
1
0.1
0.01
0.001
0
10
20
30
40
50
60
70
CALCULATED AGE (MY)

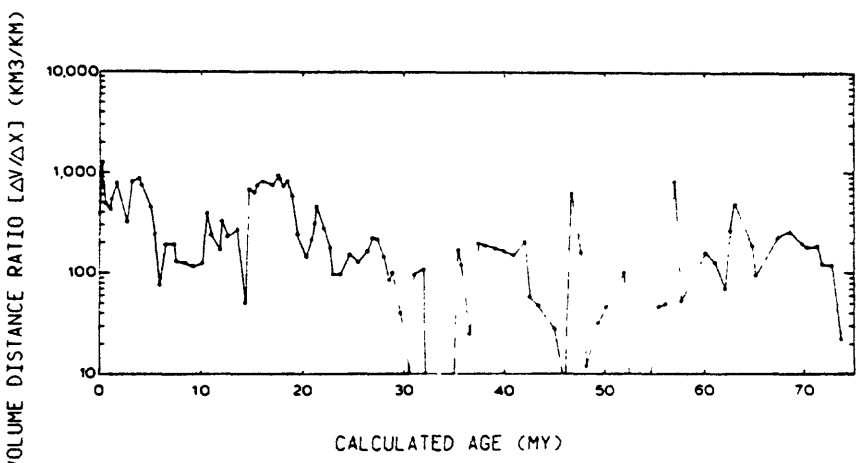
VOLUME DISTANCE RATIO [ΔV/ΔX] (KM3/KM)
10,000
1,000
100
10
0
10
20
30
40
50
60
70
CALCULATED AGE (MY)

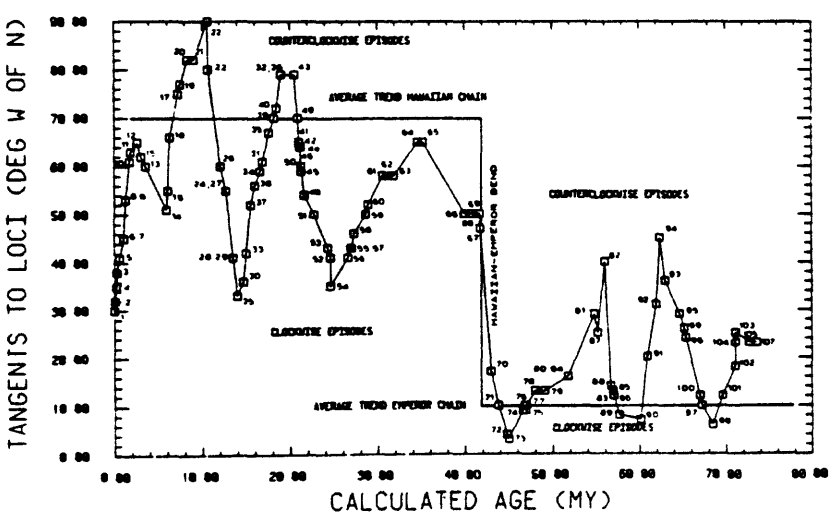
TANGENTS TO LOCI (DEG W OF N)
CALCULATED AGE (MY)
AVERAGE TREND HAWAIIAN CHAIN
AVERAGE TREND EMPEROR CHAIN
HAWAIIAN-EMPEROR BEND

Fig.2

Figure 3. Moving window averages for H-E tangent azimuth data from Tables 1 and 2 of Shaw et al. (1980) using a 4 Myr window with shifts of 2 Myr. Notice that dominant peak locations are about the same as in Figure 2, but minor peaks are suppressed. For reference, curves are shown for geomagnetic reversal frequencies redrawn from Mazaud et al. (1983) and for the smoothed cratering frequencies redrawn from Alvarez and Muller (1984); compare with Figure 11A in this paper. Vertical lines represent the peak positions of the three latest extinction events of Raup and Sepkoski (1984). Variations in the average lengths of geomagnetic polarity intervals are also shown (broken curve), redrawn from Moberly and Campbell (1984). Note correlation of maxima with curve of azimuth variations. In Hawaiian portion synchronization of maxima is almost exact; in Emperor portion form is similar but timing is out of phase, or age correlations disagree (geomagnetic time scale is that of Lowrie and Alvarez, 1981, while azimuth events are age calibration of Shaw et al. 1980). If azimuth events refer to plate motions (Jackson and Shaw, 1975), then geomagnetic correlation reflects signature of plate motions. As discussed in text, this suggests that core dynamo may respond in part to 'outside-in' magnetic signatures rather than being only causative mechanism. Cause-effect correlations suggested by Moberly and Campbell (1984) are not supported (cf., Figures 7 and 10).

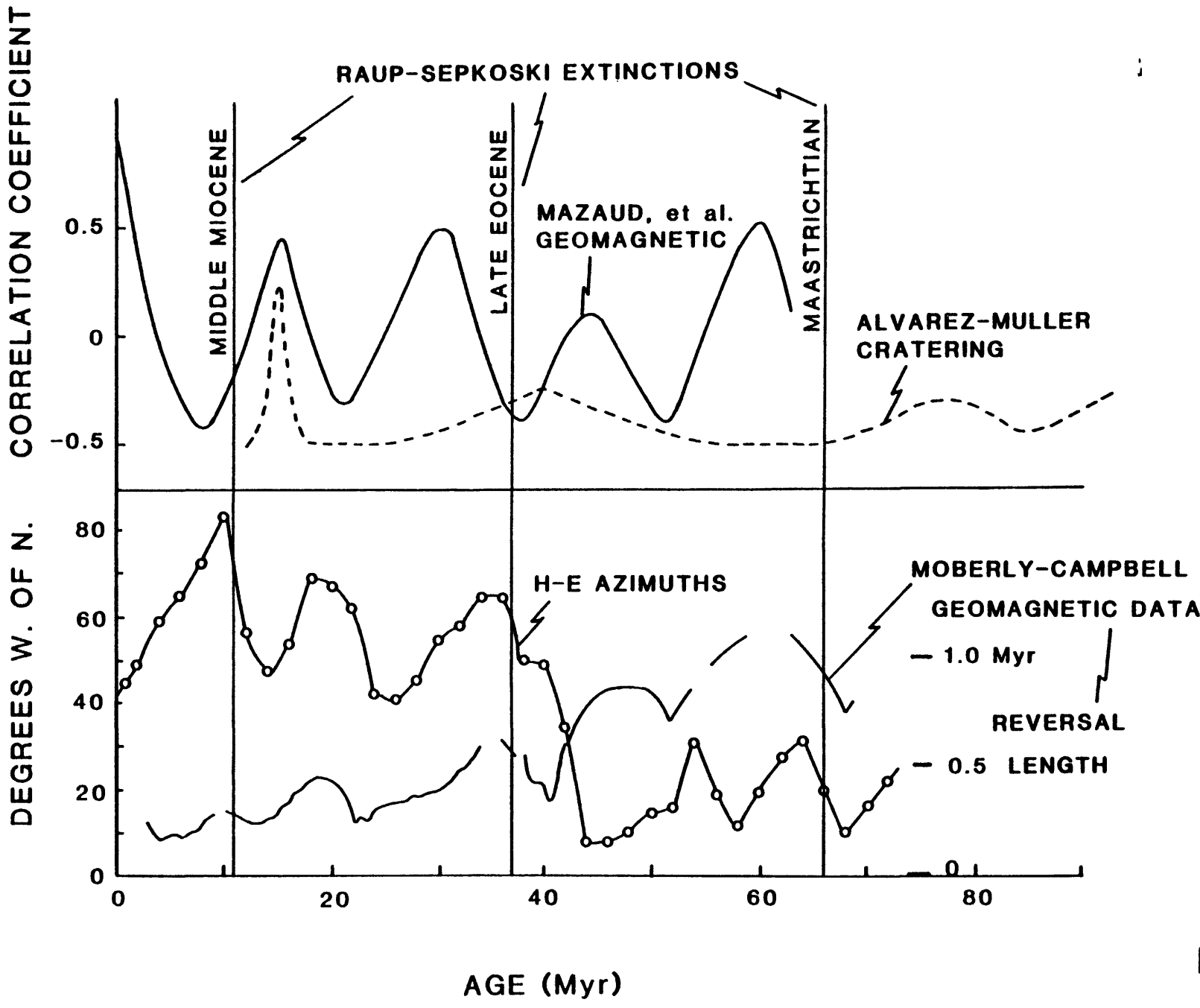
CORRELATION COEFFICIENT
0.5
0
-0.5
RAUP-SEPKOSKI EXTINCTIONS
MIDDLE MIOCENE
LATE EOCENE
MAASTRICHTIAN
MAZAUD, et al.
GEOMAGNETIC
ALVAREZ-MULLER
CRATERING
DEGREES W. OF N.
80
60
40
20
0
H-E AZIMUTHS
MOBERLY-CAMPBELL
GEOMAGNETIC DATA
— 1.0 Myr
REVERSAL
— 0.5 LENGTH
0
0
20
40
60
80
AGE (Myr)

Fig.3

Figure 4. Moving window averages as in Figure 3 for H-E edifice volumes (top) and average volumes per unit length of the chain (bottom). Peak positions are essentially the same in these two graphs (average volume peak at 4 Myr in upper graph is in part artifact of truncation at zero age; this occurs despite fact that youngest volcanoes are the most voluminous because several low-volume edifices in numerous volcanoes of latest 4 Myr bring average down). Reference curves as given in Figure 3.

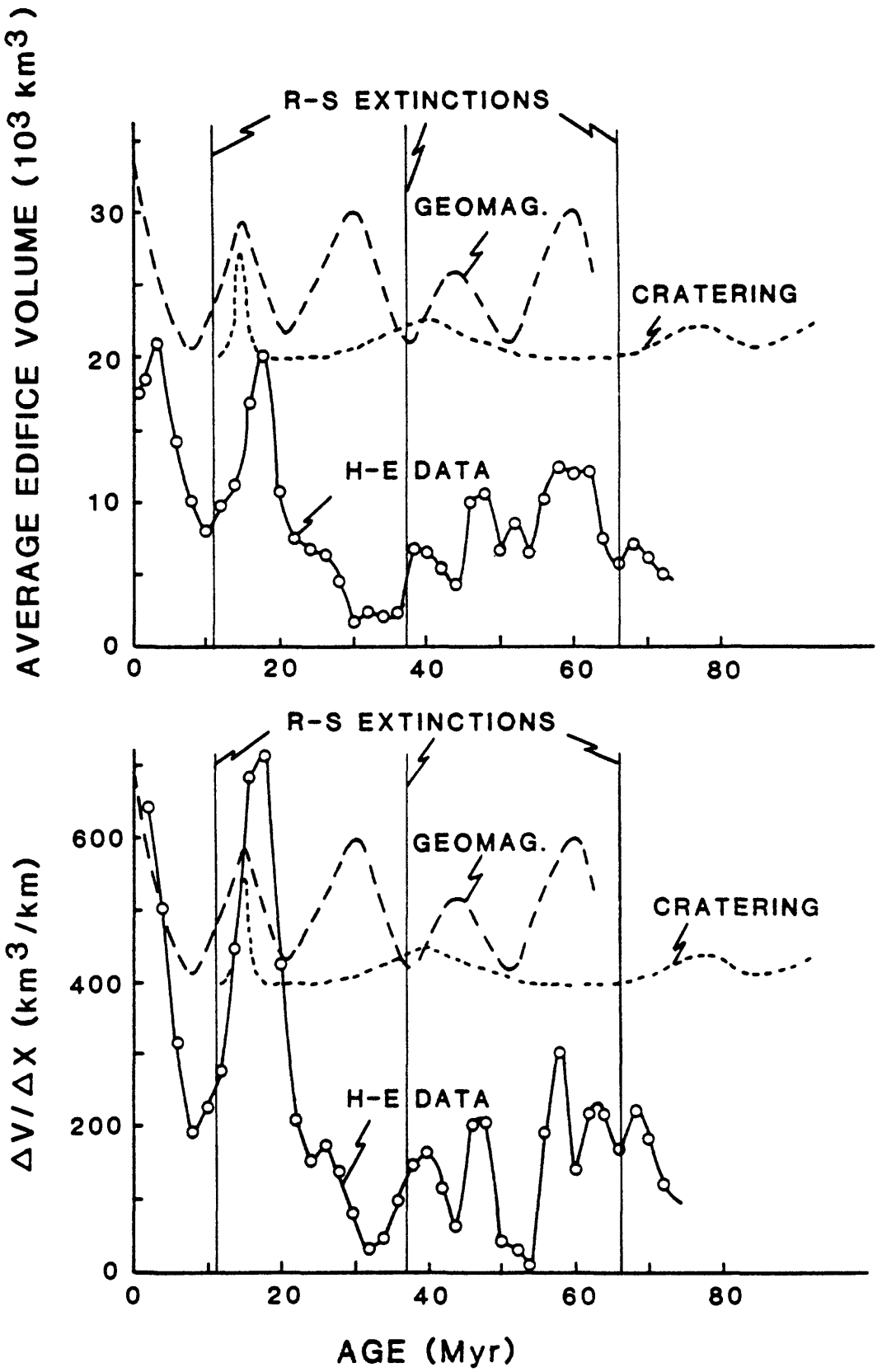
AVERAGE EDIFICE VOLUME (10^3 km^3)
R-S EXTINCTIONS
GEOMAG.
CRATERING
H-E DATA
0
10
20
30
0
20
40
60
80
$\Delta V/\Delta X$ (km^3/km)
R-S EXTINCTIONS
GEOMAG.
CRATERING
H-E DATA
0
200
400
600
0
20
40
60
80
AGE (Myr)

Fig.4

Figure 5. Moving window averages for H-E volume rates (top) and propagation rates (bottom) of data as in Figure 3. Propagation rates at 45 to 55 Myr are partially artifacts of extreme apparent melting rates during synchronous activitiy on straight segments of Emperor loci (also causing greater age ambiguity in method of correlating azimuths). Coherence of peaks at 15 Myr is noted (in Figure 4 peaks are at about 18 Myr, but in Figure 3 an azimuth reversal occurs at about 15 Myr; see Jackson and Shaw, 1975, and Jackson et al., 1975). Reference curves as in Figure 3.

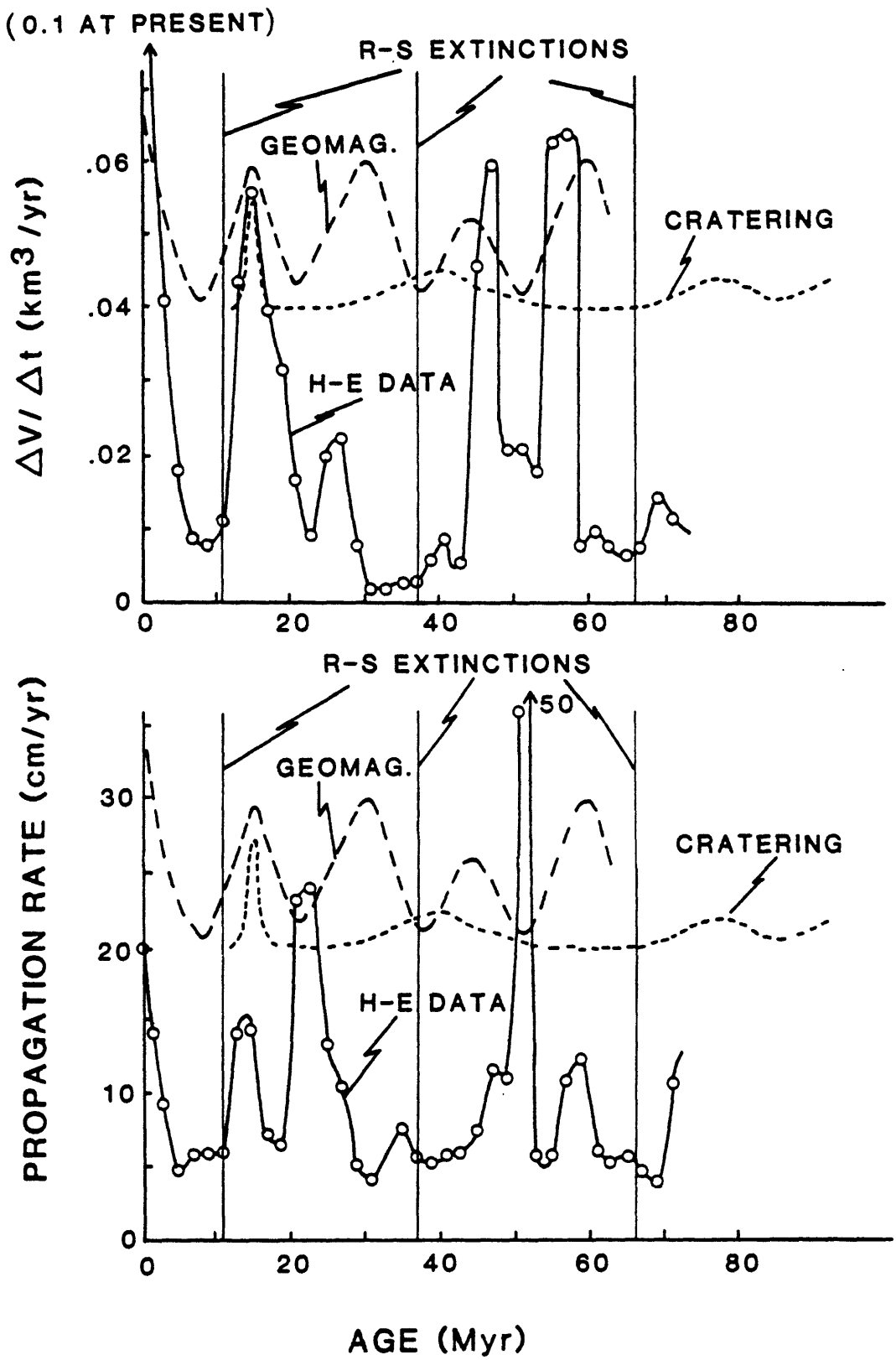
(0.1 AT PRESENT)
R-S EXTINCTIONS
GEOMAG.
CRATERING
H-E DATA
ΔV/ Δt (km³/yr)
.06
.04
.02
0
0
20
40
60
80
R-S EXTINCTIONS
50
GEOMAG.
CRATERING
H-E DATA
PROPAGATION RATE (cm/yr)
30
20
10
0
0
20
40
60
80
AGE (Myr)

Fig.5

Figure 6. Cumulative edifice volumes for the H-E chain. Data points (crosses) obtained by plotting data from Table 2 of Shaw et al. (1980) on large graph and interpolating at 0.4 Myr intervals. Average rate is based on the total volume divided by the total age. Step-like episodes are equivalent to variations of Figure 5, but incremental effects are smoothed differently (see Figure 7).

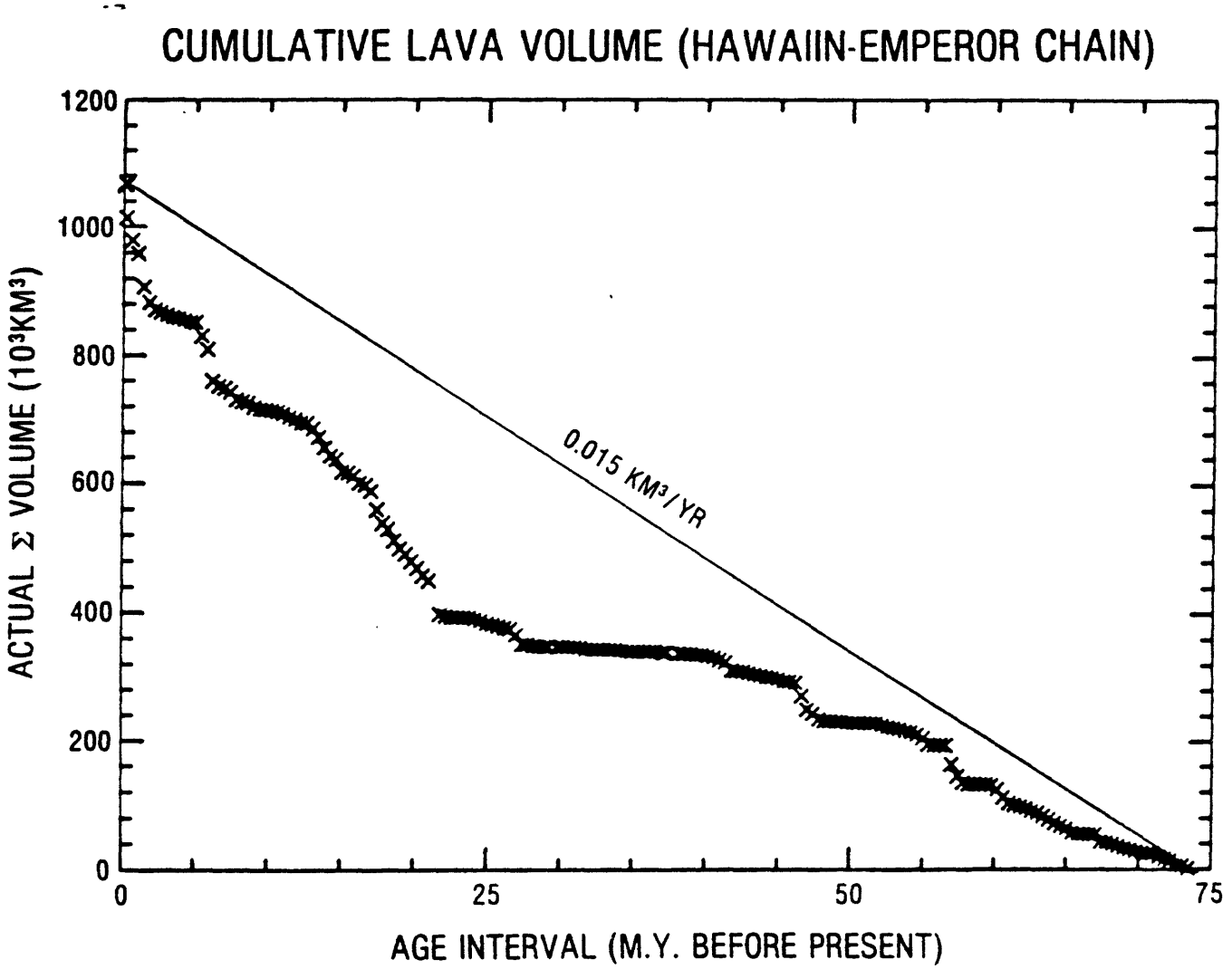
CUMULATIVE LAVA VOLUME (HAWAIIN-EMPEROR CHAIN)
ACTUAL Σ VOLUME (10³KM³)
1200
1000
800
600
400
200
0
0.015 KM³/YR
0
25
50
75
AGE INTERVAL (M.Y. BEFORE PRESENT)

Fig.6

Figure 7. Rate episodes of H-E chain from cumulative volume data.

A. Differences between observed cumulative volume and cumulative volume calculated from the mean rate of 0.015 km^3/yr in Figure 6. Positive slopes correspond to rates smaller than mean rate (increasing difference with decreasing age) and negative slopes to rates larger than mean rate. History was of generally decreasing rates with episodes of accelerations between 74 and 22 Myr; the Hawaiian segment younger than 22 Myr was of generally increasing rates with episodes of deceleration (overall variation identifies long-term oscillation of 70 Myr or more, but oldest portion too uncertain to identify possible maximum). Numbers indicate rate reversals thought to mark significant shifts in dynamic balances; rate maxima (steepest negative slopes) reflect maxima of magma generation (see B). Profile at bottom of A (also at top of B) tracks variations in geomagnetic polarity signature of Hawaiian-Emperor chain according to Moberly and Campbell (1984) based on time scale of Lowrie and Alvarez (1981). Correlation may exist between high normal polarity percentage and slope reversals in magma transport rates (positive and negative) but not with peaks of magma transport rates (see B).

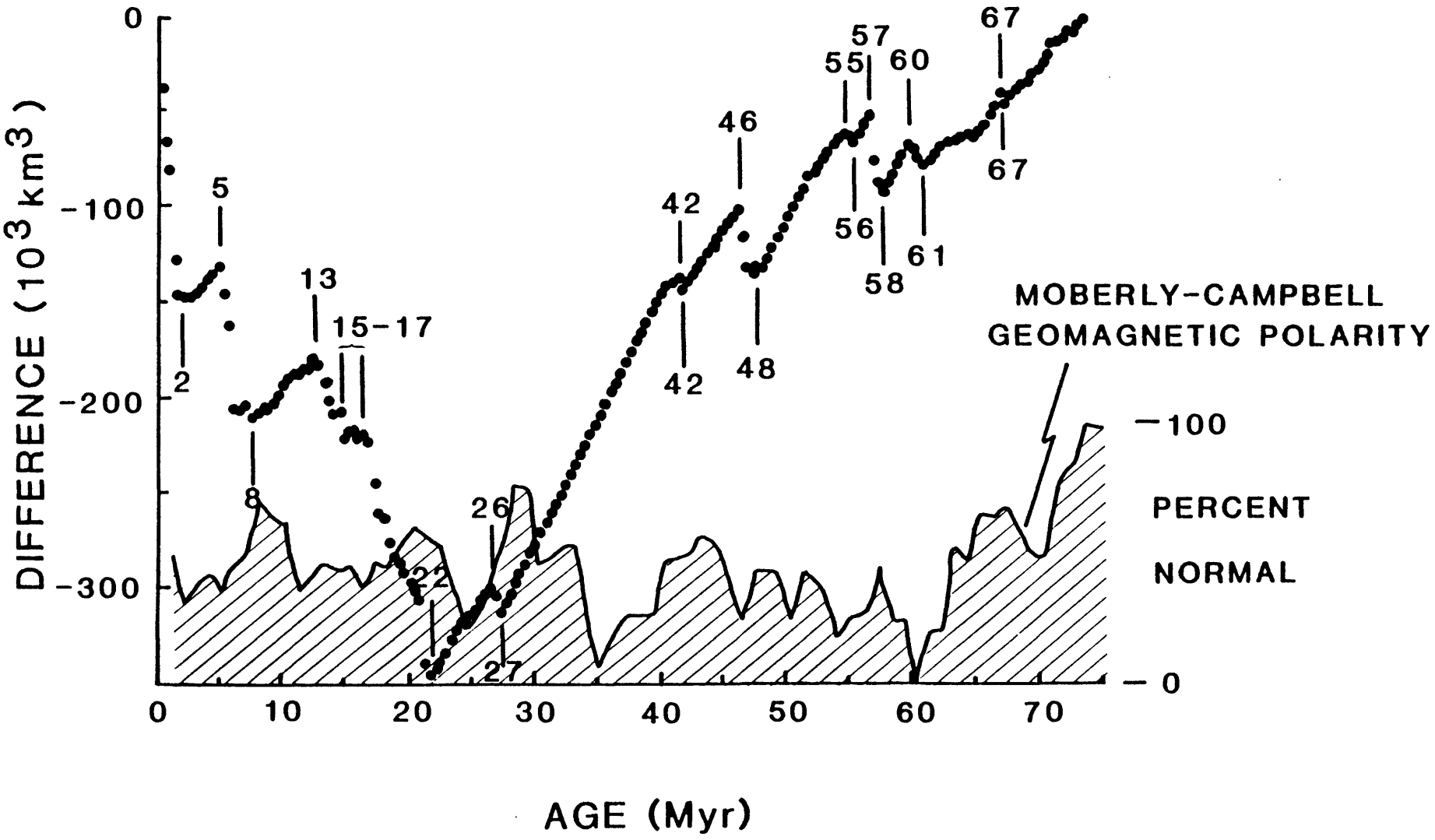
DIFFERENCE (10^3 km^3)
0
-100
-200
-300
0
10
20
30
40
50
60
70
AGE (Myr)
2
5
8
13
15-17
22
26
27
42
42
46
48
55
56
57
58
60
61
67
67
MOBERLY-CAMPBELL
GEOMAGNETIC POLARITY
-100
PERCENT
NORMAL
-0

Fig.7A

Figure 7. Rate episodes of H-E chain from cumulative volume data.

B. Mean slopes of difference curve in A (mean rate in Figure 6 is zero line). Horizontal bars indicate durations of rate episodes; peak intervals differ from times of change in slope except for accelerative episodes that nearly coincide with positive-negative reversals. This graph has more episodes than moving window plots because of finer resolution; peak-to-peak intervals are included in Table 1. One-to-one correlation of magma transport maxima with normal polarity peaks not evident, in contrast with Moberly and Campbell (1984), but higher average normal polarity goes with higher average transport rates as they concluded (Hawaiian portion is generally greater in both cases).

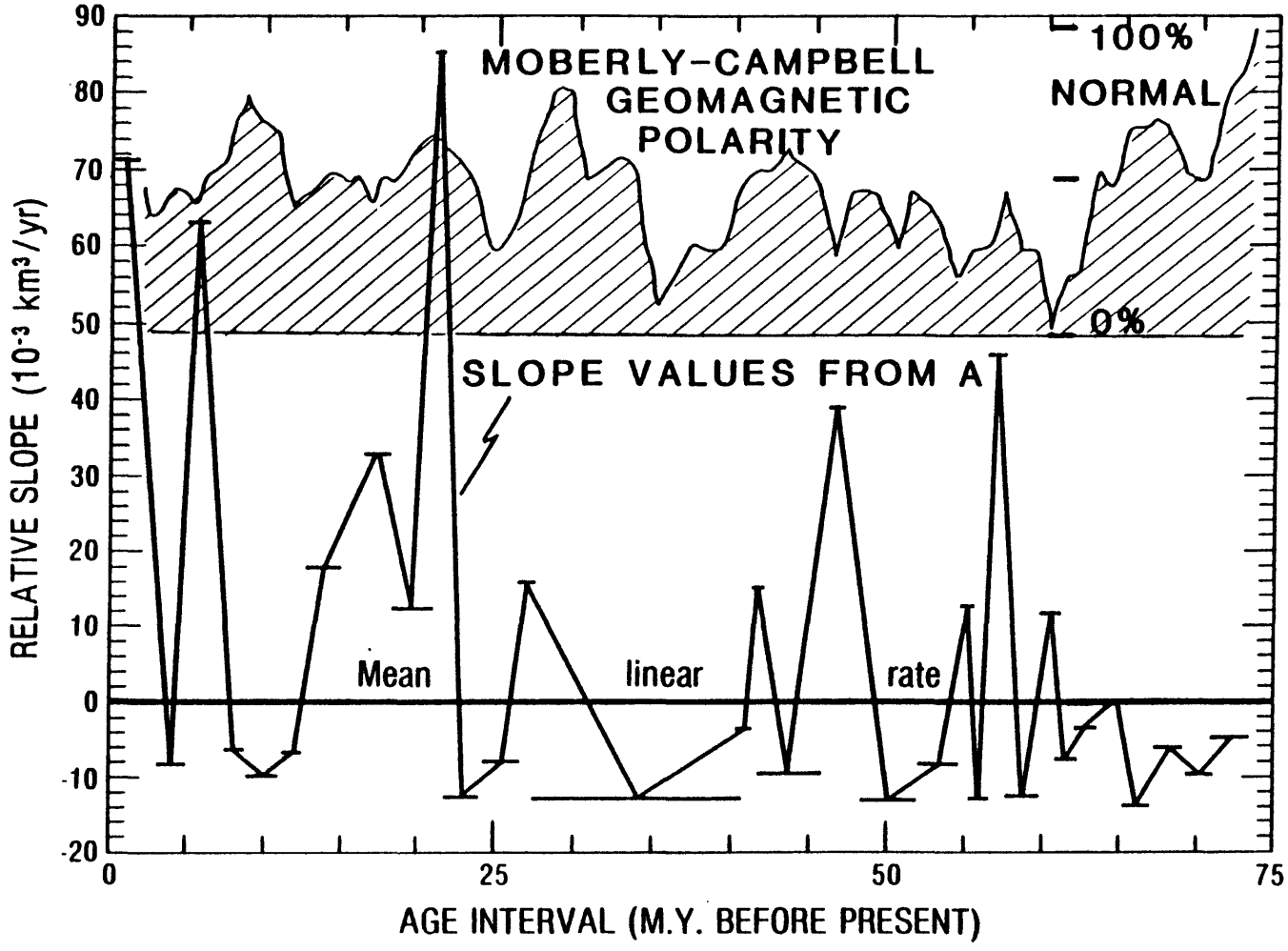
MOBERLY-CAMPBELL
GEOMAGNETIC
POLARITY
100%
NORMAL
0%
SLOPE VALUES FROM A
Mean
linear
rate
RELATIVE SLOPE (10⁻³ km³/yr)
AGE INTERVAL (M.Y. BEFORE PRESENT)
90
80
70
60
50
40
30
20
10
0
-10
-20
0
25
50
75

Fig.7B

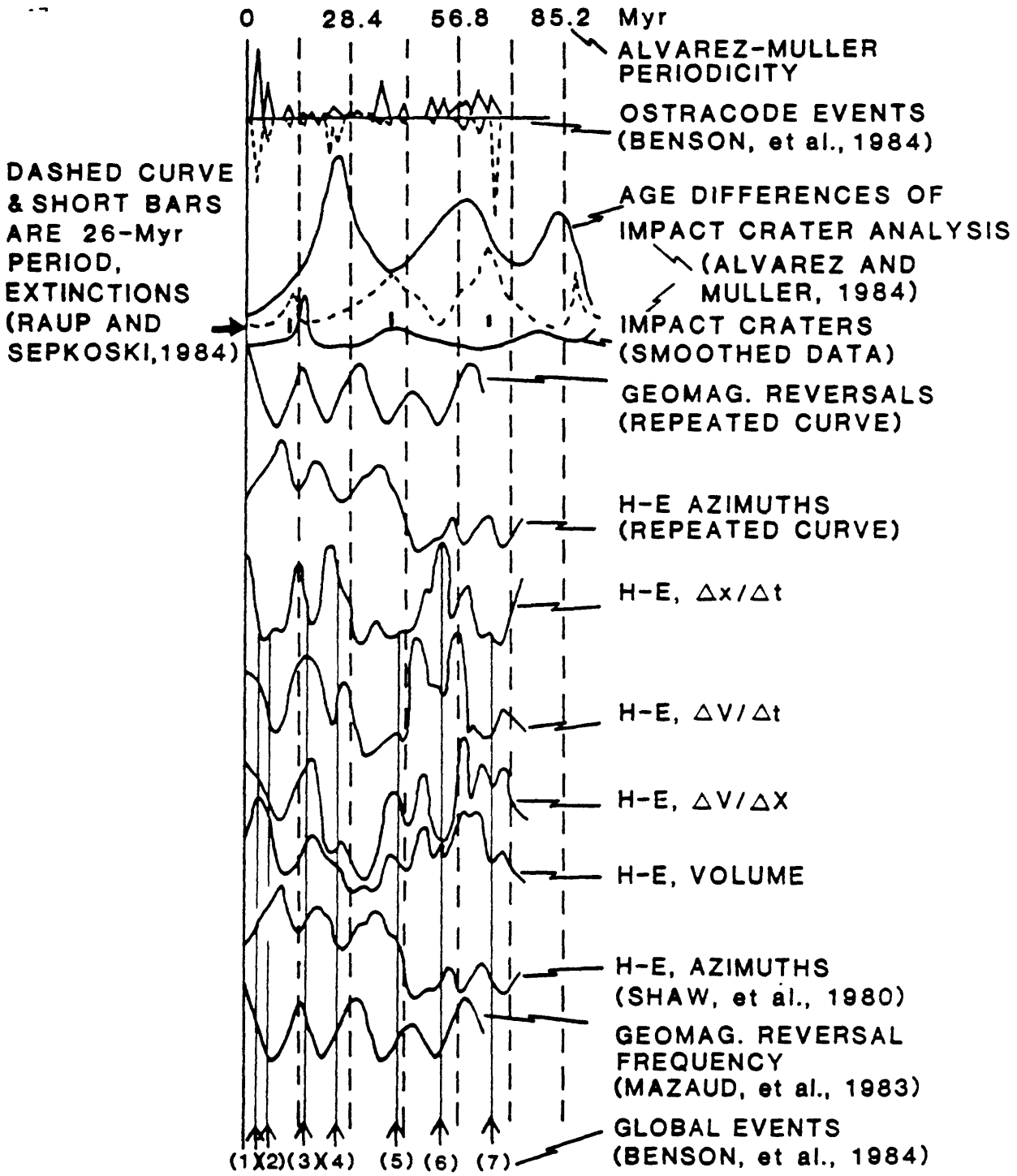
0
28.4
56.8
85.2
Myr
ALVAREZ-MULLER PERIODICITY
OSTRACODE EVENTS (BENSON, et al., 1984)
DASHED CURVE & SHORT BARS ARE 26-Myr PERIOD, EXTINCTIONS (RAUP AND SEPKOSKI, 1984)
AGE DIFFERENCES OF IMPACT CRATER ANALYSIS (ALVAREZ AND MULLER, 1984)
IMPACT CRATERS (SMOOTHED DATA)
GEOMAG. REVERSALS (REPEATED CURVE)
H-E AZIMUTHS (REPEATED CURVE)
H-E, Δx/Δt
H-E, ΔV/Δt
H-E, ΔV/ΔX
H-E, VOLUME
H-E, AZIMUTHS (SHAW, et al., 1980)
GEOMAG. REVERSAL FREQUENCY (MAZAUD, et al., 1983)
GLOBAL EVENTS (BENSON, et al., 1984)
(1)(2)(3)(4) (5) (6) (7)

Fig.8

Figure 8. Composite of H-E time series compared with selected time series of other phenomena. Peak heights of the H-E curves were shortened in some cases to fit curves together; see original sources for accurate numerical values. Geomagnetic, impact cratering and biologic extinction episodes are from Figure 3; tick marks show the statistical 26-Myr period calculated by Raup and Sepkoski (1984). Dashed vertical lines are 28.4 Myr periodicity of Alvarez and Muller (1984) shown for visual comparison with other peaks (see Figure 9 for comparison with 26-Myr grid). Arrows at bottom are global events of biostratigraphic correlations in oceanic sedimentary sections discussed by Benson et al. (1984); their record of ostracode extinctions (dashed lines) and originations (solid lines) is at top. Maxima and minima of H-E azimuth data (Figure 3) are directional extrema (minima are most northerly excursions, maxima most westerly); note almost direct correspondence of northerly extrema and maxima of reversal frequencies in analysis of Mazaud et al. (1983).

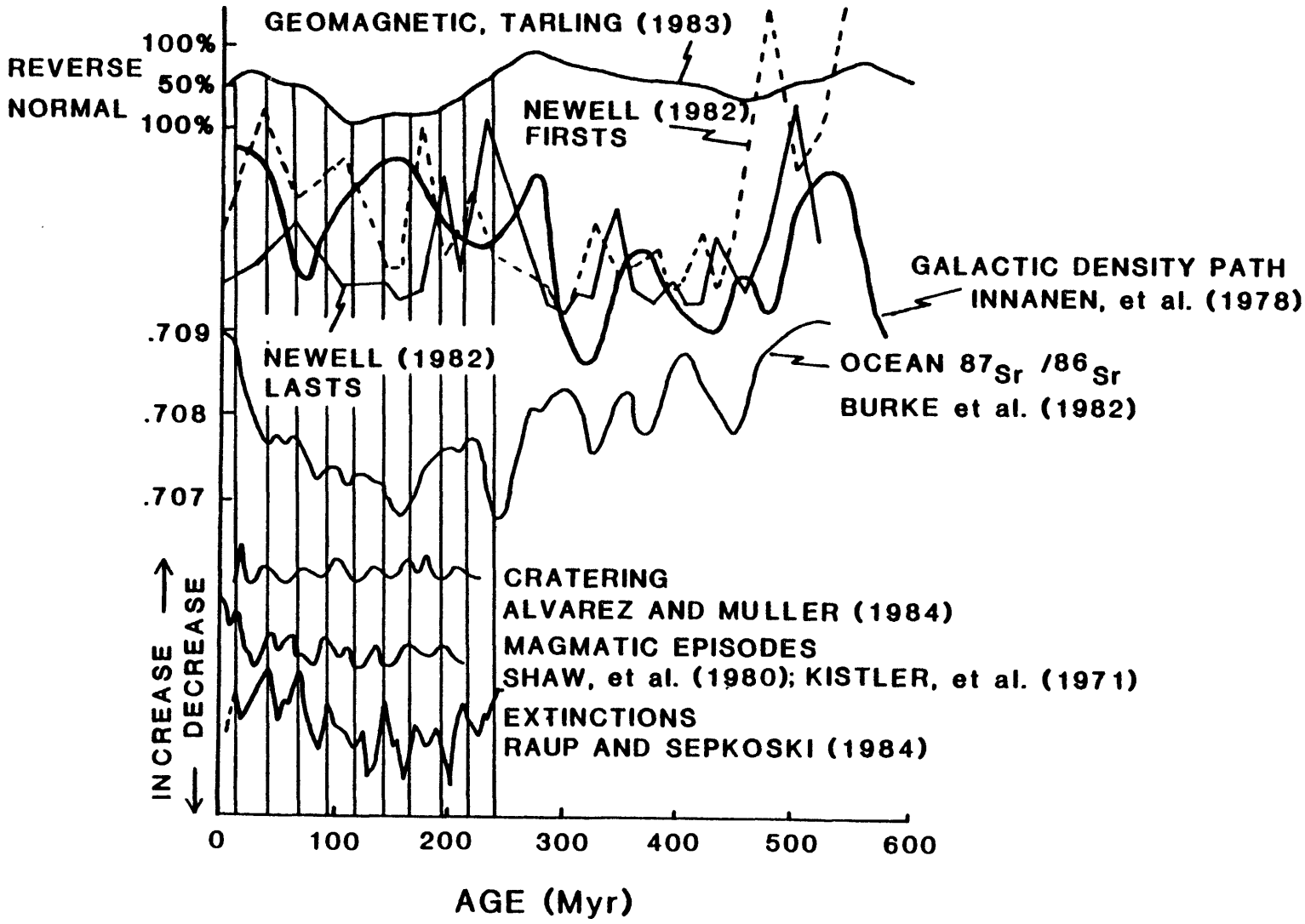
GEOMAGNETIC, TARLING (1983)
100%
REVERSE
50%
NORMAL
100%
NEWELL (1982)
FIRSTS
GALACTIC DENSITY PATH
INNANEN, et al. (1978)
.709
NEWELL (1982)
LASTS
OCEAN 87Sr /86Sr
BURKE et al. (1982)
.708
.707
CRATERING
ALVAREZ AND MULLER (1984)
MAGMATIC EPISODES
SHAW, et al. (1980); KISTLER, et al. (1971)
EXTINCTIONS
RAUP AND SEPKOSKI (1984)
INCREASE
DECREASE
0
100
200
300
400
500
600
AGE (Myr)

Fig.9

Figure 9. Comparison of several Phanerozoic time series. Vertical grid lines for latest 250 Myr are Raup-Sepkoski periodicity of 26 Myr (cf., Figures 10 and 25, Table 1, and discussion of mixed periods in text). Curve for magmatic episodes is composite of H-E rate peaks of Figure 5 (top) and plutonic maxima in Sierra Nevada batholith of Evernden and Kistler (1970) and Kistler et al. (1971); figurative curve is rationalized on evidence of basaltic system support of silicic cratonic systems (see Shaw et al., 1971). From top, other curves are: long-term geomagnetic reversals from Tarling (1983; Figure 8.10), major extinction and origination events in fossil record from Newell (1982), calculations of galactic densities encountered by solar system from Innanen et al. (1978), and record of strontium isotope variations in ocean from Burke et al. (1982). Note rough correlations among bottom three curves; also note resemblance of galactic density curve and average behavior (not drawn) of extinction-origination oscillations (galactic curve lags extinction curve 30 to 80 Myr, and extinctions lag originations about 10 to 30 Myr; forward shift of galactic density by about 50 Myr puts Paleozoic records nearly in phase).

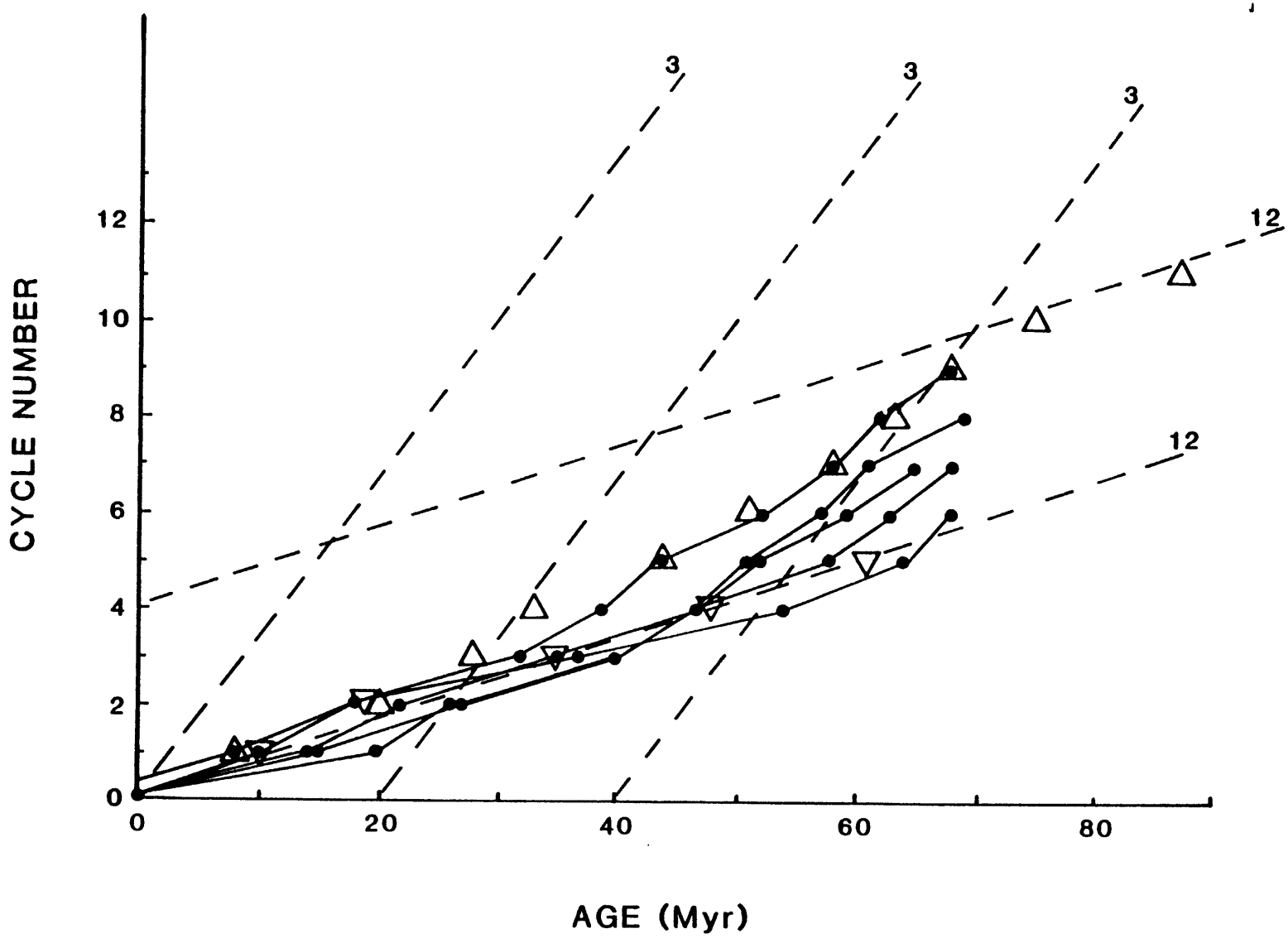

Fig. 10A

Figure 10. Cycle plots from geologic time series data.

A. Cycle plot of Hawaiian-Emperor data of Figures 3 through 7 (solid circles connected by lines; all maxima of volume-distance-age data and all reversals in azimuth record) and H-E geomagnetic data of Moberly and Campbell (1984) (upward pointing triangles are maxima of percent normal polarity, using peaks with at least 20 percent peak-to-trough change on one or both sides; inverted triangles are maxima from data for length of polarity intervals in Figure 3). Geomagnetic pattern has same variability as magmatic pattern; periodicity mixing among bases 2^n and 3^m indicated by reference curves (dashed lines) at 3 and 12 Myr.

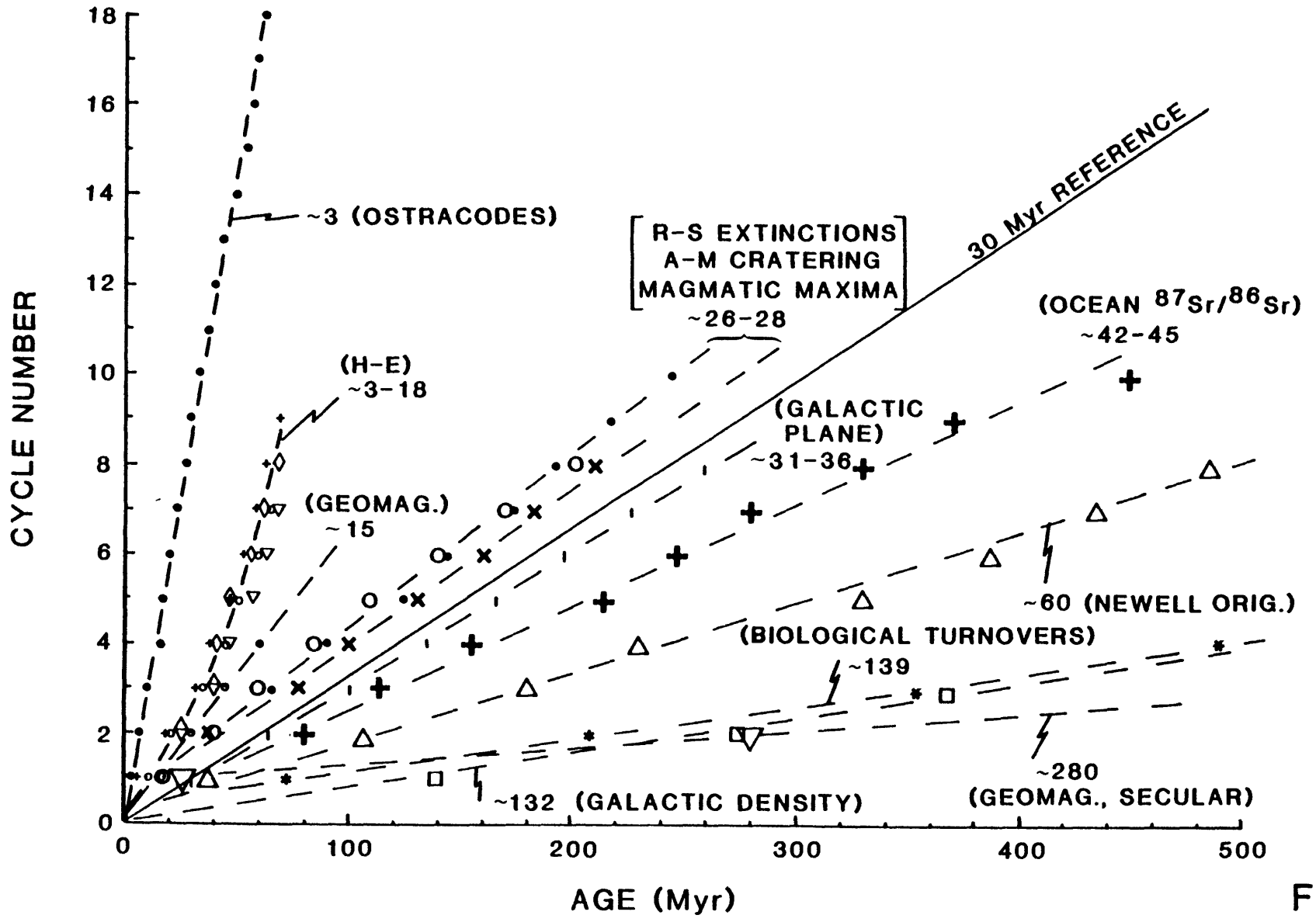
CYCLE NUMBER
AGE (Myr)
0
2
4
6
8
10
12
14
16
18
0
100
200
300
400
500
~3 (OSTRACODES)
(H-E)
~3-18
(GEOMAG.)
~15
R-S EXTINCTIONS
A-M CRATERING
MAGMATIC MAXIMA
~26-28
30 Myr REFERENCE
(OCEAN 87Sr/86Sr)
~42-45
(GALACTIC
PLANE)
~31-36
~60 (NEWELL ORIG.)
(BIOLOGICAL TURNOVERS)
~139
~280
(GEOMAG., SECULAR)
~132 (GALACTIC DENSITY)

Fig.10B

Figure 10. Cycle plots from geologic time series data.

B. Cycle plot of all data sources (see Figures 3 through 9 for data sources). Note linearity of ostracode episodes (originations and extinctions) obscured by seeming haphazard pattern in Figure 8 . Linearities drawn on basis of constant mean age intervals. Hawaiian-Emperor cycles are curved toward shorter periodicities at older ages (see A) reflecting more complex variations in Emperor portions of records. H-E trends are typical of dynamically complex phenomena: multiple periodicities vary with time but proportionalities remain similar over longer times (given detail, other records may show self-similar excursions from mean trends; e.g., mean trend of magmatic maxima includes H-E data). Simple common denominators such as 2 and 3 may descibe higher frequency oscillations (see Figure 25 and text for discussion of mixed periods). 30-Myr reference line (solid) demarks grouping of terrestrial cycles in range 26 to 28 Myr relative to galactic plane crossings from Innanen et al. (1978); see Figure 20. All sets vary in period and phase and may represent subintervals of more inclusive complex spectra (e.g., long-term biological, geomagnetic, and galactic density cycles).

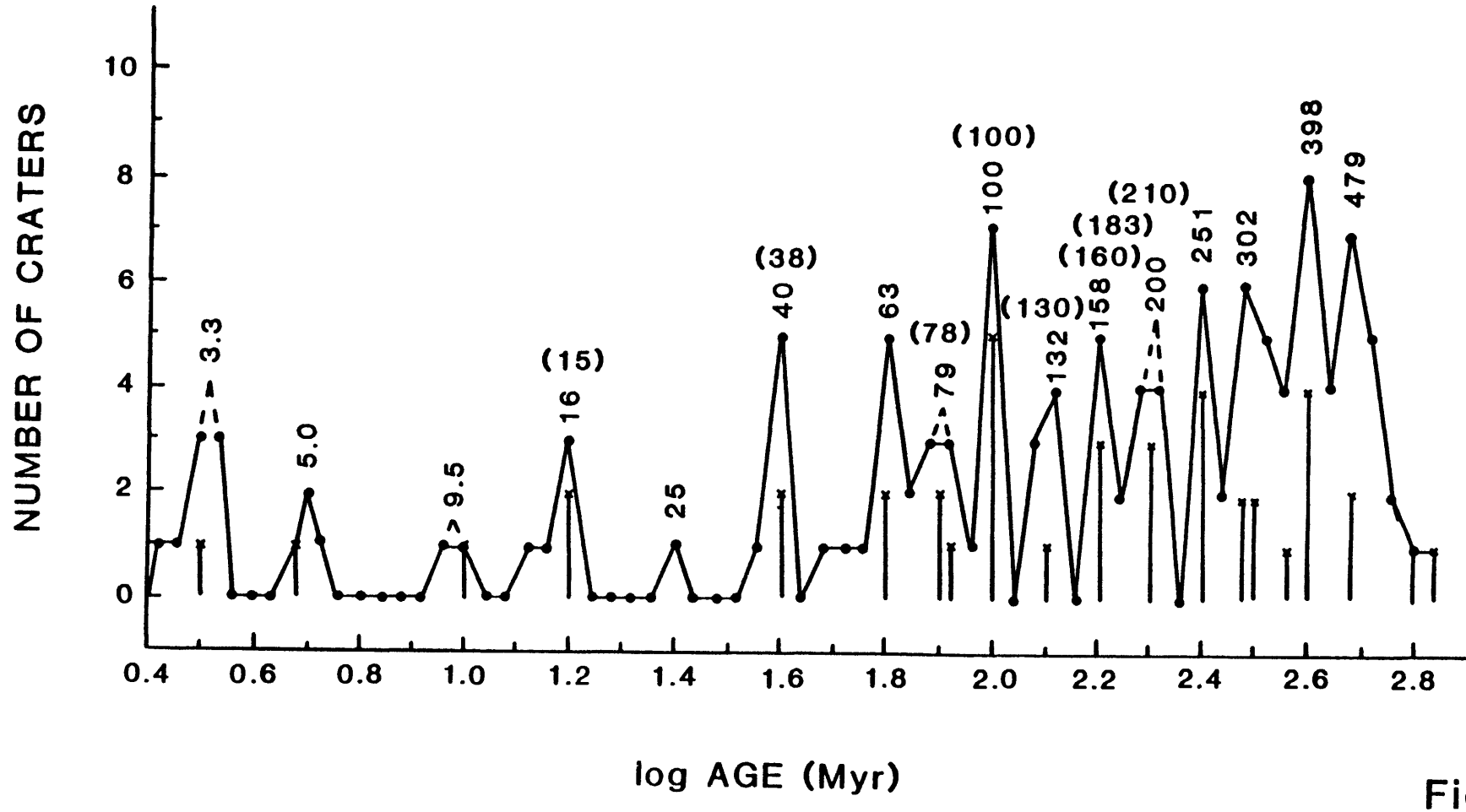
NUMBER OF CRATERS
10
8
6
4
2
0
0.4
0.6
0.8
1.0
1.2
1.4
1.6
1.8
2.0
2.2
2.4
2.6
2.8
log AGE (Myr)
3.3
5.0
> 9.5
(15)
16
25
(38)
40
63
(78)
79
(100)
100
(130)
132
(160)
158
(183)
(210)
200
251
302
398
479

Fig.11A

Figure 11. Logarithmic time series of known impact craters on Earth.

A. Logarithmic moving window averages of impact-cratering record based on compilation of Grieve (1982); window is 0.08 log units shifted by 0.04 log units between 2.88 (758 Myr) and .32 (2 Myr) (window varies from about 130 Myr with 70-Myr shift at oldest age to about 0.5 Myr with 0.1-Myr shift at youngest age; range is larger than age uncertainties at oldest age and smaller at youngest age). Two events occur at about 1 Myr (offscale at left); one is well-dated 10-km diameter structure discussed by Shoemaker (1983). Vertical bars and crosses represent specific counts of cratering events equal to or larger than 10 km in diameter. Approximate event ages given for each peak based on cratering events of all sizes; numbers in parentheses are events of Alvarez and Muller (1984) for selected subset of well-dated large craters (note agreement between age sets; peak at 63 Myr is not in their spectrum because their uncertainty filtering excluded some large events in that vicinity).

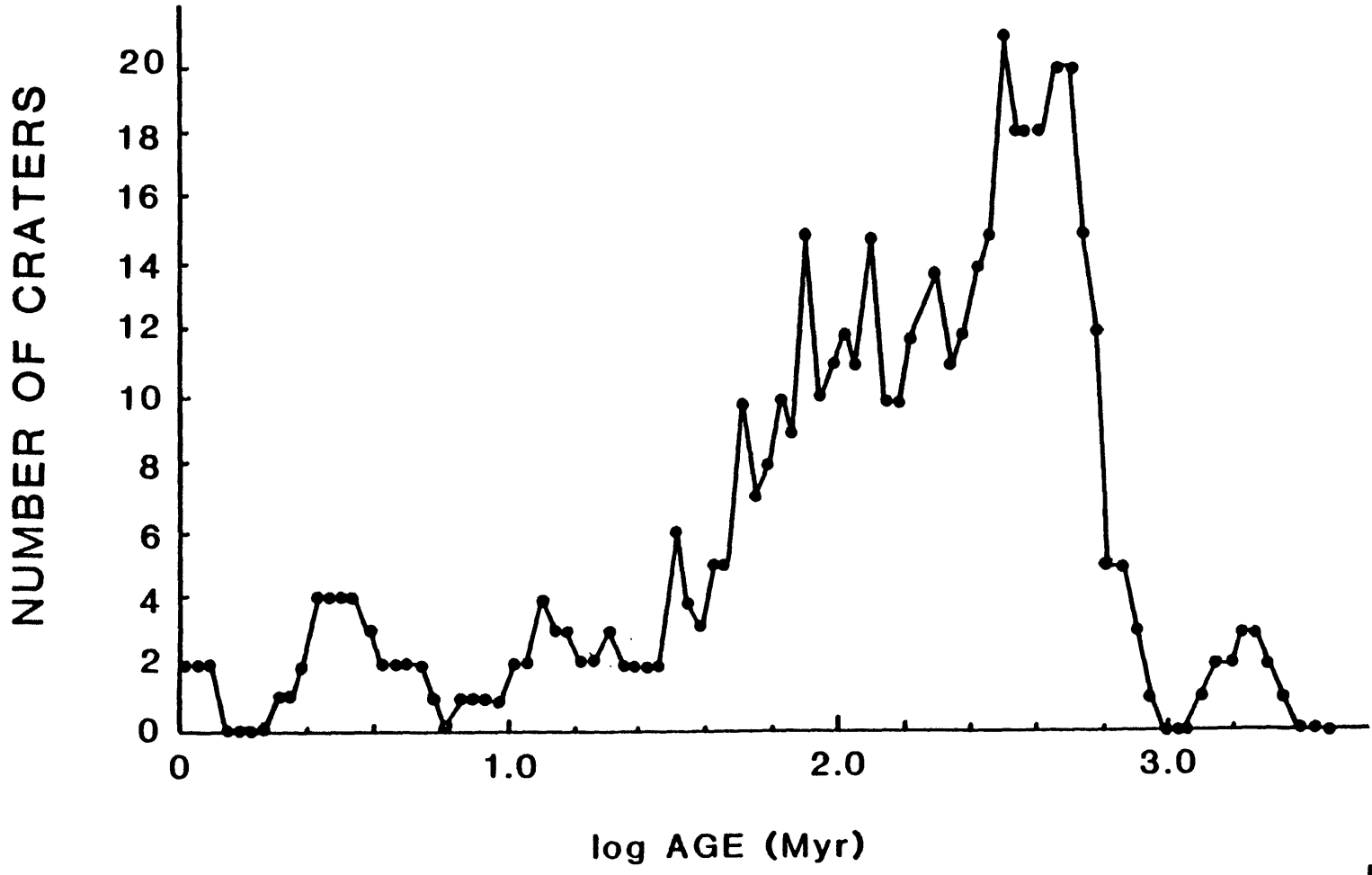

Fig.11B

Figure 11. Logarithmic time series of known impact craters on Earth.
B. Moving window averages with large window of 0.2 log units and 0.1 unit shift. This graph emphasizes Paleozoic dominance in cratering record; small peaks in graph A are suppressed and dominant peaks are shifted to younger ages because of large window.

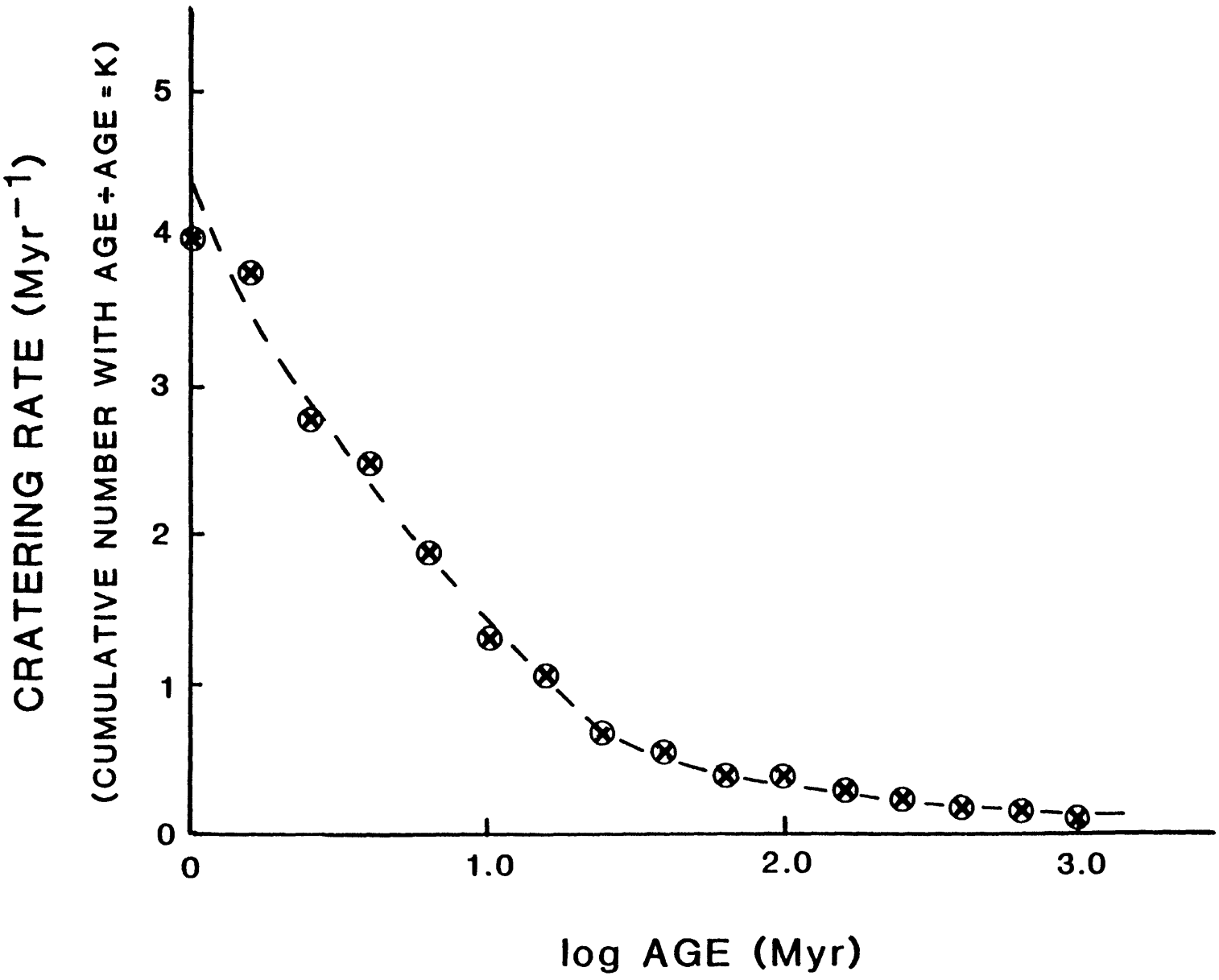
CRATERING RATE (Myr^{-1})
(CUMULATIVE NUMBER WITH AGE ÷ AGE = K)
0
1
2
3
4
5
0
1.0
2.0
3.0
log AGE (Myr)

Fig. 12A

Figure 12. Variation of impact cratering in time.

A. History of average cratering rates (K): summations of numbers of all events to a given age divided by age and plotted against logarithm of age. Graph shows apparent increase in cratering rates with decreasing age despite dominance of counts having Paleozoic-Mesozoic ages in Figure 11 (see text).

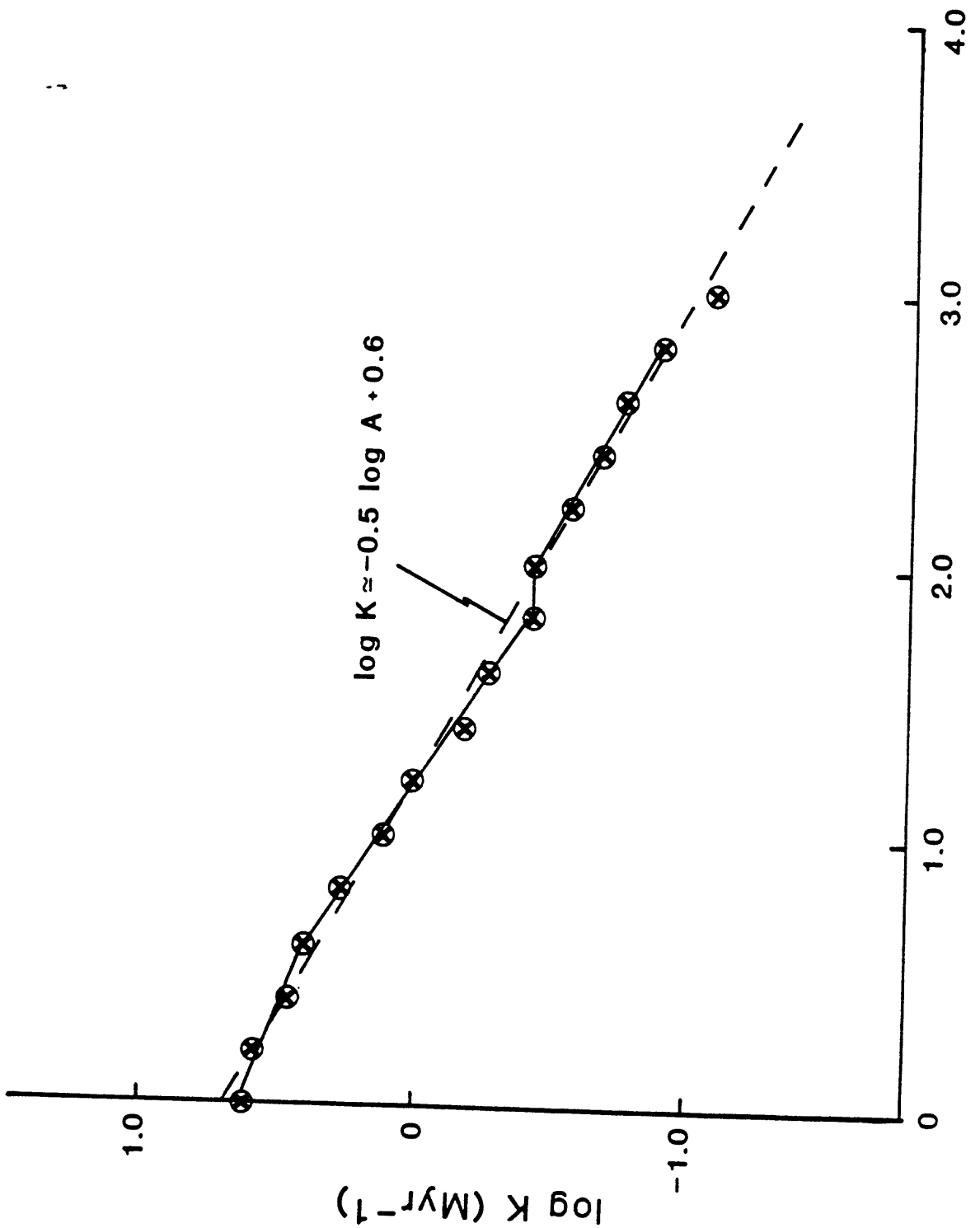

Fig.12B

Figure 12. Variation of impact cratering in time.

B. Logarithm of rate coefficient (K from graph A) against logarithm of age. Average regression line (dashed) demonstrates nearly constant proportionality to inverse square root of age (projects to about 4 Myr^{-1} at age 1 Myr). Rate episodes are suggested by solid lines. There are 4 events at ages younger than 1 Myr (offscale to left). Rates calculated from events at 0.1 and 0.01 Myr are same as rates extrapolated from steeper slope in interval $0.6 \leq \log A \leq 1.8$; equation for this interval is roughly $\log K \approx -0.7 \log A + 0.8$ giving 32 Myr^{-1} at 0.1 and 160 Myr^{-1} at 0.01 Myr. There is either a systematic relation for age-dependence of recognizable craters or a systematic increase in rates of smaller cratering events with decreasing age; latter may be likely based on size distributions in Figure 13 and discussion in text. If young events with sizes smaller than 10 km were representative of cratering rates for older small events, the slope would be near zero with constant total rate of order 100 Myr^{-1} (this would give order of 10^4 total craters of order 1 km diameter or greater during Phanerozoic compared to less than 100 known craters in Figure 11).

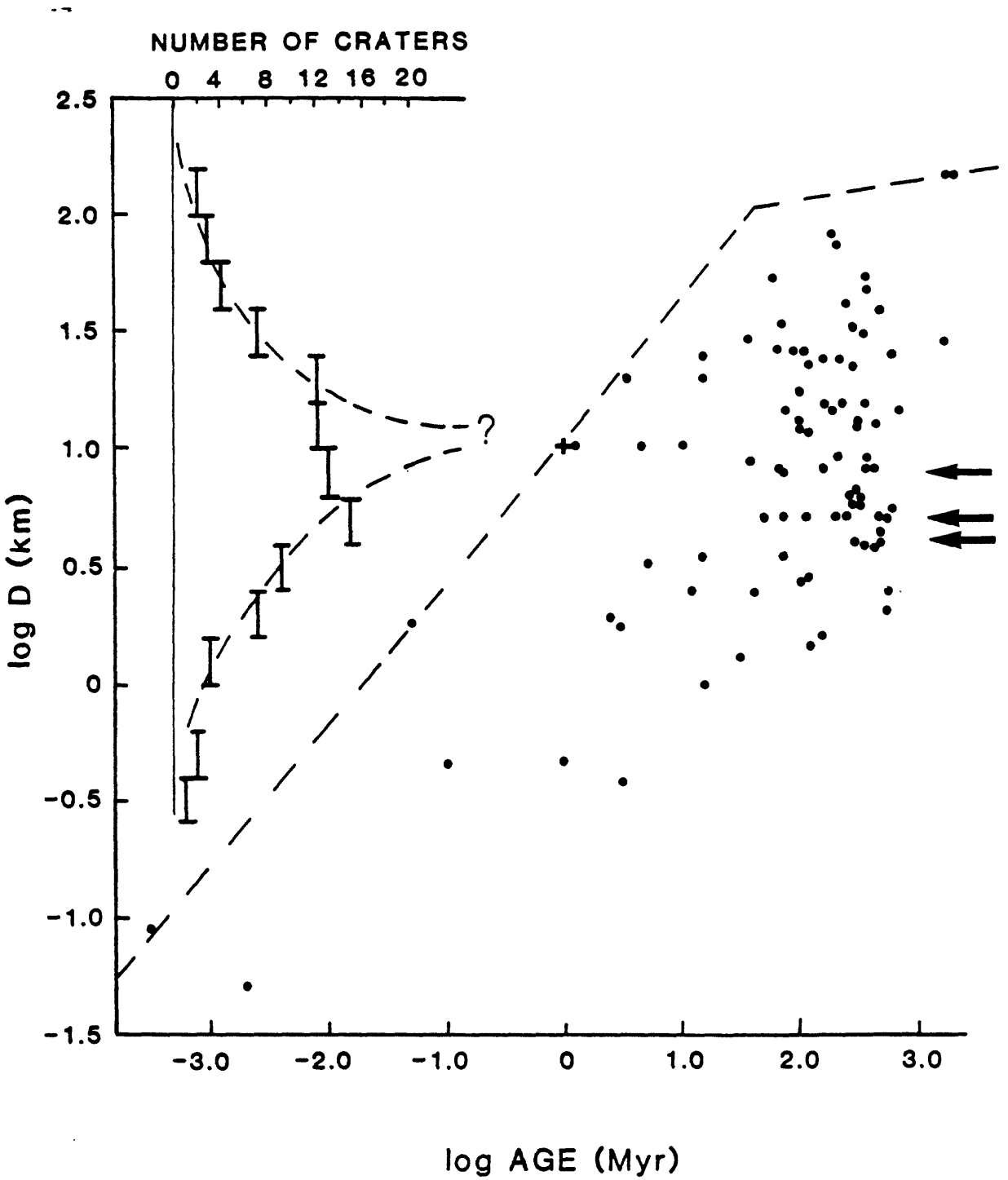
NUMBER OF CRATERS
0 4 8 12 16 20
2.5
2.0
1.5
1.0
0.5
0
-0.5
-1.0
-1.5
log D (km)
?
-3.0
-2.0
-1.0
0
1.0
2.0
3.0
log AGE (Myr)

Fig.13A

Figure 13. Size variations in impact cratering on Earth.

A. Logarithmic size vs age distribution of cratering events tabulated by Grieve (1982). Straight dashed lines demark size truncation of the distribution (see Eq. 3 in text). The 1 Myr-old 10-km crater discussed by Shoemaker (1983) is shown by plus sign; adjacent dot is same crater in Grieve's tabulation (horizontal arrows at right indicate sizes of undated craters in his list). Inset at left gives total frequency distribution vs logarithm of diameter, D, with maximum in neighborhood of 10-km. Sharp falloff in number of small craters is poor representation in older rocks and(or) possibility of real increase of small-diameter craters at young ages (see Figure 12 and text).

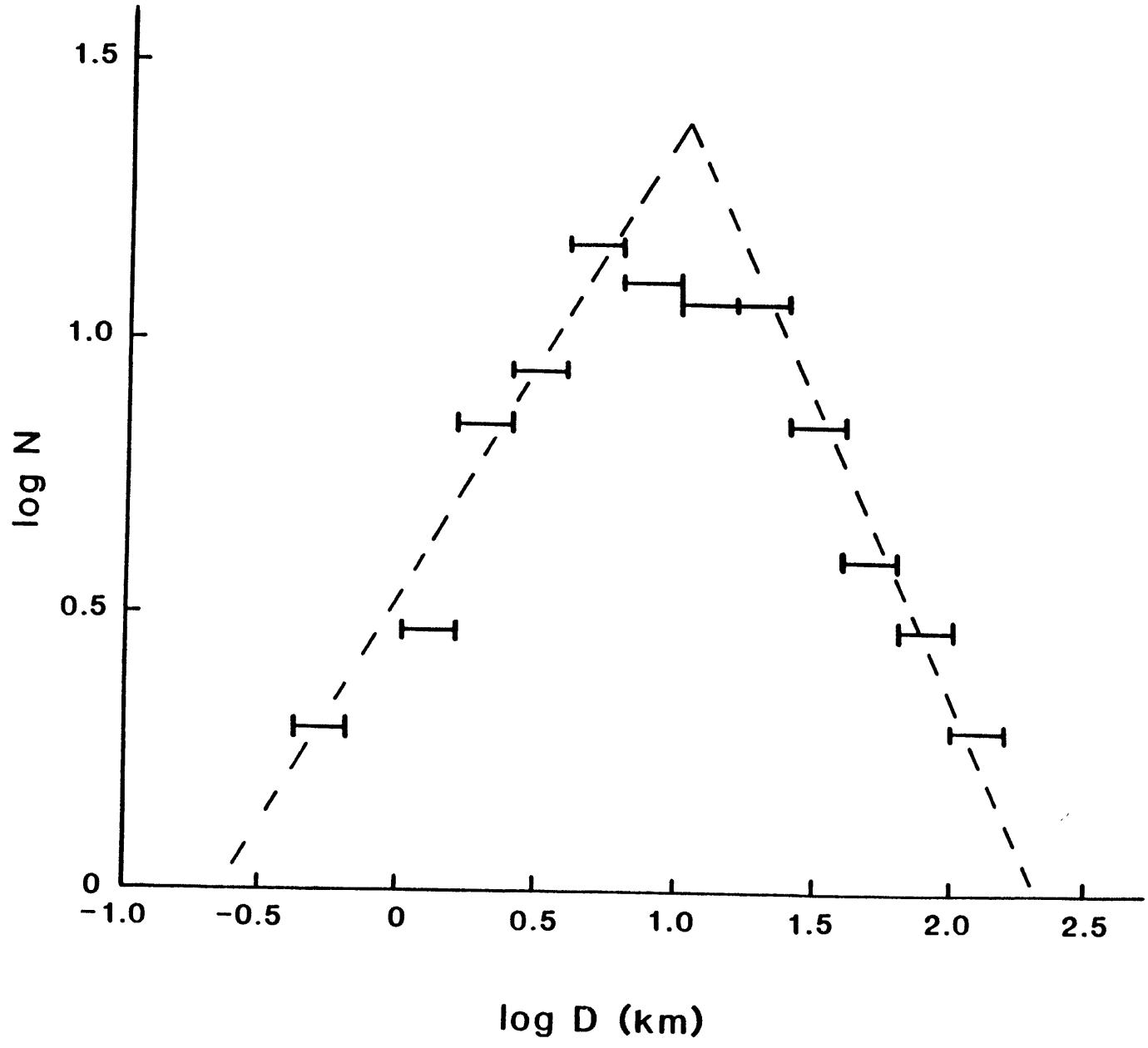

Fig. 13B

Figure 13. Size variations in impact cratering on Earth.
B. Log N vs log D from A illustrating focus at log D ≈ 1. The righthand limb is approximated by Eq. 2 in text (cf., caption Figure 12).

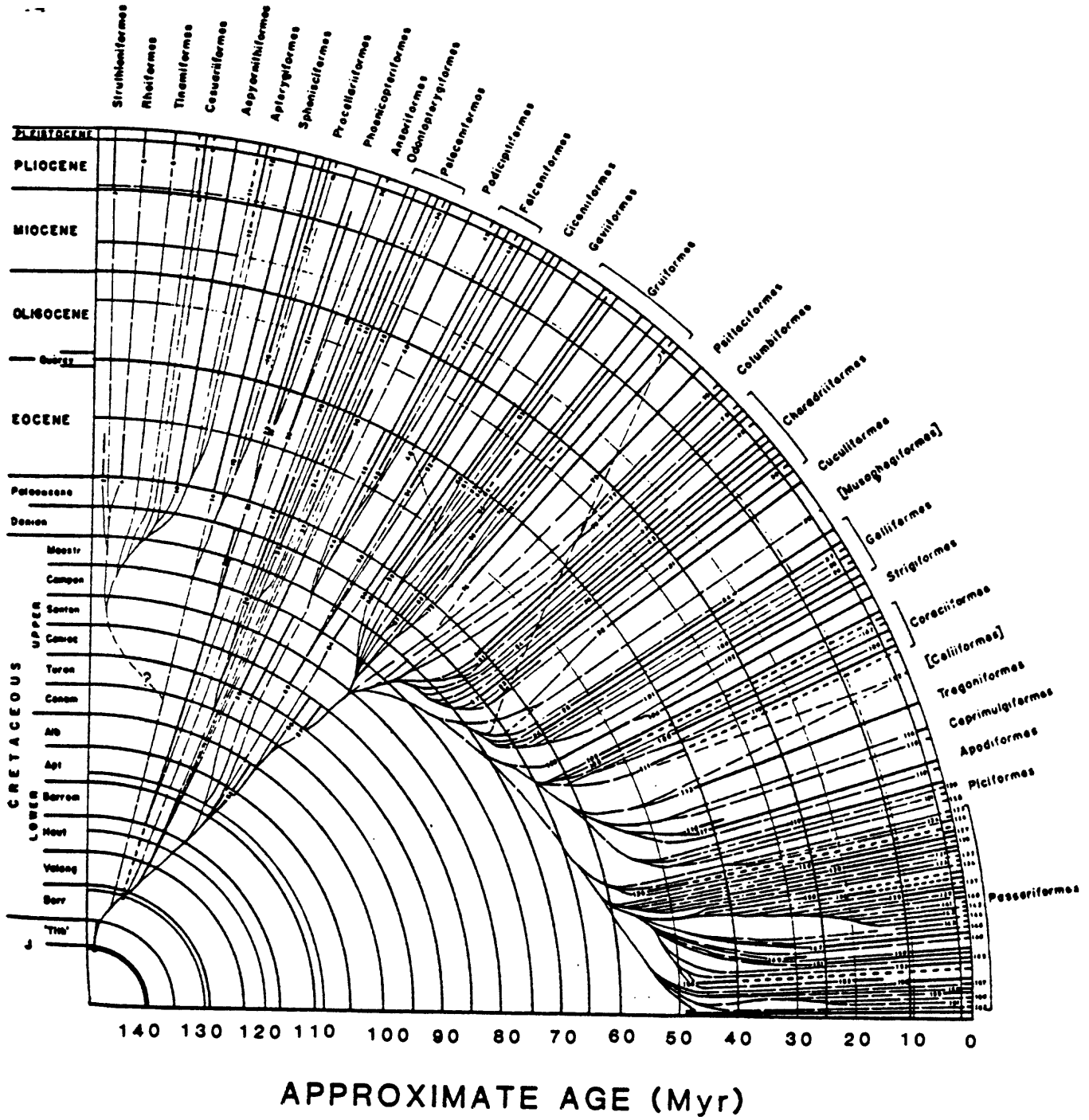
Struthioniformes
Rheiformes
Tinamiformes
Casuariformes
Aepyornithiformes
Apterygiformes
Sphenisciformes
Procellariiformes
Phoenicopteriformes
Anseriformes
Odontopterygiformes
Pelecaniformes
Podicipitiformes
Falconiformes
Ciconiiformes
Gaviiformes
Gruiformes
Psittaciformes
Columbiformes
Charadriiformes
Cuculiformes
[Musophagiformes]
Galliformes
Strigiformes
Coraciiformes
[Coliiformes]
Trogoniformes
Caprimulgiformes
Apodiformes
Piciformes
Passeriformes
PLEISTOCENE
PLIOCENE
MIOCENE
OLIGOCENE
EOCENE
Paleocene
Danian
CRETACEOUS
UPPER
LOWER
Maastr.
Campan.
Santon.
Coniac.
Turon.
Cenom.
Alb.
Apt.
Barrem.
Haut.
Valang.
Berr.
'Tith'
J
?
140 130 120 110 100 90 80 70 60 50 40 30 20 10 0
APPROXIMATE AGE (Myr)

Fig. 14

Figure 14. Record of Avian adaptive radiation at levels of Orders and Families from Fisher (1967). Ages are approximate; comparison of this timescale with that of Harland et al. (1982) is given in Figure 16. This classification is currently being revised on the basis of DNA hybridization methods (Sibley and Ahlquist, 1983), but this is not likely to change overall bifurcation pattern.

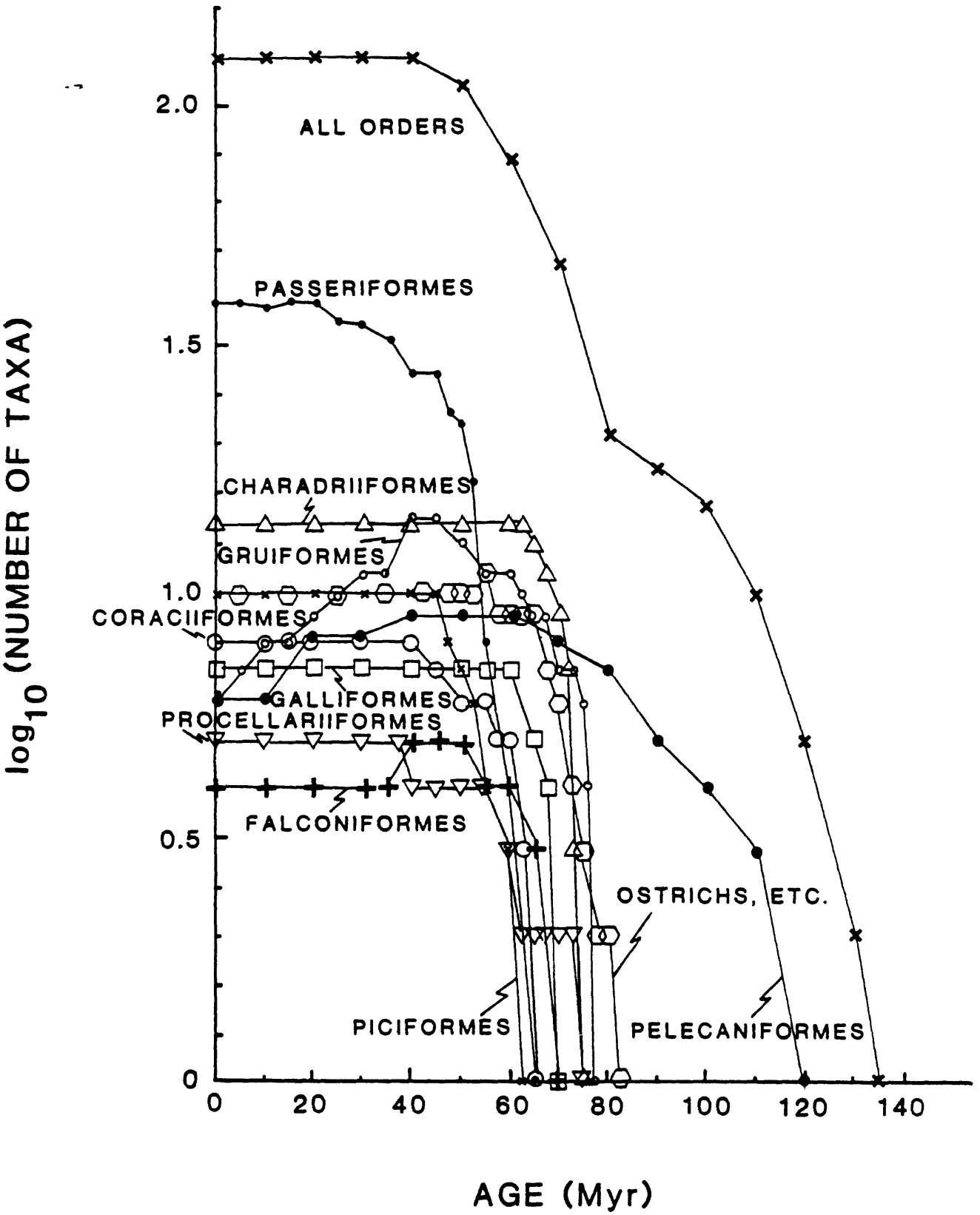
2.0
1.5
1.0
0.5
0
$\log_{10}$ (NUMBER OF TAXA)
ALL ORDERS
PASSERIFORMES
CHARADRIIFORMES
GRUIFORMES
CORACIIFORMES
GALLIFORMES
PROCELLARIIFORMES
FALCONIFORMES
OSTRICHS, ETC.
PICIFORMES
PELECANIFORMES
0
20
40
60
80
100
120
140
AGE (Myr)

Fig.15

Figure 15. Logarithm of cumulative number of taxa with decreasing age in Figure 14 (same timescale). Counts were made near times of bifurcation where changes are rapid and at intervals of 5 to 10 Myr within intervals of relatively slow changes.

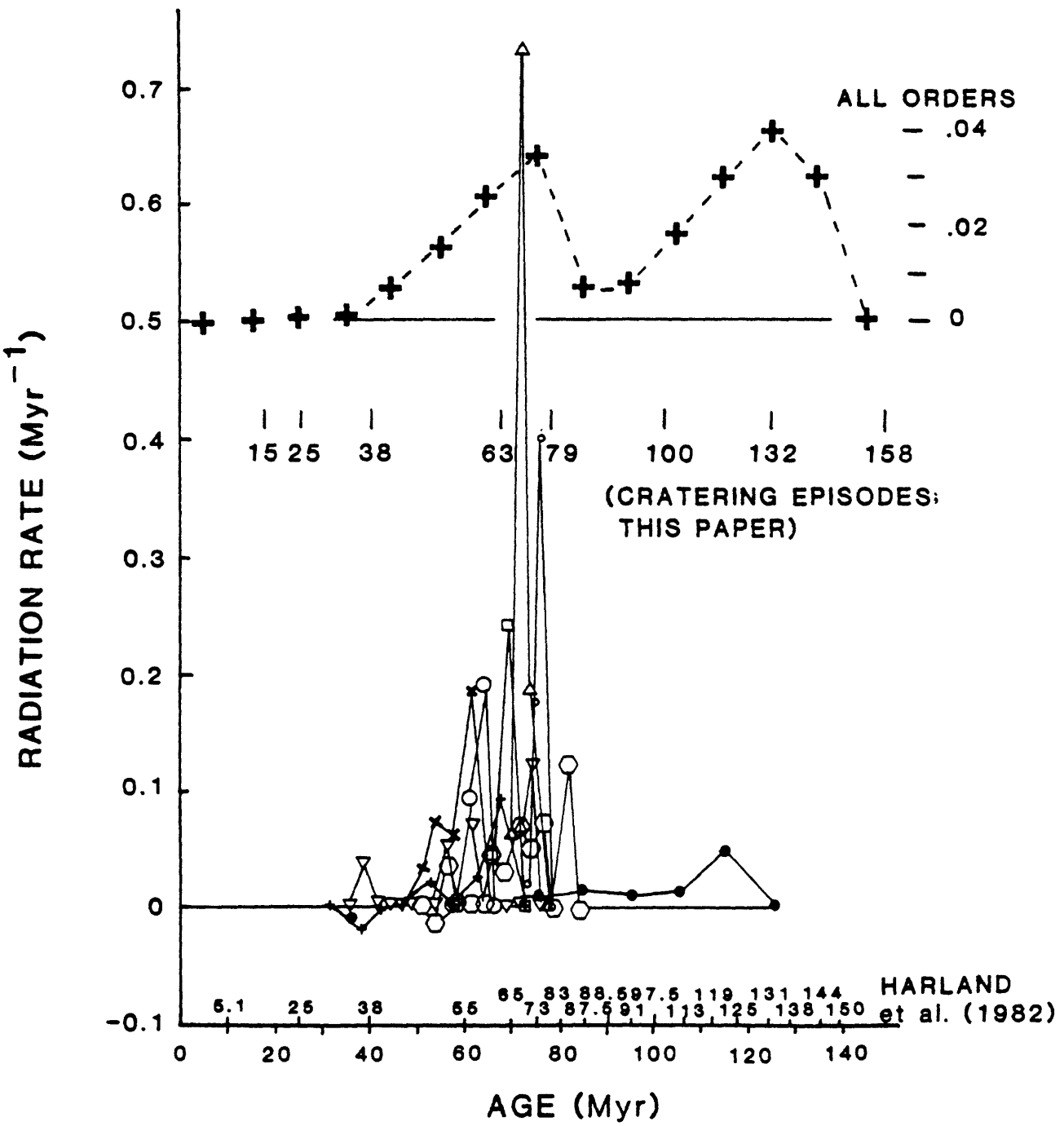
RADIATION RATE (Myr^{-1})
0.7
0.6
0.5
0.4
0.3
0.2
0.1
0
-0.1
ALL ORDERS
.04
.02
0
15 25 38 63 79 100 132 158
(CRATERING EPISODES: THIS PAPER)
5.1 25 38 55 65 73 83 87.5 88.5 91 97.5 113 119 125 131 138 144 150
HARLAND et al. (1982)
0 20 40 60 80 100 120 140
AGE (Myr)

Fig.16

Figure 16. Incremental slopes from Figure 15 expressed as radiation rates dlog(# of taxa)/dt vs. age based on timescale of Figure 14; revised ages according to Harland et al. (1982) also shown. Revised ages do not significantly affect rates and peak heights in age ranges of interest. Upper (dashed) curve gives average rates as defined by the curve of "all orders" in Figure 15; tick marks show cratering episodes from Figure 11A on Harland et al. (1982) timescale. Zero slopes at beginning of each curve represent the interval of constancy of the immediately preceding ancestral lineage in Figure 14 prior to its first bifurcation (incremental slope values in Figure 15 do not reflect local changes in vicinities of bifurcation points in Figure 14). Negative slope values represent reversals in lineage diversity (extinctions exceed originations; extinctions at levels of genera and species could be high and not be seen in Figure 14 if even one species survives to represent a family).

Figure 17. One-dimensional bifurcation diagrams based on nonlinear dynamics.

B. Period-doubling regime of A expressed as function proportional to logarithm of difference between tuning parameter and critical value, $\log(\lambda_c-\lambda)$, vs function proportional to $\log\Delta X$, redrawn from Helleman (1983). Plot logarithmically expands bifurcation range revealing scale invariance. Bifurcations over narrow intervals of λ in A occur at nearly equal intervals of $-\log(\lambda_c - \lambda)$; density of X-values in linear plot expanded in self-similar bundles (each bundle has same form regardless of absolute scale). Similar functions apply to other sets expressed relative to characteristic values of tuning parameter. This illustrates universality of attractor structures first demonstrated by Feigenbaum (1980); see Helleman (1983). Avian bifurcations in Figure 14 resemble B, with maximum number stabilized at approximately n = 7 (there are roughly 2^7 = 128 families; see Figure 18).

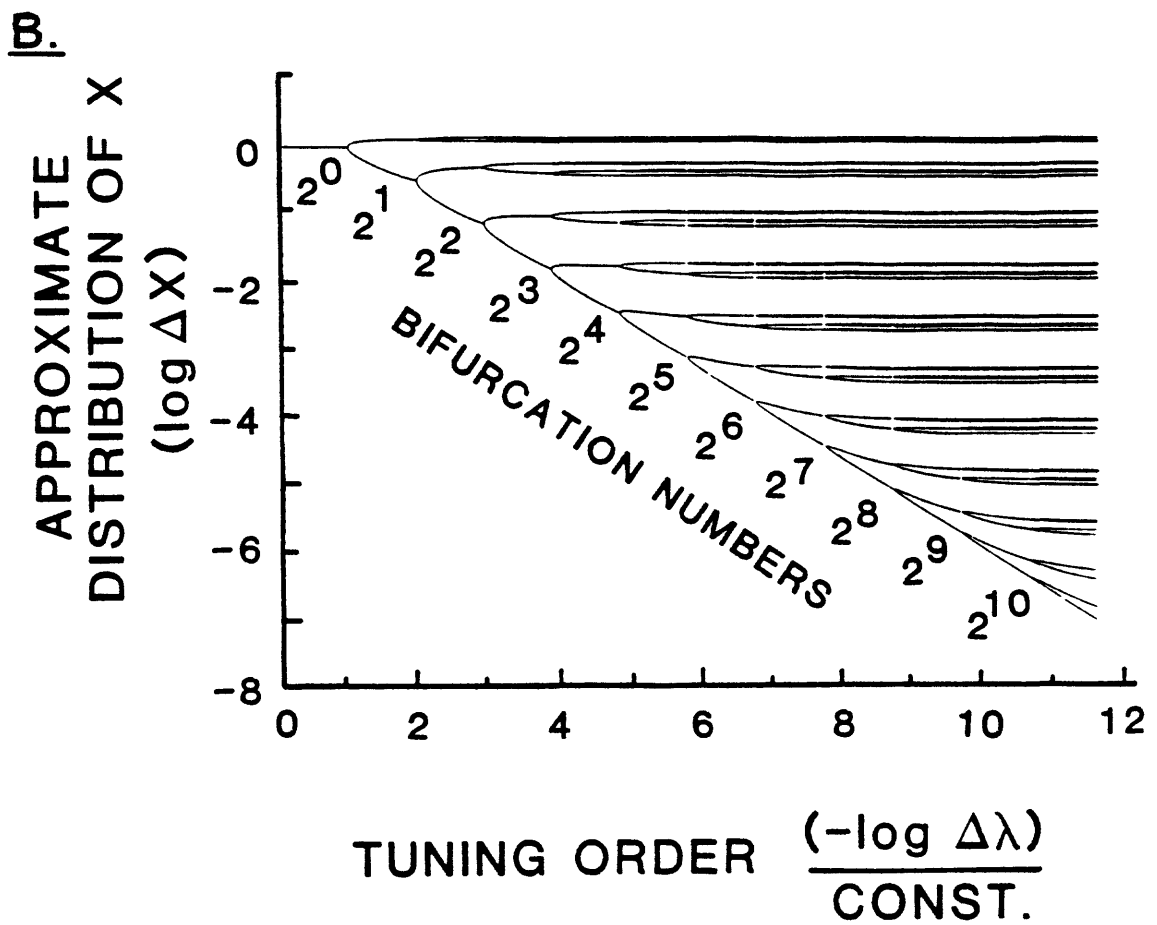

6

Figure 17. One-dimensional bifurcation diagrams based on nonlinear dynamics.

A. Diagram illustrating principal regimes of one-dimensional attractor systems, redrawn from May (1976). This is case of parabolic function called 'logistic equation' in population dynamics (a feedback curve with one maximum); in difference form expressed: $X_{n+1} = 4\lambda X_n(1-X_n)$, where X_n is population at given time that determines the population at the next increment of time, X_{n+1}, and λ is the 'tuning parameter' determined by amplitude of quadratic curve. For $4\lambda < 4\lambda_{c2} \approx 3.5700$ bifurcations occur as unlimited period-doubling sets as the critical value is approached (2^n X-values, where n is integer bifurcation state defined by λ). For $4\lambda > 3.5700$ chaotic sets and sets of odd and even periods exist. For $3.8284 \leq 4\lambda \leq 4\lambda_{c3,2} = 3.8495$ periods involve series $3x2^n$ also increasing indefinitely as λ_{c3x2} approached (dashed portions are unstable). Diagram hints at varieties of bifurcations of attractors and sensitivity to variations of λ (cf., Figure 19).

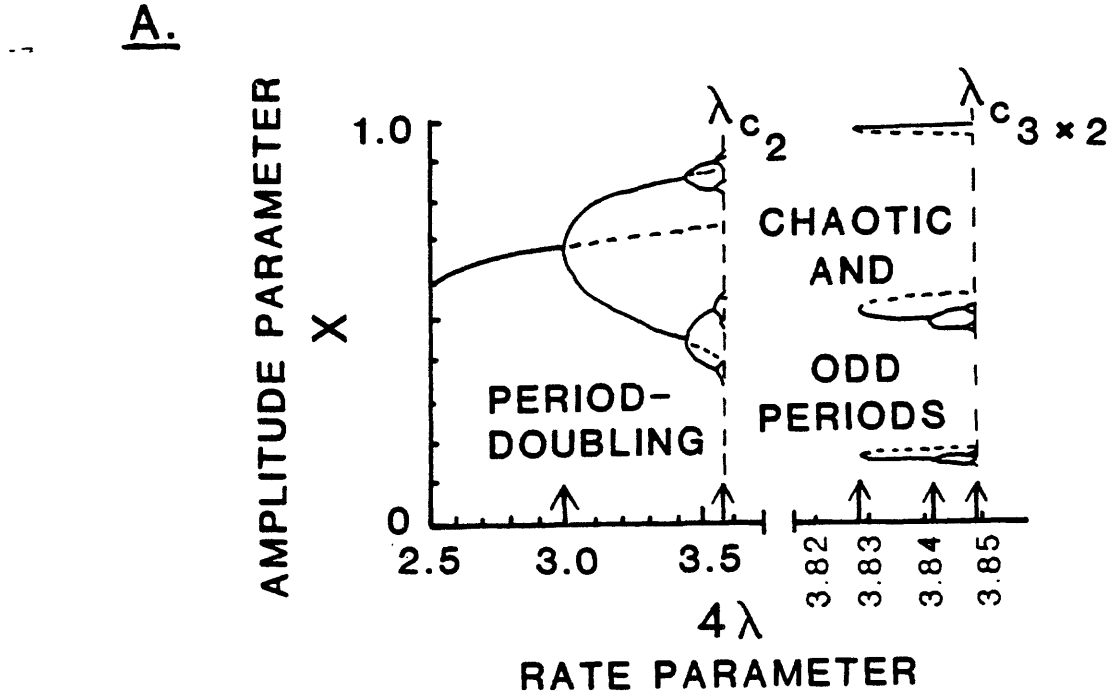

Figure 18. Schematic prism illustrating hypothetical paths in time of tuning parameters and period-doubling sets of Figure 17B.

B. Prism unfolded to show steady-state bifurcations projected to plane X vs t. Constancy of sets implies breakoff in curve f(λ) vs t to constant limit short of critical transition to chaos.

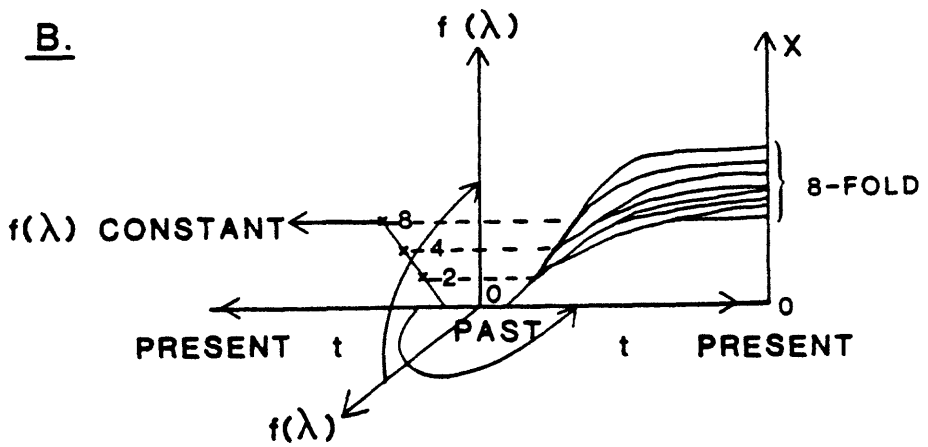

Figure 18. Schematic prism illustrating hypothetical paths in time of tuning parameters and period-doubling sets of Figure 17B.

A. Bifurcation sets are projected to front and right face of prism. Expressed by three variables t, f(λ), and X they would plot within volume of prism vertically above dotted path f(λ) vs t. Only a few bifurcations are shown.

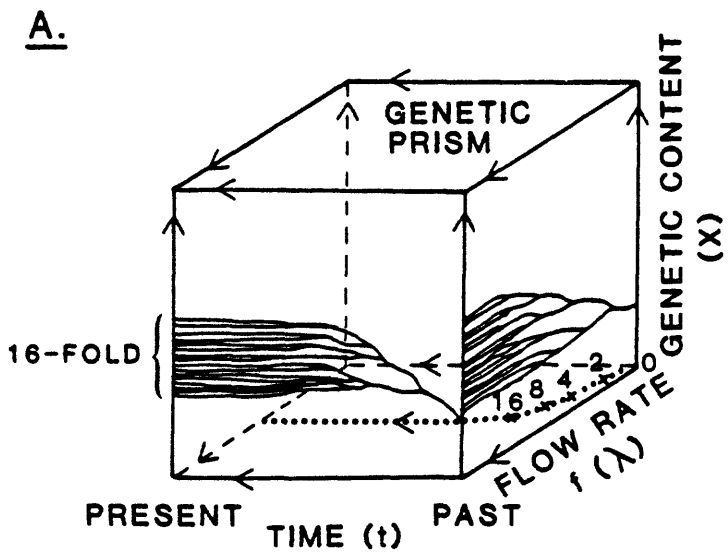

Figure 18. Schematic prism illustrating hypothetical paths in time of tuning parameters and period-doubling sets of Figure 17B.

C. Monotonically increasing rates result in unlimited bifurcations and eventual chaotic bifurcations.

Avian adaptive radiation resembles B., where rates increase for some time then become constant or decrease. Paths of constant or increasing $f(\lambda)$ represent, respectively, freezing to a constant bifurcation state and acceleration of bifurcation states (exponentially with linearly increasing rates); Figure 17(b) shows that to linearize or stabilize an increase in bifurcation numbers with time, the rate of increase in tuning parameter must decelerate with time and stop short of the critical value where infinite bifurcations and(or) a jump to chaotic patterns occur. With invariant tuning, system 'coasts' on previous impetus at plateaus of constant or standardized complexity. However, Figure 14 shows that some sublineages reach stabilized bifurcation state while others progress to higher bifurcation states (bifurcation bundles are not regularly aligned as in Figure 17B). This suggests multiple tuning subject to relative variations (see Figure 19).

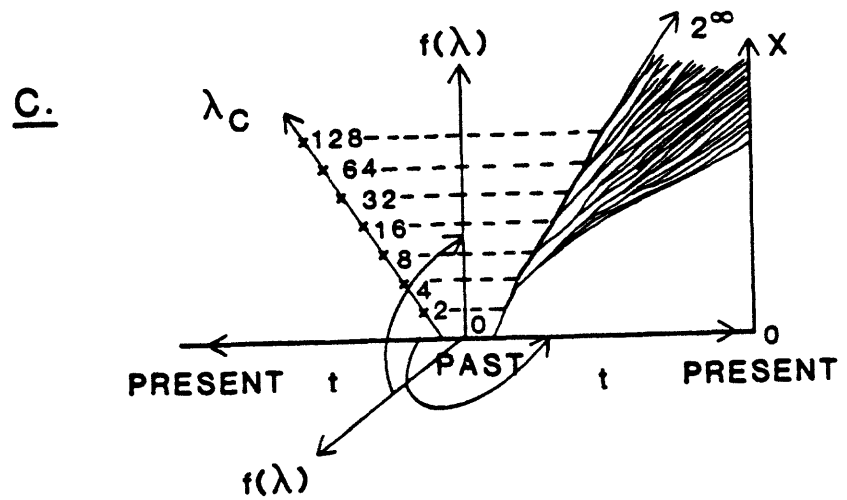

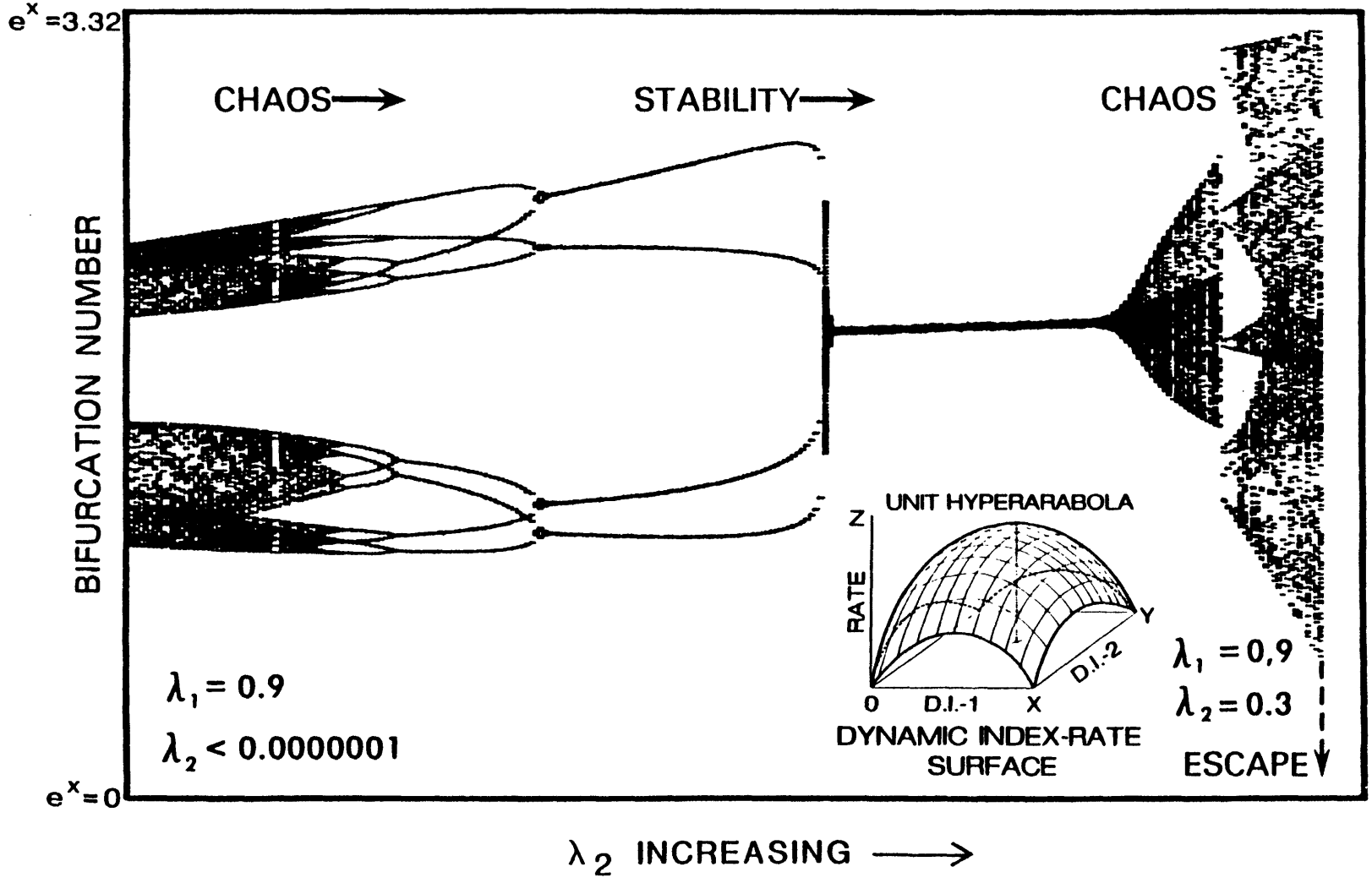
e^x =3.32
CHAOS
STABILITY
CHAOS
BIFURCATION NUMBER
e^x = 0
λ_1 = 0.9
λ_2 < 0.0000001
UNIT HYPERARABOLA
Z
RATE
Y
0
D.I.-1
X
D.I.-2
DYNAMIC INDEX-RATE SURFACE
λ_1 = 0,9
λ_2 = 0.3
ESCAPE
λ_2 INCREASING

Fig. 19A

Figure 19. Attractor bifurcation structures for multiple tuning parameters.

A. Example of patterns produced by two tuning parameters; dynamically similar to Figure 17 except that two degrees of freedom allow multiple sets of bifurcations in some regions, stabilization in others, and reversals of bifurcation sense in other regions. λ_1 held constant at value exceeding λ_{c2} for one-dimensional case (chaotic regime) and λ_2 increased from zero to about 0.3. Inset is surface governing paths of λ-variation. For values of $(\lambda_1 + \lambda_2)$ approaching 1.2 trajectories 'escape' (are repelled) from attractor. Initially, intervals of two state values, X and Y, follow reversed bifurcation paths and stabilize (X and Y converge to simple sets of fixed points); symbolizes standardization of populations controlled by rate functions each with different time-dependence. For net increase, chaos and escape ('extinction') occurs as in one-dimensional case; 'extinction' also occurs as attraction to fixed point at zero if λ-values are too low (below $4\lambda=1$ in one-dimensional attractor of Figure 17; for multiple λ's threshold is lower). Values of X and Y plotted together on ordinate (exponentials spread out distribution); values of λ_1, λ_2 given by abscissa (linear interpolation between indicated limits). Points in diagram are 'steady-state' X and Y for given pairs, λ_1 and λ_2 (points are plotted after initial transient values attain characteristic state, periodic or chaotic). Range of λ-values divided into about 300 pairs with 200 iterations per pair before incrementing (10^5 total iterations).

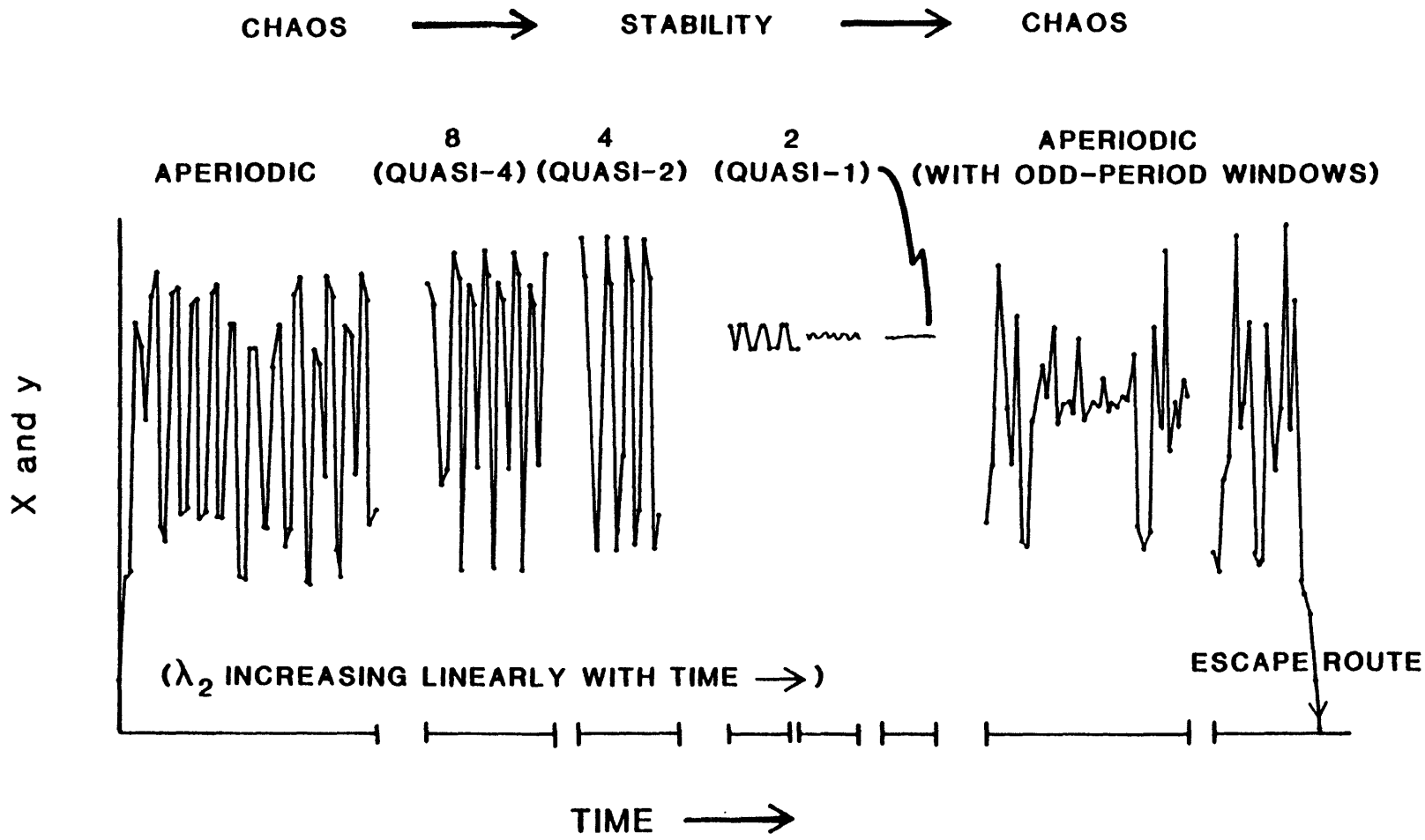
CHAOS
STABILITY
CHAOS
APERIODIC
8
(QUASI-4)
4
(QUASI-2)
2
(QUASI-1)
APERIODIC
(WITH ODD-PERIOD WINDOWS)
X and y
(λ_2 INCREASING LINEARLY WITH TIME →)
ESCAPE ROUTE
TIME

Fig.19B

Figure 19. Attractor bifurcation structures for multiple tuning parameters.

B. Time-series from A; t vs (X,Y) plotted on time axis normal to A. Left-hand region of chaos in A is more regular than right-hand chaotic region. Period-doubling series have redundancies; values of X and Y are superposed. Low and high amplitude excursions on the right increase in 'sling-shot' effect leading to escape condition. Compare with volcanic time series of Figure 2.

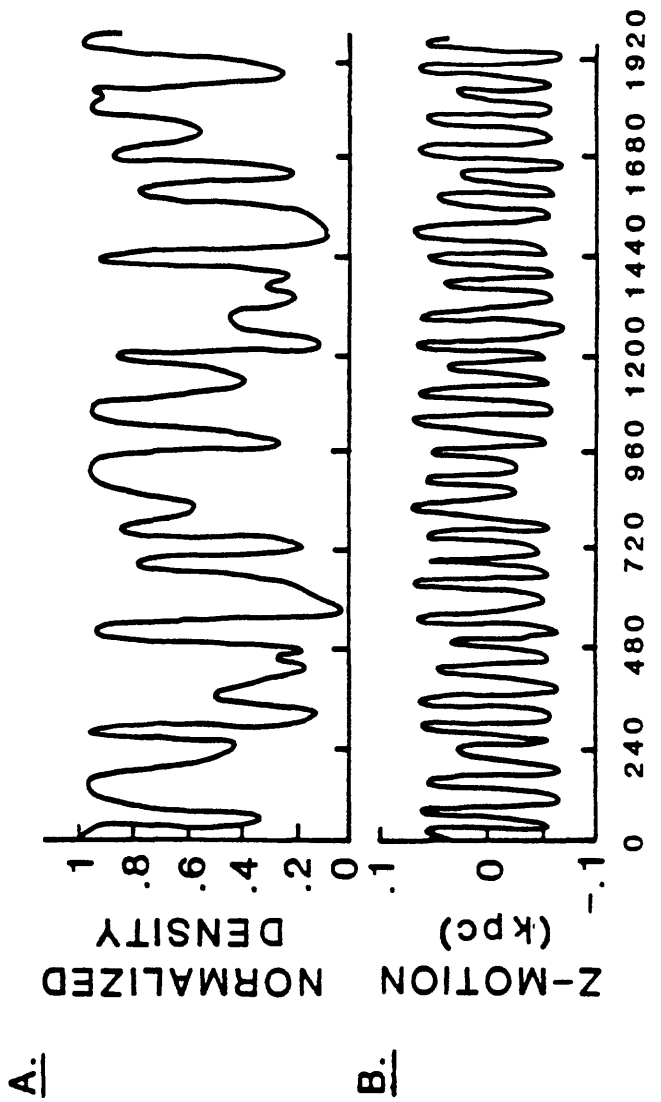
A.
NORMALIZED DENSITY
1
.8
.6
.4
.2
0
B.
Z-MOTION (kpc)
.1
0
-.1
0 240 480 720 960 1200 1440 1680 1920
AGE (Myr)

Fig.20

Figure 20. Time series for motion of solar system in Milky Way galaxy redrawn from Innanen et al. (1978); calculations based on empirical computer model described by Clutton-Brock et al. (1977).

A. Irregularly repetitive variations of galactic density in Sun's vicinity normalized to a standard state.

Figure 20. Time series for motion of solar system in Milky Way galaxy redrawn from Innanen et al. (1978); calculations based on empirical computer model described by Clutton-Brock et al. (1977).

B. Oscillations of Sun's motion relative to galactic plane at z=0 ('plane-crossing rhythm' in text); unit of distance is kiloparsec (kpc) defined in text and Figure 21.

Note qualitative resemblance between these series and artificial time series in Figure 19B. Galactic motion is complex in three dimensions as in plot of X and Y versus time in Figure 19B for chaotic intervals with almost periodic repeats (systems with rate parameters oscillating between stable and chaotic intervals in Figure 19 give both periodic and aperiodic time series). Behavior is 'mixing' in sense that trajectories eventually sample most of attractor space though repeats are almost periodic.

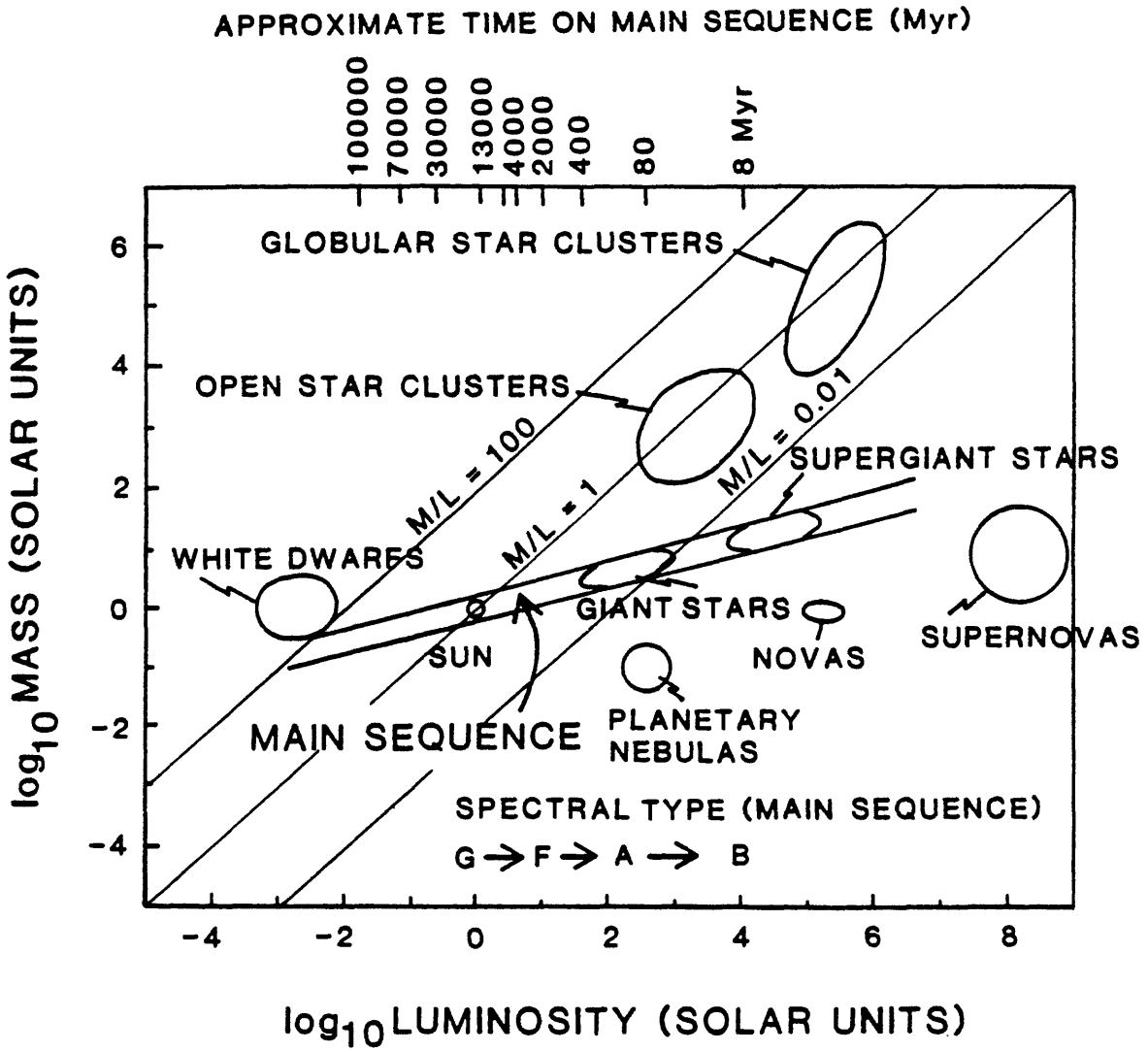
APPROXIMATE TIME ON MAIN SEQUENCE (Myr)
100000
70000
30000
13000
4000
2000
400
80
8 Myr
GLOBULAR STAR CLUSTERS
OPEN STAR CLUSTERS
M/L = 100
M/L = 1
M/L = 0.01
SUPERGIANT STARS
WHITE DWARFS
GIANT STARS
SUN
NOVAS
SUPERNOVAS
MAIN SEQUENCE
PLANETARY NEBULAS
SPECTRAL TYPE (MAIN SEQUENCE)
G → F → A → B
log10 MASS (SOLAR UNITS)
log10 LUMINOSITY (SOLAR UNITS)
6
4
2
0
-2
-4
-4
-2
0
2
4
6
8

Fig.21A

Figure 21. Stellar setting of solar system.

A. Generalized diagram showing mass and luminosity of stars, modified from Rubin (1984); spectral types for stars on the Main Sequence are indicated at the bottom with generalized ages shown at the top, after Huang (1975). Giant and Supergiant stars on Main Sequence are relatively young. Lines labeled M/L represent constant ratios of mass to luminosity delineating different styles and paths of evolution. Birth and aging of stars on Main Sequence discussed in text relative to processes of this paper.

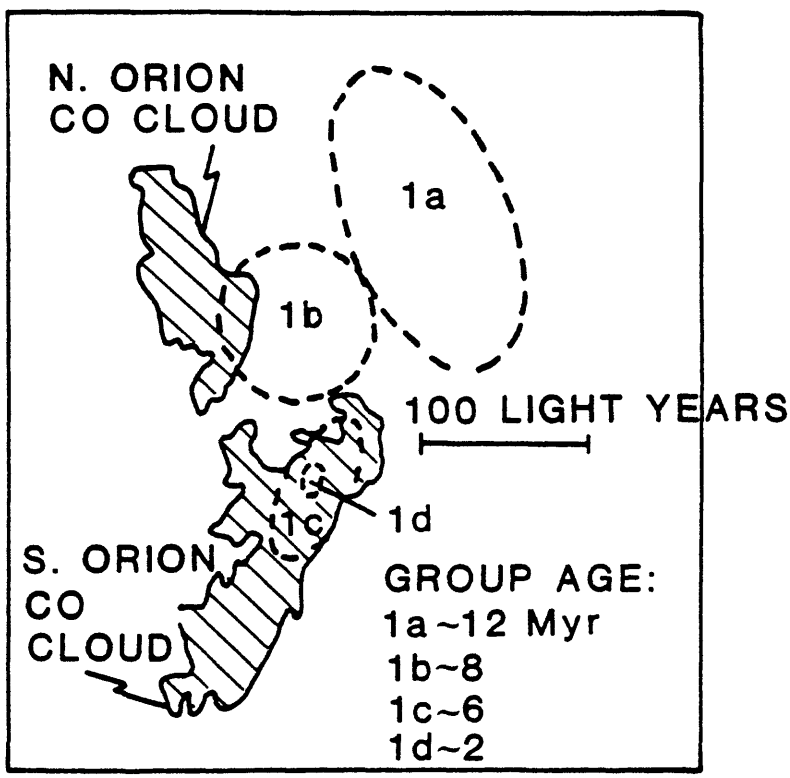
N. ORION
CO CLOUD
1a
1b
100 LIGHT YEARS
1c
1d
S. ORION
CO
CLOUD
GROUP AGE:
1a~12 Myr
1b~8
1c~6
1d~2

Fig.21B

Figure 21. Stellar setting of solar system.

B. Localized region of Orion arm of Milky Way galaxy within which young events of star formation have taken place in the vicinities of CO cloud complexes; they continue to occur at the present epoch (redrawn from Spitzer, 1982). The solar system is presently located within the Orion arm, a subarm of generalized 2-arm (4-spoke) spiral of Milky Way, at distance of about 1500 light years from region of active star formation (0.5 kiloparsec, kpc; typical width of spiral arm in galactic plane is about 1 kpc). Sun's distance from rotational center of galaxy is about 8 kpc; radius of galactic disc is about ten times this distance, and thickness of disc (Figure 20) is about 0.2 kpc at Sun's distance from galactic nucleus.

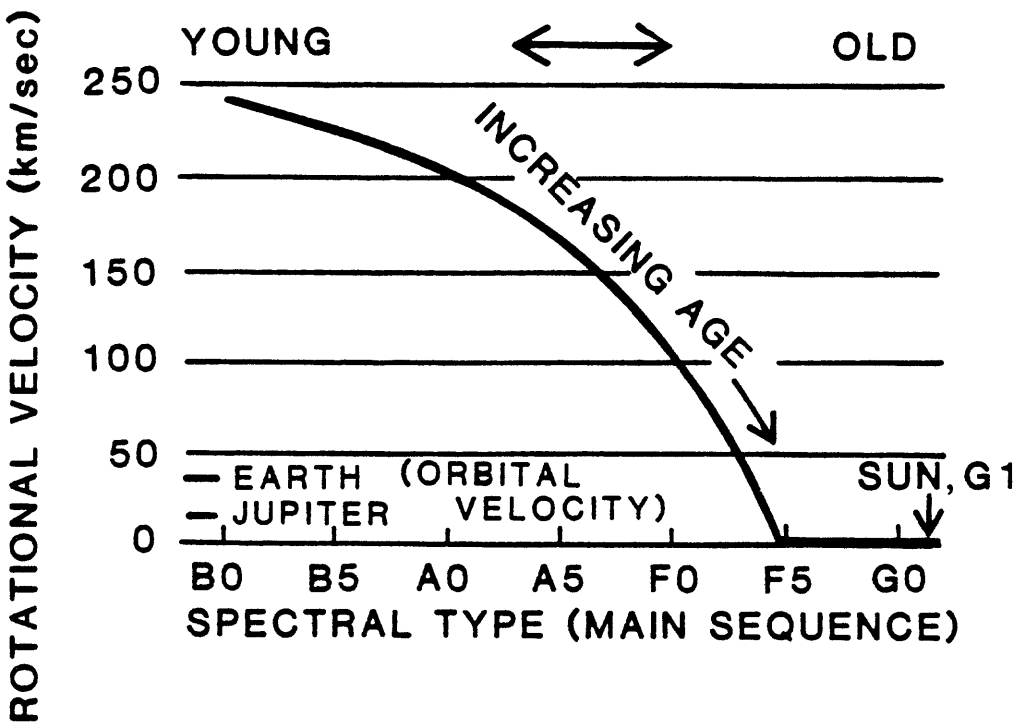
ROTATIONAL VELOCITY (km/sec)
YOUNG
OLD
250
200
150
100
50
0
INCREASING AGE
EARTH (ORBITAL VELOCITY)
JUPITER
SUN, G1
B0
B5
A0
A5
F0
F5
G0
SPECTRAL TYPE (MAIN SEQUENCE)

Fig.22

Figure 22. Generalized relation between rotation velocities of stars and spectral type, modified from Huang (1975). Upper limit is about same as orbital velocity of stars in galaxy; Sun's velocity in Milky Way is about 220 km/sec (Rubin, 1983). Orbital velocities of Earth and Jupiter in solar system are shown for comparison (rotational velocity of Sun about spin axis is about 2 km/sec). Loss of rotational kinetic energy by primary explained by exchange with orbital kinetic energies of planetary systems during their evolution.

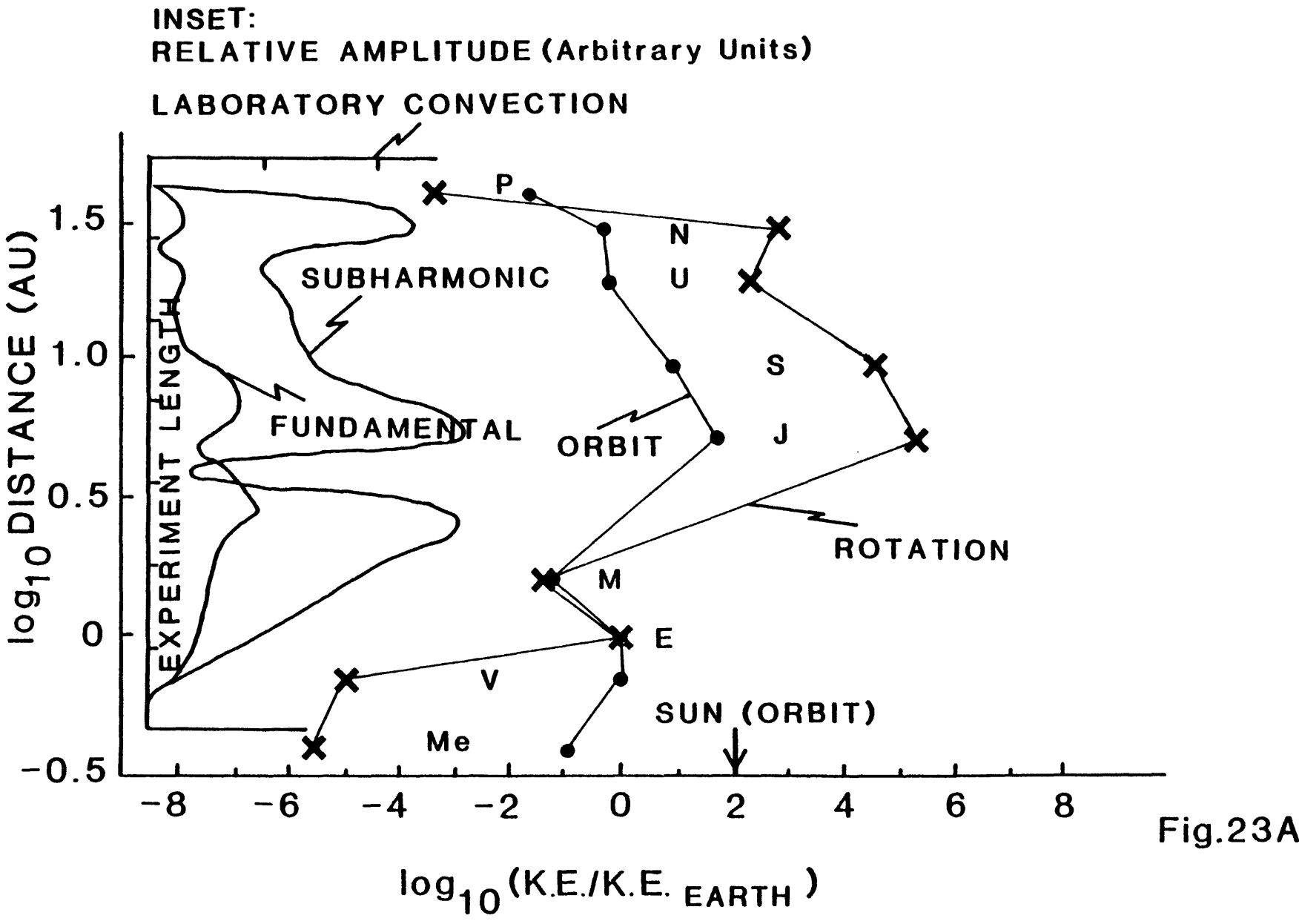
INSET:
RELATIVE AMPLITUDE (Arbitrary Units)
LABORATORY CONVECTION
EXPERIMENT LENGTH
SUBHARMONIC
FUNDAMENTAL
ORBIT
ROTATION
SUN (ORBIT)
P
N
U
S
J
M
E
V
Me
1.5
1.0
0.5
0
-0.5
-8
-6
-4
-2
0
2
4
6
8
log10 DISTANCE (AU)
log10 (K.E./K.E. EARTH)

Fig.23A

Figure 23. Energy-distance-mass relationships in solar system.

A. Relationships between orbital and rotational kinetic energies (K.E.) of the planets versus distance (Shaw, 1983b) calculated from standard data for solar system (Kaula, 1968, Tables 5.1 through 5.4). Orbital K.E. for Sun refers to revolution about solar system center of mass. Inset is laboratory experiment demonstrating quasiperiodic patterns of flow in which geometries of subharmonic motions mimic fundamental period of general circulation (modified from Gollub et al., 1980). Particle trajectories in such experiments plotted as phase portraits generate geometries of strange attractors (cf., Figure 24). Note resemblance to galactic structure in sense of complex periodic motions (Figure 20). Inset analogous to patterns in orbital and rotational kinetic energies of solar system (mimicry between two different scales of motion; pattern of planetary 'days' mimics that of planetary 'years'). Mimicry may record stages in process of transition from stellar to planetary system in Figure 22. Precision of present planetary periods represent resonant regime of stellar strange attractor (latter defined over long cycle times relative to timescales of planetary rotation and revolution).

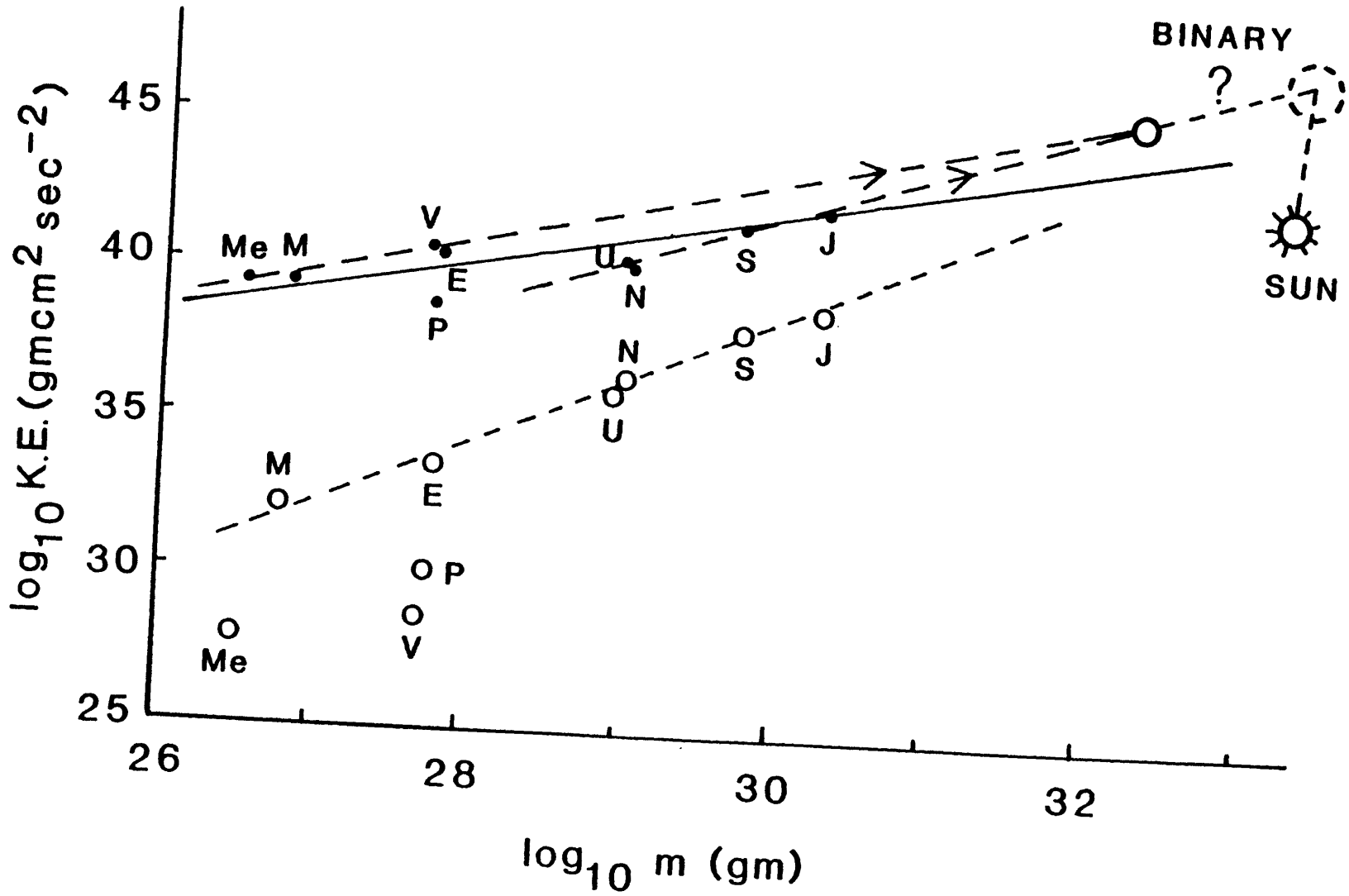
BINARY
?
SUN
45
40
35
30
25
26
28
30
32
$\log_{10}$ K.E. ($gmcm^2 sec^{-2}$)
$\log_{10}$ m (gm)
Me M
V
E
P
U
N
S
J
M
O
Me
V
E
P
U
N
S
J

Fig.23B

Figure 23. Energy-distance-mass relationships in solar system.

B. Relationships between kinetic energies and masses of planets and Sun illustrating hypothesis for binary star stage in evolution of solar system. Regression lines through subsets of points for orbital kinetic energies of inner and outer planets (long dashes and solid circles) converge at value roughly one-tenth Sun's mass. Rotational kinetic energies (short dashes and open circles) converge to mass-energy state in that vicinity. This pattern, mimicry in A, and Titius-Bode relation for planetary spacings record memory effects from early stage of stellar evolution (Shaw, 1983b); missing mass satisfied by companion star of ~ 0.1 solar mass postulated by Davis et al. (1984) and by Whitmire and Jackson (1984)? Dashed circle symbolizes stellar state prior to loss of rotational kinetic energy to planetary spinup (Figure 22) and partial loss of original mass.

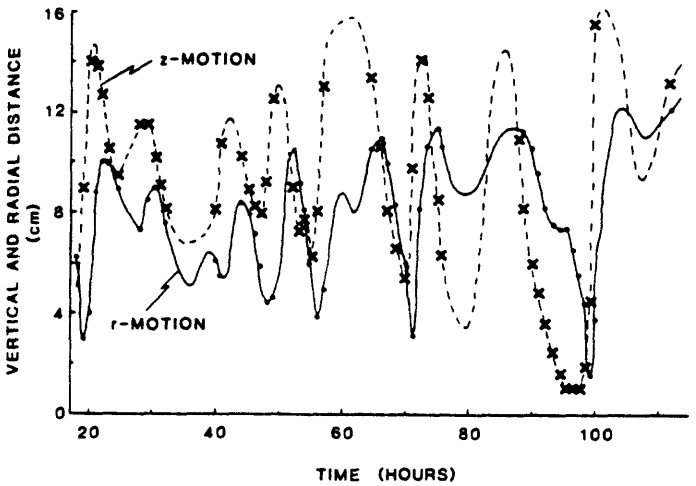

PIERCING POINTS IN X-Z PLANE
10^6 AT CENTER
10^3 NEAR EDGE
VISCOSITY 1000 POISE

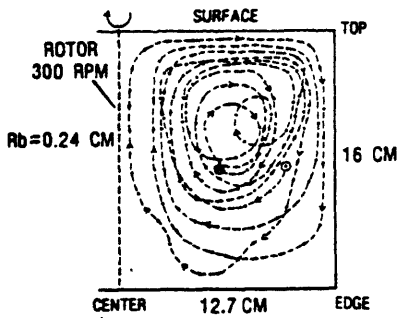

24 TOROIDAL REPEATS
TOTAL CYCLE: 112 HOURS

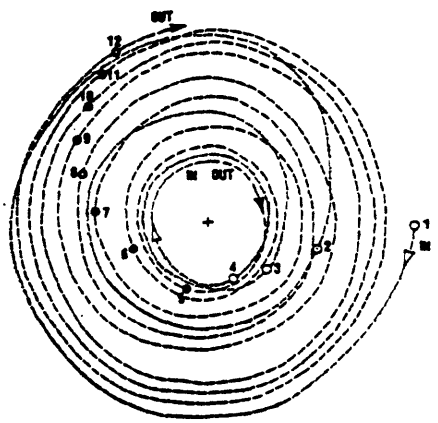

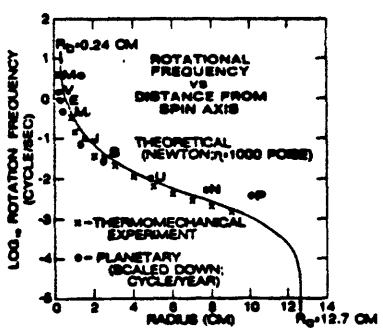

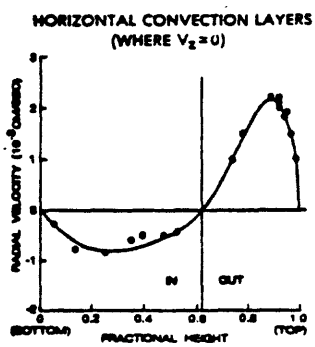

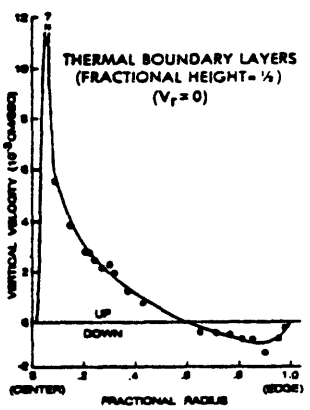

Fig.24

Figure 24. Laboratory experiment (H.R. Shaw, unpub. data, 1967) demonstrating mixed periodicities in system of combined forced and natural convection. Top diagram is time series record of trajectories of neutrally buoyant marker (analogous to Sun as marker for galactic 'convection' over about half the record in Figure 20A). Time and distance scales illustrated in other graphs. Forcing is by spin of small-diameter mechanical rotor (left center graph) driven by constant-speed motor causing viscous dissipation and thermal convection (center and bottom graphs); walls of container approximately isothermal, and no other heat sources (temperatures exceeded ambient by up to about $30^{\circ}C$): total time 112 hours, length scales 16 cm vertically and 12.7 cm radially, maximum power about 10 watts. Marker moves in-and-out and up-and-down synchronized crudely with angular rotation (center and bottom), an exaggerated analog of Sun's galactic rotation: r-motion (top) simulates effect of galactic mass fluctuations in Figure 20A; z-motion is roughly periodic, as in galactic plane-crossing rhythm, but of frequency similar to r-motion. In experiment radial and vertical motions are similar scale because aspect ratio is about 1; galaxy has aspect ratio, r/z, of order 10^3 so periods of r-motions greatly exceed periods of z-motions). Nonlinear pulsations (thermal instabilities) recorded by rapid temperature oscillations; dissipation is enhanced by high viscosity, small rotor diameter, and high torque (left center). In galaxy analogous pulsations are related to star-formation. Despite nonlinearities, average rotational motion agrees with theoretical velocity profiles calculated from linear models of flow (bottom left, crosses and solid curve); heat transfer fits standard correlations for annular convection in plots of Nusselt vs. Rayleigh numbers (not shown). Convective systems with strange attractors are consistent with Newtonian effects and fixed periods (e.g., period of rotor, length-of-day, year, etc., are constant relative to other periods).

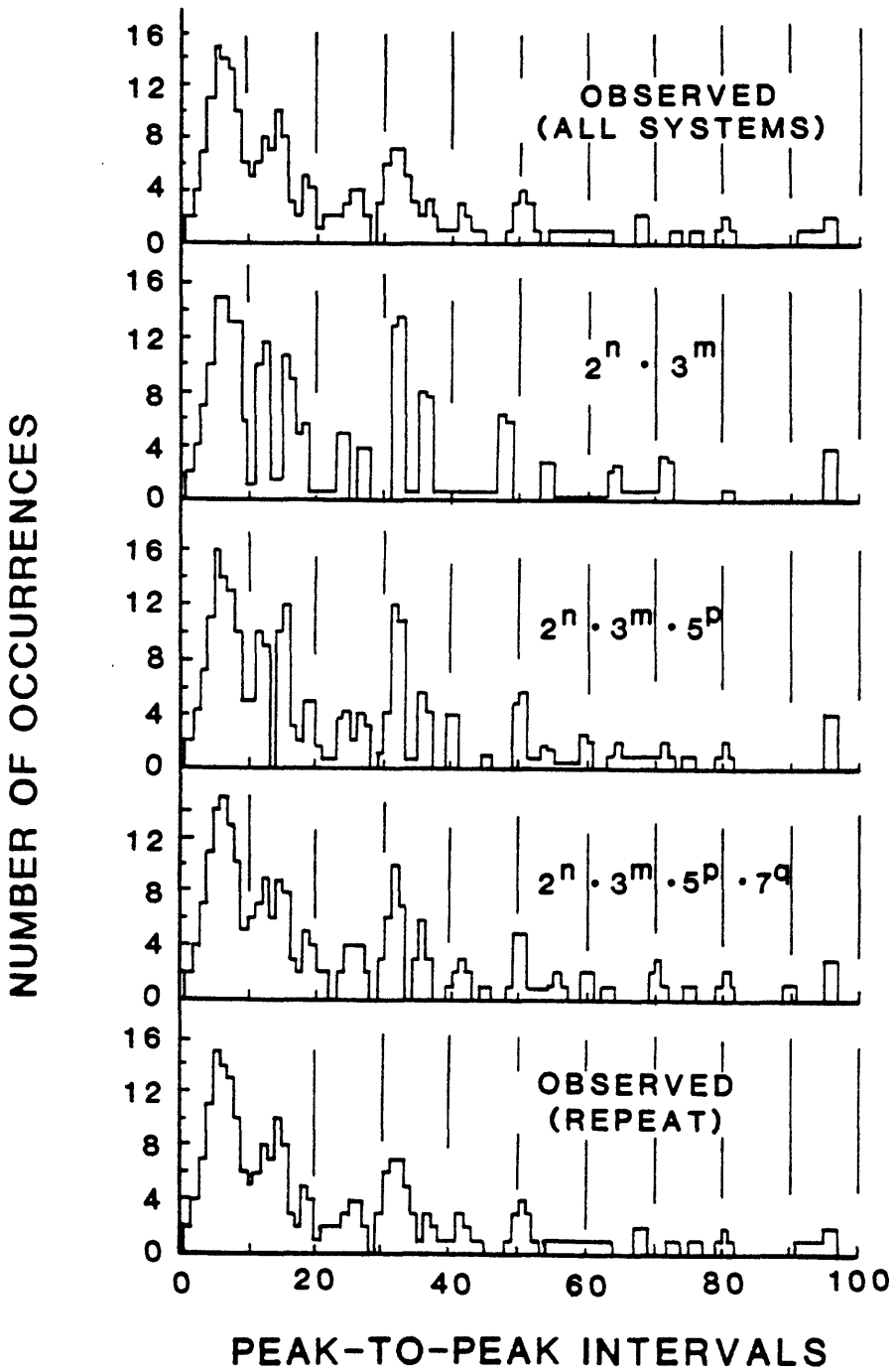
NUMBER OF OCCURRENCES
16
12
8
4
0
OBSERVED
(ALL SYSTEMS)
$2^n \cdot 3^m$
$2^n \cdot 3^m \cdot 5^p$
$2^n \cdot 3^m \cdot 5^p \cdot 7^q$
OBSERVED
(REPEAT)
0
20
40
60
80
100
PEAK-TO-PEAK INTERVALS

Fig.25A

Figure 25. Histograms of periodic phenomena in geological record.

A. Histograms of peak-to-peak age intervals based on data in Table 1 (sources given in footnotes of Table 1; H-E geomagnetic data not included because they overemphasize volcanic periods). Counts were made for observed age intervals; differences read in original graphs to $\pm$ 1 Myr. Unit count is rectangle 2 Myr in length on abscissa and one unit in height on ordinate. Where counts overlapped they were summed at 1-Myr intervals. Histograms for artificial geometric series $(2^n)(3^m)$, $(2^n)(3^m)(5^p)$, and $(2^n)(3^m)(5^p)(7^q)$ derived in same way for values nearest to observed period. A nearest value usually was close to only one observed value; where it was equidistant between two observed values the full range was plotted and the count interval reduced proportionately (a 4-Myr spread was counted as a bar 1/2 unit in height and 4 units in width, a 6-Myr spread as 1/3 unit in height and 6 units in width, etc.). These histograms are weighted most by processes considered by others to show periodicities in neighborhood of 30 Myr: ostracode data (column 8, Table 1) and shortest intervals of H-E record (column 4, Table 1) excluded in A. Counts at 2 and 3 Myr are weighted by intervals in Figure 16 for various peaks of Avian adaptive radiation in vicinity of K/T boundary (column 9, Table 1). Maxima at about 6, 15, 26, and 32 Myr resemble various periods reported in literature (see Figures 3 through 10 and references); the maximum at 6 Myr is approximately same as average duration of geologic stage in latest 250 Myr (Raup and Sepkoski, 1984).

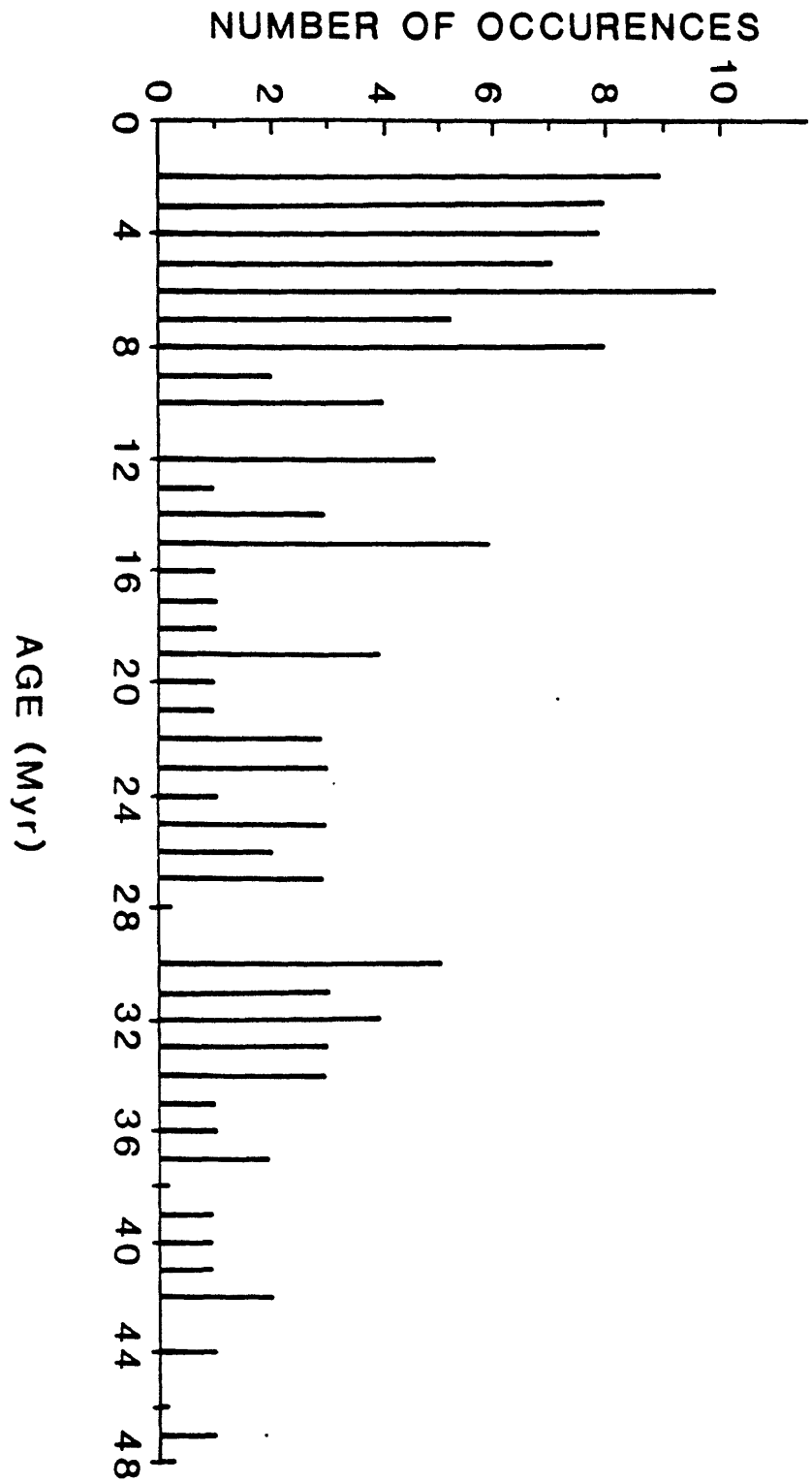
NUMBER OF OCCURENCES
0
2
4
6
8
10
AGE (Myr)
0
4
8
12
16
20
24
28
32
36
40
44
48

Fig.25B

Figure 25. Histograms of periodic phenomena in geological record.
B. Histogram of short-period intervals from all data in Table 1 plotted at specific values without overlap, for age differences of 48 Myr and less. Note episodic increases from about 45 to 30, and 30 to 2 Myr. Similar trends are seen in A and C and are mimicked in overall set (episode of order 100 Myr). These effects suggest self-similarities in frequency ratios (e.g., above episodes suggest ratios of about 2 to 6).

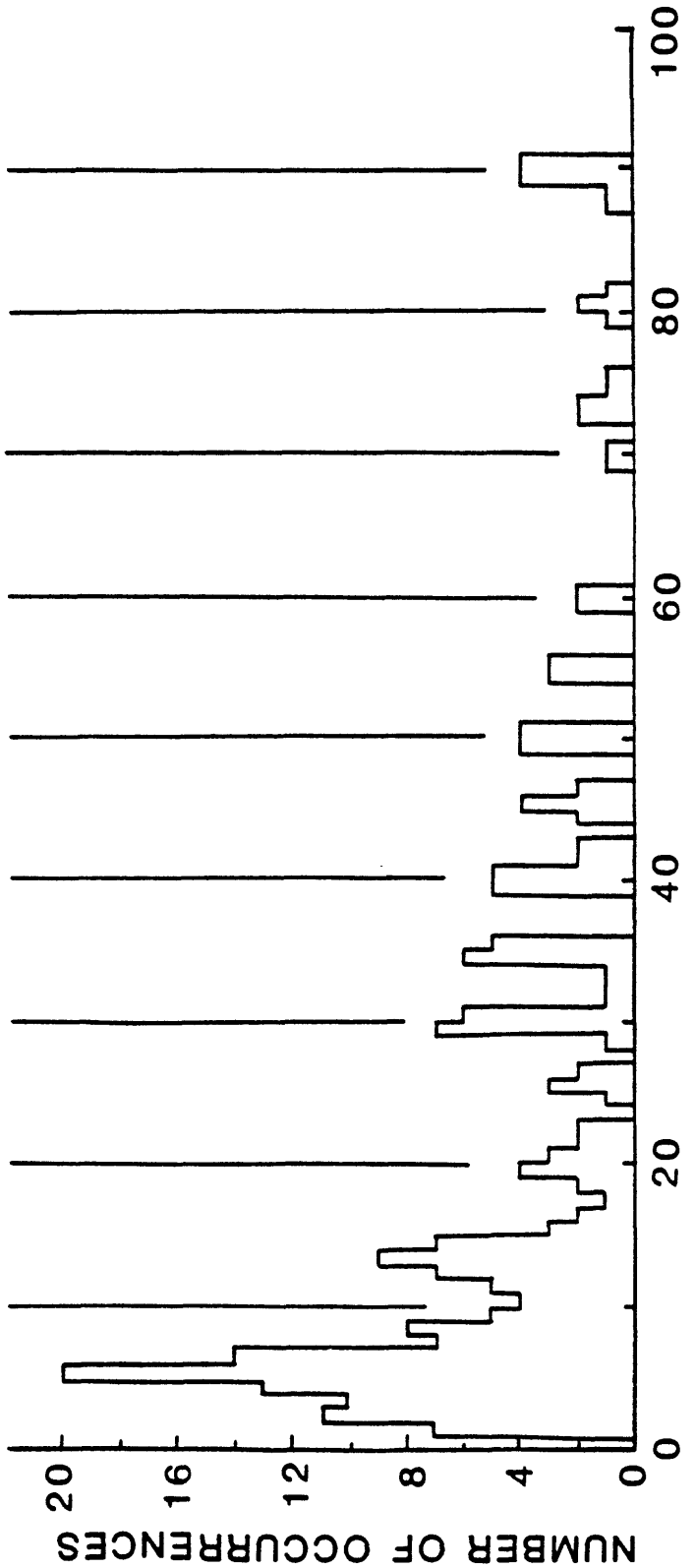
NUMBER OF OCCURRENCES
0
4
8
12
16
20
0
20
40
60
80
100
INTERVALS BETWEEN MINIMA (Myr)

Fig.25C

Figure 25. Histograms of periodic phenomena in geological record.

C. Histogram constructed as in A using observed age intervals between minima rather than maxima of data sources in Table 1; counts at less than 10 Myr are higher than in A because short-period events, including ostracode originations, have been included. This histogram is alternative data set representing same spectrum of mixed periodicities (see text for discussion of differences between A and C). Short-period maxima resemble signatures of H-E volcanism (see Figures 2, 7, and 10, and column 4, Table 1); Fourier transform analysis of H-E time-volume data gave power peaks near periods of 2, 3, 4, 6, and 12 Myr, power increasing with period (International Mathematics and Statistics Library (IMSL), Ed. 9, Vol. 2, Chapt. F, FTFREQ, p. 1-3, 1982; analysis by P. Doherty, Information Systems Division, U.S. Geological Survey).